EPSC2018

TP5 abstracts

EPSC Abstracts
Vol. 12, EPSC2018-36-1, 2018
European Planetary Science Congress 2018

Ensemble Forecast Sensitivity to Observations (EFSO) of the Venus data assimilation system

N. Sugimoto (1), A. Yamazaki (2), T. Kouyama (3), H. Kashimura (4), T. Enomoto (2, 5), and M. Takagi (6)
(1) Keio University, Yokohama, (nori@phys-h.keio.ac.jp / Fax: +81-45-566-1320), (2) JAMSTEC, Yokohama, (3) AIST, Tsukuba, (4) Kobe University, Kobe, (5) Kyoto University, Uji, (6) Kyoto Sangyo University, Kyoto, Japan.

Abstract

Last year, we developed the data assimilation system based on the local ensemble transform Kalman filter (LETKF) for a Venusian general circulation model (VAFES) [1]. This system reduces errors between analysis and forecast quickly, and successfully reproduced the thermal tide excited by the diurnal component of the solar heating. Recently, Ensemble Forecast Sensitivity to Observations (EFSO) technique has been implemented to quantify impact of each observation. The system would be useful for datasets from the Venus Climate Orbiter 'Akatsuki'.

1. Introduction

The data assimilation is an effective tool widely used in the planetary atmospheric science. Since observation data are irregularly sampled in space and time, global and continuous analysis fields produced by general circulation models (GCMs) with the data assimilation are quite useful to study atmospheric dynamics because the produced data are dynamically consistent.

However, the data assimilation has not been attempted for the Venusian atmosphere so far. In recent years, we have developed a Venusian Atmospheric GCM [2] named AFES-Venus (VAFES) on the basis of Atmospheric GCM For the Earth Simulator (AFES) [3]. Using VAFES, we have succeeded in reproducing the realistic structure of the Venusian atmosphere, such as planetary scale waves [4], cold collar [5], polar vortex [6], and thermal tide [7]. Comparison between the VAFES simulations and Akatsuki observations suggests that VAFES could be used for the data assimilation at this moment. Therefore, we developed a new data assimilation system for the Venusian atmosphere, named VALEDAS (Venus AFES LETKF Data Assimilation System) [1], based on AFES-Venus and the local ensemble transform Kalman filter (LETKF) [8] which is one of the most powerful and efficient schemes for the data assimilation. In the present study, we have implemented Ensemble Forecast Sensitivity to Observations (EFSO) technique to quantify how much each observation would improve the VAFES forecasts, and conducted several test cases using idealized and real observation data.

2. VAFES-LETKF system

VAFES is a full nonlinear Venus GCM with simplified physical processes [2]. The resolution is set to T42L60 (128 times 64 horizontal grids and 60 vertical levels). The vertical domain extends from the flat ground to ~120 km. The infrared radiative process is simplified by a Newtonian cooling scheme and the temperature is relaxed to a prescribed horizontally uniform temperature field based on VIRA. Vertical and horizontal distributions of the solar heating are based on previous observations and decomposed into a zonal mean component and a deviation from the zonal mean (diurnal component), which excite the mean meridional (Hadley) circulation and the thermal tide, respectively. Other details of the model settings are described in our previous works [2, 4].

The initial state is assumed to be an idealized superrotating flow in solid-body rotation. The zonal wind increases linearly with height from the ground to 70 km. We perform numerical time integrations for more than 4 Earth years. The model atmospheres reached quasi-steady states within approximately an Earth year. Quasi-equilibrium data sampled at 1-hour intervals are used for the *idealized observations*, and those at 8-hour intervals are for initial conditions of each member of the ensemble.

In data assimilation schemes, an improved estimate (called analysis) is derived by combining observations and short time forecasts. The LETKF [8] seeks the analysis solution with minimum error variance. Using an ensemble of VAFES runs,

uncertainty of the model forecast is characterized. Details of the VALEDAS are described in [1].

EFSO can estimate impacts of assimilated observations using the 12-hour forecasts with the ensemble-based method [9]. Such estimations are usually made by data-denial experiments or Observing System Experiments (OSEs), but these experiments with various observation datasets are computationally very expensive. EFSO is simpler, more computationally efficient, and gives similarly accurate results without using the adjoint model. Here, several idealized observations at the cloud top level with different intervals of the VAFES run are used to test EFSO.

3. Results

The VALEDAS quickly reduces the analysis and subsequent forecast root-mean-square (RMS) error. Furthermore, though the observation data are given at 70 km only, the three-dimensional structure associated with the thermal tide appears clearly.

Figure 1 shows time series of EFSO value and total energy (TE) that has been improved by all observations. A correlation coefficient of ~86.9% clearly indicates that the EFSO value successfully estimates impact of observations.

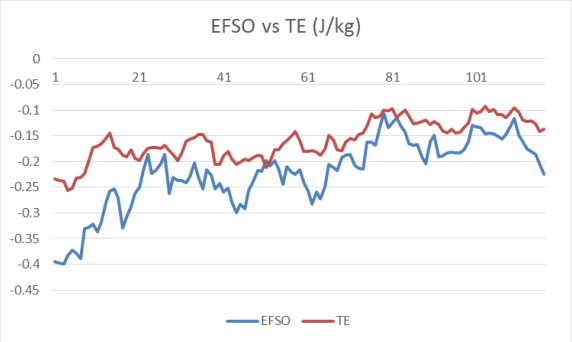

Figure 1: Time series of EFSO value and total energy (TE) that has been improved by all observations.

4. Summary and Conclusions

The VAFES-LETKF data assimilation system (VALEDAS) applicable to the Venus atmosphere has been developed and Ensemble Forecast Sensitivity to Observations (EFSO) technique was newly implemented to quantify impact of each observation. The VALEDAS with EFSO would enable us to reproduce more reliable structures of the Venus atmosphere by using Akatsuki observations.

Acknowledgements

This study was conducted under the joint research project of the Earth Simulator Center entitled 'Simulations of Atmospheric General Circulations of Earth-like Planets by AFES.'

References

[1] Sugimoto, N. et al.: Development of an ensemble Kalman filter data assimilation system for the Venusian atmosphere, Scientific Rep., 7, 9321, 2017.

[2] Sugimoto, N. et al.: Baroclinic instability in the Venus atmosphere simulated by GCM, J. Geophys. Res., Planets, 119, 1950–1968, 2014.

[3] Ohfuchi, W. et al.: 10-km mesh meso-scale resolving simulations of the global atmosphere on the Earth Simulator: Preliminary outcomes of AFES, J. Earth Simulator, 1, 8–34, 2004.

[4] Sugimoto, N. et al.: Waves in a Venus general circulation model, Geophys. Res. Lett., 41, 7461–7467, 2014.

[5] Ando, H. et al.: The puzzling Venusian polar atmospheric structure reproduced by a general circulation model, Nat. Commun., 7, 10398, 2016.

[6] Ando, H. et al.: Vertical structure of the axi-asymmetric temperature disturbance in the Venusian polar atmosphere: Comparison between radio occultation measurements and GCM results, J. Geophys. Res., Planets, 122, 1687–1703, 2017.

[7] Takagi, M. et al.: Three dimensional structures of thermal tides simulated by a Venus GCM, J. Geophys. Res., Planets, 123, 335–352, 2018.

[8] Hunt, B. R. et al.: Efficient data assimilation for spatiotemporal chaos: A local ensemble transform Kalman filter, Physica D, 230, 112–126, 2007.

[9] Kalnay, E. et al.: A simpler formulation of forecast sensitivity to observations: application to ensemble Kalman filters, Tellus 64A, 18462, 2012.

EPSC Abstracts
Vol. 12, EPSC2018-64, 2018
European Planetary Science Congress 2018

Water in the martian thermosphere and its effect on hydrogen escape

Vladimir A Krasnopolsky
Moscow Institute of Physics and Technology, Moscow, Russia (vlad.krasn@verizon.net)

Please make sure that your pdf conversion results in a document with a page size of 237 x 180 mm!

Abstract

Recent HST, MEX, and MAVEN observations reveal significant variations of hydrogen escape from Mars in the perihelion season (L_S = 200 to 330º) with values that reach 10^9 cm^{-2} s^{-1} and exceed the diffusion limit for H_2. This correlates with high H_2O abundances observed by MEX up to ≈80 km in this season. Here we present a 1D self-consistent photochemical model of neutral and ion composition at 80-300 km that accounts for H_2O chemistry. The model explains the observed hydrogen escape if the dayside-mean H_2O can reach 40 ppm at 80 km. This abundance is well within those observed by MEX.

1. Introduction

The martian hydrogen corona is described by two parameters: density of H at 250 km and temperature. However, the altitude extent in the orbiter observations may be insignificant for measurement of T, and the Mariner 6 and 7 flybys and HST imaging could provide more reliable data (Fig. 1).

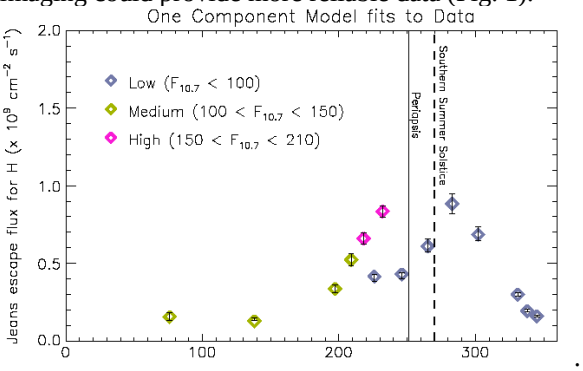

Fig, 1. HST observations of hydrogen escape from Mars in 2007-2017 [1].

These observations confirm the MEX data [2] that the escape rate at the perihelion season (L_S = 200-330º) may be very large and exceed the diffusion limit of 4×10^8 cm^{-2} s^{-1} for H_2 = 17 ppm [3, 4]. The observations correlate with the recent detections of high H_2O abundances up to ≈80 km in the perihelion season using the SPICAM IR solar occultations [5, 6]. If H_2O can reach the thermosphere, it may significantly affect its chemistry and increase hydrogen escape. However, the MAVEN/NGIMS measurements of the ion composition [7, 8] do not support significant abundances of water in the thermosphere. Here we will create a photochemical model to account for all aspects of the problem.

2. Model

Our one-dimensional self-consistent model of neutral and ion composition in the martian atmosphere at 80-300 km is based on the model [3] with nonthermal escape of light species (H, H_2, D, HD, and He) from [4]. The model accounts for vertical transport of species by eddy, molecular, and ambipolar diffusion.

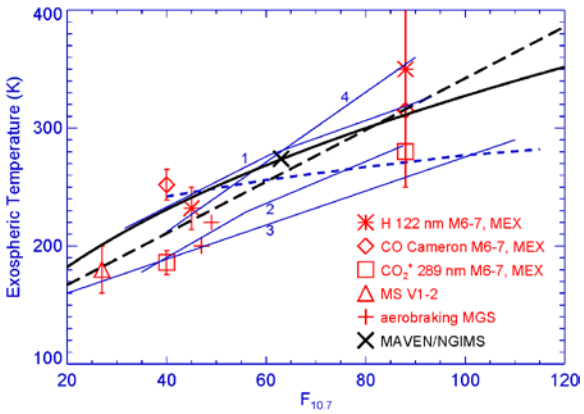

Fig. 2. Observed exospheric temperatures and their linear fit (long dashes). Blue lines are the MGTM versions of 2000, 2008, 2009, and 2015 at fall equinox. Solid line is a fit to the MAVEN point by thermal balance equation.

Temperature profiles are adopted by the least-square linear fit to observed exospheric temperatures (Fig. 2) that results in

$T_\infty = 123 + 2.19\, F_{10.7}$.

Temperature at 80 km is either 128 K with no water or that for the saturation conditions of water. Temperatures from 80 and 300 km are interpolated using an analytic expression. 30 reactions, which account for the basic photochemistry of H_2O, H_2O^+, H_3O^+, O_2, and their products, are added to the model.

3. Results

Photolysis of H_2O increases significantly the productions of H and H_2 and their escape. The following sequence of the ion reactions is also important in the balance of H_2O and its products:

$CO_2^+ + H_2O \rightarrow H_2O^+ + CO_2$
$H_2O^+ + CO \rightarrow HCO^+ + OH$
$HCO^+ + H_2O \rightarrow H_3O^+ + CO$
$H_3O^+ + e \rightarrow OH + H + H$
$(OH + O \rightarrow O_2 + H)\times 2$
$2\ H_2O + 2\ O + CO_2^+ + e \rightarrow CO_2 + 2\ O_2 + 4\ H$

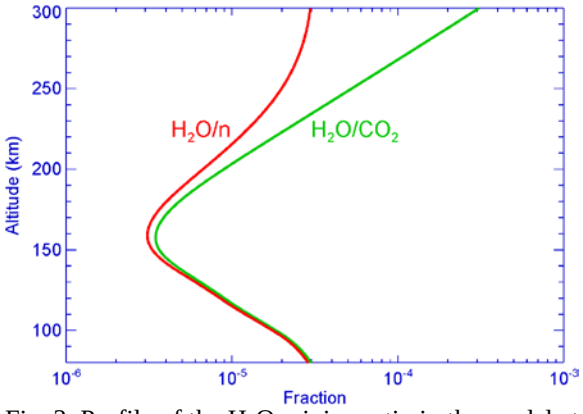

Fig. 3. Profile of the H_2O mixing ratio in the model at $F_{10.7}$ = 70 and f_{H2O} = 30 ppm at 80 km.

Both photolysis and ion chemistry strongly deplete the H_2O mixing ratio (Fig. 3) with a minimum at 160 km and further increase by the diffusive enrichment of light species.

Our models do not confirm the conclusion in [8] that significant H_2O abundances strongly deplete HCO^+ densities and are therefore incompatible with the MAVEN/NGIMS measurements. Loss of HCO^+ in our models is weaker in the reaction with H_2O than that in recombination, while the production is greater in the reaction $CO_2^+ + H$ because of the greater H for large H_2O.

Variations of the H and H_2 escape and densities at 250 km with H_2O at 80 km and solar activity are shown in Fig. 4 and 5. The escape flux of H may be approximated by

$\Phi_{H\uparrow}$ (cm^{-2} s^{-1}) = $1.6\times10^8 + 1.7\times10^7 f_{H2O}$ (ppm).

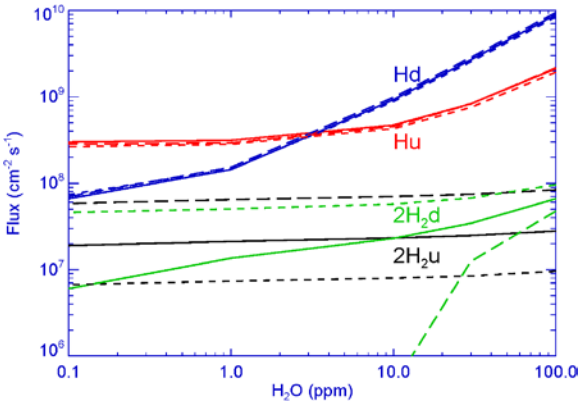

Fig. 4. Upward (u, escape) and downward (d, at 80 km) fluxes of H and H_2 for various H_2O abundances at 80 km and solar activity: $F_{10.7}$ = 40, 70, and 100 (short dashes, solids, and long dashes, respectively).

The results agree with those in Fig. 1 if H_2O reached 40 and 15 ppm at 80 km in the martian falls of 2014 and 2016, respectively.

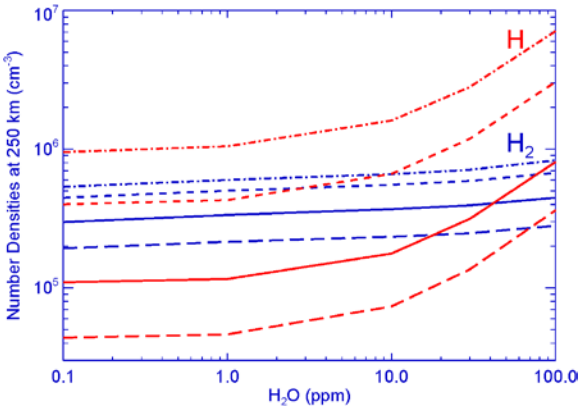

Fig. 5. Densities of H and H_2 at 250 km for various H_2O at 80 km and $F_{10.7}$ = 25, 40, 70, and 100 (dash-dots, short dashes, solid, and long dashes).

Acknowledgement. This work is supported by a grant of Russian Science Foundation to MIPT and V.A. Krasnopolsky.

References

[1] Bhattacharyya D. et al. JGR 122A, 11754, 2017.
[2] Chaufray J.Y. et al. Icarus 245, 282, 2015
[3] Krasnopolsky V.A. JGR 107E, E12, 5128, 2002
[4] Krasnopolsky V.A. Icarus 207, 638, 2010
[5] Maltagliati L. et al. Icarus 223, 942, 2013
[6] Fedorova A. et al. Icarus 300, 440, 2018
[7] Benna M. et al. GRL 42, 8958, 2015
[8] Fox J.L. et al. GRL 42, 8977, 2015

EPSC Abstracts
Vol. 12, EPSC2018-127, 2018
European Planetary Science Congress 2018

Flow associated with the Condensation and Sublimation of Carbon Dioxide Ice on Mars

Kim-Chiu Chow, Kwing-Lam Chan
Space Science Institute, Macau University of Science and Technology, Macao, China. (kcchow@must.edu.mo)

Abstract

By performing numerical experiments with a Mars general circulation model, the patterns of flow associated with the condensation and sublimation of carbon dioxide ice in the atmosphere of Mars have been interpreted.

1. Introduction

Carbon dioxide (CO_2) is the major constituent in the atmosphere of Mars. During a Martian year, the sublimation and condensation of CO_2 may result in a substantial change (up to 25%) in the total mass of the atmosphere, and so is important to the general circulation of the planet. In addition, it has been suggested that the sublimation flow near the ice cap edges may facilitate the process of dust lifting in the regions near the cap edge such as the Hellas Basin [1]. However, the patterns of the condensation and sublimation flow are not easy to be interpreted, as observational data is generally not available. A direct numerical simulation of these flows in a realistic general circulation model (GCM) is also not feasible in general. In this study, the patterns of these flows will be interpreted in an indirect way based on some numerical experiments by a Mars GCM.

2. Numerical Experiments

The GCM used is the MarsWRF [2]. The model domain has 36 x 72 grid points (horizontal resolution ~ 5 degree or 300 km), with 52 vertical layers. The model top layer is at the attitude about 80 km. The model has a radiation scheme specific to Mars [2], which has considered the heating/cooling effects of dusts and CO2. The model also includes some physical process parameterizations which are specific to Mars such as the CO2 cycle [3] and dust lifting. The parameterization of the dust process in the model includes an active dust scheme and a dust devil scheme similar to those used in [4]. The emission of dust is proportional to the surface wind stress when the stress is over a certain threshold value, while the suspended dusts may change the atmospheric radiation and so the circulation. The process of dust devils is parameterized to provide the background dust field, with amount mainly depending on the surface temperature.

The model was run for two years. The first year is considered as the spin-up period. The simulation in the second year is considered as the control simulation CTRL. Based on CTRL, some sensitivity experiments LHX5 have been performed in which the latent heat of CO_2 ice sublimation in either the northern or southern icecap is increased by 5 times starting from several chosen time instants. These are the periods when sublimation or condensation of CO_2 icecap occurs in the southern or northern hemisphere (Fig. 1). It can be shown that the effect of increasing the latent heat substantially in LHX5 is very similar to the effect of shutting down the process of sublimation or condensation.

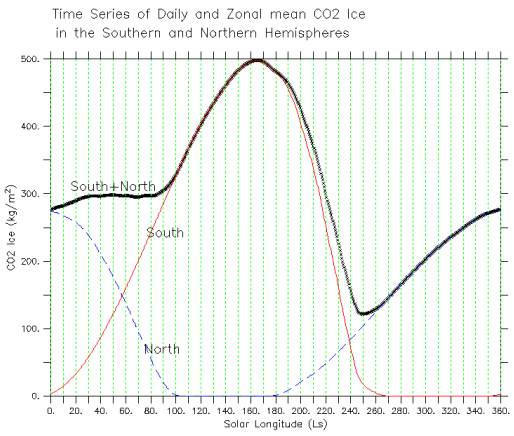

Figure 1: Seasonal variation of zonal-mean mass of CO_2 ice in the southern hemisphere (red), northern hemisphere (blue dotted) and both hemispheres (crosses) simulated in CTRL.

3. Results

The flow associated with the sublimation of CO_2 ice in the southern ice cap can be interpreted by considering the difference in the flow filed between CTRL and LHX5 after the increase in latent heat. To eliminate the signals of diurnal variation, the results averaged for 5 sols will be considered.

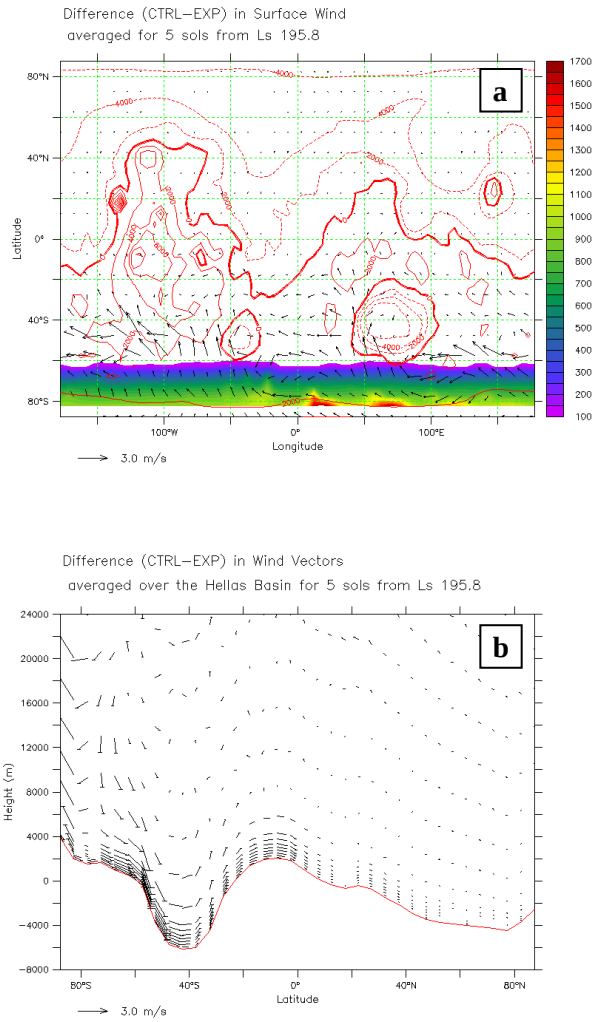

Figure 2: Five-sol mean differences in wind field between CTRL and LHX5 started at L_S = 195.8 °. (a) Surface wind field with topography in contours, and surface CO_2 ice (shading, kg m^{-2}). (b) Height-latitude profile of velocity vectors (m s^{-1}, vertical component multiplied by 100) averaged over the longitudes of the Hellas basin region.

The results of the experiments suggest that the surface wind of the sublimation flow is rather significant in the middle to high latitudes of the southern hemisphere (Fig. 2a). In fact, the sublimation flow may be rather shallow in general (Fig. 2b) except near the southern high latitude region.

It is interested to perform a similar analysis to interpret the sublimation flow at the northern icecap. The results suggest that the sublimation flow in the northern hemisphere is much weaker than that in the southern hemisphere (Fig. 3a). Compared with the sublimation flow, the magnitude of the condensation flow is generally much weaker in both hemispheres. However, the magnitude is still generally stronger in the southern hemisphere (Fig. 3b).

Acknowledgements

This research is funded by the grants from the FDCT of Macau (grant no. 119/2017/A3 and 080/2015/A3).

4. Summary and Conclusions

The results of the numerical experiments suggest that the sublimation flow in the southern hemisphere is much stronger than that in the northern hemisphere, and the maximum magnitude of the flow is generally around L_S ~ 240 °. The sublimation flow is rather shallow and is significant mainly near the surface.

References

[1] Chow, K. C., Chan, K. L., Xiao, J.: Dust Activity over the Hellas Basin of Mars during the Period of Southern Spring Equinox. *Icarus*, v311, 306 – 316, 2018.

[2] Richardson, M.I., Toigo, A.D., Newman, C.E.: PlanetWRF: A general purpose, local to global numerical model for planetary atmospheric and climate dynamics, *J. Geophys. Res. 112*. doi:10.1029/2006JE002825, 2007.

[3] Guo, X., Lawson, W.G., Richardson, M.I., et al.: Fitting the Viking Lander surface pressure cycle with a Mars General Circulation Model. *J. Geophys. Res. 114*, E07006. doi:10.1029/2008JE003302, 2009.

[4] Newman, C.E., Richardson, M.I.: The impact of surface dust source exhaustion on the martian dust cycle, dust storms and interannual variability, as simulated by the MarsWRF General Circulation Model. *Icarus 257*, 47 – 87, 2015.

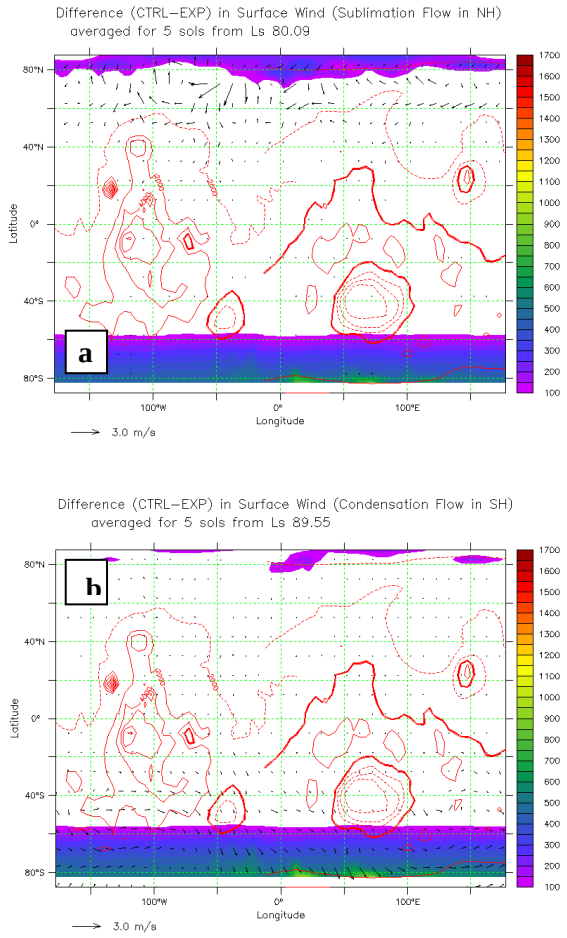

Figure 3: Similar to Fig. 2a, but for interpreting the sublimation flow in the northern icecap around L_S = 80 ° in (a), and the condensation flow in the southern icecap around L_S = 90 ° in (b).

EPSC Abstracts
Vol. 12, EPSC2018-157, 2018
European Planetary Science Congress 2018

Simulation of the coupled atmosphere and hydrosphere on early Mars using a GCM

Takeshi Kuroda (1,2), Arihiro Kamada (1), Katsushige Toriumi (1), Yasumasa Kasaba (1), Naoki Terada (1) and Hiromu Nakagawa (1)
(1) Department of Geophysics, Tohoku University, Sendai, Japan, (2) National Institute of Information and Communications Technology, Koganei, Japan. (tkuroda@nict.go.jp)

Abstract

We have adopted a Mars Global Climate Model (MGCM) for the early Martian climate (Paleo-Mars GCM, hereafter PMGCM) with the surface pressures of up to 2 bars, introducing the water cycle scheme with the liquid phase, liquid ocean/lakes on surface and their freezing/thermodynamic processes, and surface fluvial activities. We reproduced the warm surface condition to allow the fluvial activities except during winter, and the comparison of the simulated distributions of fluvial and sediment discharges with the observed valley networks was made.

1. Introduction

Martian valley networks are considered the evidence of a climate warm enough to allow the existence of long-term fluvial systems on early Mars during the Noachian and Hesperian boundary (3.85-3.6 Ga). The isotopic ratios detected from Martian meteorites showed the evidence of surface pressure of >0.5 bars in ~4.1 Ga [1] and surface water abundance of ~550 m global equivalent layer around that time [2], which should indicate that the surface liquid water made the observed fluvial traces.

However, 3-dimensional numerical studies using MGCMs had shown that the reproduction of surface temperature of above 273K (melting point of water) assuming the Martian environment of 3.8 Ga (with 25% weaker solar luminosity than the present value) would be difficult with only the radiative effects of thick (up to 7 bars) CO_2 atmosphere, water vapor and clouds [3,4]. To solve this contradiction, some studies has shown that higher surface temperature may be achieved by adding the radiative effects of SO_2[5] or H_2[6,7], but no 3-dimensional simulation study of early Martian climate had been done including the effects of the spatial changes of surface parameters such as thermal inertia of liquid water surface (ocean/lake) and estimating the fluvial features on surface for the accurate understanding of the environment.

2. Model Description

The PMGCM used in this study has been developed based on DRAMATIC (Dynamics, RAdiation, MAterial Transport and their mutual InteraCtions) MGCM, with the dynamical core of CCSR/NIES/FRCGC MIROC [8], which has reproduced various dynamical and physical processes for the current Martian atmosphere [9-11]. Here we simulated the possible early Martian climate assuming a pure CO_2 atmosphere with surface pressures of up to 2 bars, decreased solar flux to be 75% of the present value, a radiative scheme with the coupling of CO_2/H_2O gases and clouds, and water cycle including the large scale condensation and cumulus convection. We also implemented the ocean/land thermodynamics and land hydrology with the ocean mixed layer of 20 m and formation of sea ice, variable thermal inertia and surface albedo, and water penetration/fluvial transport/sediment transport processes.

Figure 1 shows the surface condition of the PMGCM assuming an ocean and lakes with the sea level of -2.54 km altitude on the topography of current Mars.

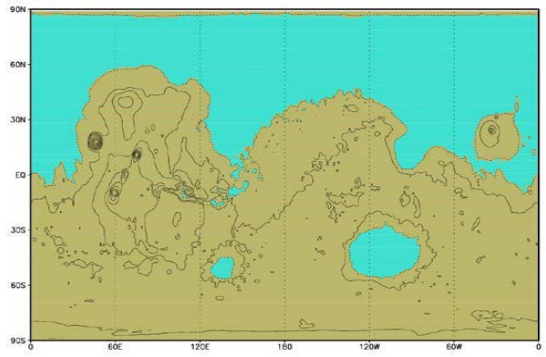

Figure 1: Surface condition of the PMGCM. Aqua regions represent the ocean/lakes.

3. Results

Figures 2 and 3 show the annual mean surface temperature and annual precipitation (sum of rain and snow), respectively. Due to the assumption of high thermal inertia of the ocean, we reproduced the warm surface temperature exceeding 273K from spring to autumn allowing seasonal melting of snow-ice deposits, while cold surface (< 273 K) during winter to produce considerable snow precipitation and accumulation, with the surface pressures of higher than 1.5 bars.

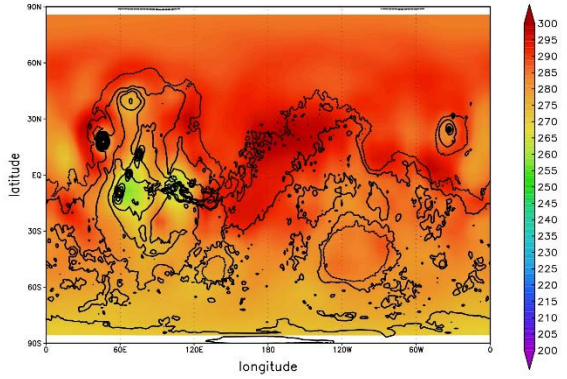

Figure 2: Simulated annual mean surface temperature [K] in our PMGCM with surface pressure of 2 bars.

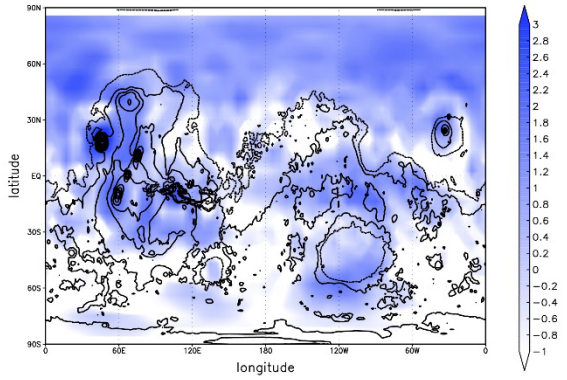

Figure 3: Same as Figure 2 except the annual precipitation [$\log_{10}$ of mm/Martian year].

Figures 4 and 5 show the annual mean fluvial and sediment discharges, respectively, simulated with the surface pressure of 2 bars. The results indicate the existence of fluvial sediment transport in the southern low- and mid-latitudes enough to reproduce Martian valley networks within a relatively short time (less than 10 million years) in the early Martian climate. However, there are some differences between the distributions of simulated discharges and observed valley networks which should be discussed.

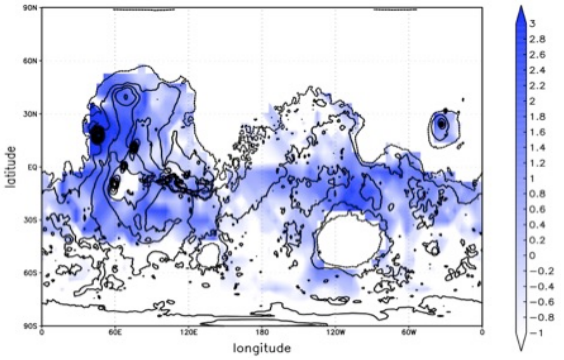

Figure 4: Same as Figure 2 except the annual mean fluvial discharge [$\log_{10}$ of m^3/Martian year].

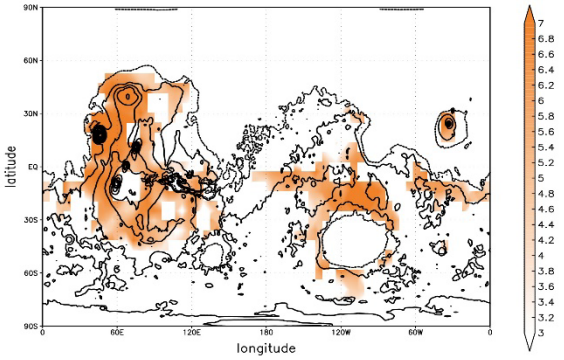

Figure 5: Same as Figure 2 except the annual mean sediment discharge [$\log_{10}$ of m^3/Martian year].

Our study first showed the possibilities of the clement and aqueous early Martian environment using a coupled atmospheric–hydrospheric MGCM in a 3-dimensional manner [12].

References

[1] Kurokawa et al., Icarus 299, 443–459. 2018.
[2] Kurokawa et al., Geochem. J. 50, 67–79, 2016.
[3] Forget et al., Icarus 222, 81-99, 2013.
[4] Wordsworth et al., Icarus 222, 1–19, 2013.
[5] Mischna et al., J. Geophys. Res. Planets, 118, 560–576, 2013.
[6] Ramirez et al., Nature Geosci., 7, 59–63, 2014.
[7] Ramirez, Icarus 297, 71–82, 2017.
[8] K-1 Model Developers, K-1 Tech. Rep., 1, Univ. of Tokyo, 2004.
[9] Kuroda et al., J. Meteor. Soc. Japan 83, 1-19, 2005.
[10] Kuroda et al., Geophys. Res. Lett., 40, 1484-1488, 2013.
[11] Kuroda et al., Geophys. Res. Lett., 42, 9213–9222, 2015.
[12] Kamada et al., Icarus, under revision.

EPSC Abstracts
Vol. 12, EPSC2018-166, 2018
European Planetary Science Congress 2018

D and H in the Upper Atmosphere of Mars

Majd Mayyasi, John Clarke, Dolon Bhattacharyya, SOHO SWAN and MAVEN Teams
Center for Space Physics, Boston, MA, USA,
(majdm@bu.edu)

Abstract

The atmosphere of Mars has been remotely sounded at Ultraviolet wavelengths using the NASA Mars Atmosphere and Volatile Evolution (MAVEN) mission [1]. A high-resolution echelle channel on board MAVEN, capable of resolving Lyman-α emissions of hydrogen and deuterium at 121.567 nm and 121.535 nm, respectively, has been used to measure emission brightness from these atomic species along the disk, limb and corona of Mars with unprecedented coverage. The remotely-sensed MAVEN observations have been consistently calibrated using Solar Wind Anisotropy (SWAN) instrument observations and model estimates of diffuse interplanetary H [2]. In situ and remote sensing measurements are collectively used in order to determine properties of H and D in the martian upper atmosphere. This presentation highlights the results of these efforts to date.

1. Introduction

A key scientific goal of the MAVEN mission is to understand water escape at Mars. One way to quantify this escape is to examine the ratio of D and H abundances in the upper atmosphere in order to examine the rate of preferential loss of the lighter to heavier isotopologue. The classical (pre-MAVEN) perception of H loss originates with the atomic and molecular photo-dissociated byproducts of water diffusing slowly (timescale of years) to higher altitudes where chemistry liberates atomic H and allows a population of those atoms to leave the planet's upper atmosphere via Jeans escape [3]. D undergoes similar processes as H but escapes at a slower rate due to its larger mass. Therefore, determining the properties of D and H in the upper atmosphere would improve our understanding of water escape rates, the water cycle, and ultimately, would help to constrain the amount of primordial water at the planet.

2. Summary of Variability Studies

MAVEN measurements of D and H brightness have been mapped across nearly two Mars Years. These measurements have shown that both D and H vary on multiple timescales, all of which are much faster than the classical theory suggests. Analysis of MAVEN echelle observations has revealed several trends in the D and H brightnesses. These variations are summarized below, in order of increasing timescale:

1) Lyman-α is a solar resonant scattering emission. Therefore, to first order, the brightness of this emission exhibits trends consistent with solar flux variability, such as solar zenith angle variations as well as periodic trends with a solar-rotation timescale (~28 days) [4, 5, 6].

2) Changes in Mars' orbital distance from the Sun triggers climate dynamics and seasonal dust storms that affect the water cycle and the flux of D and H atoms into the upper atmosphere. These lower-atmospheric processes vary with a seasonal and repeatable periodicity that affects the properties of H and D in the upper atmosphere with timescales of months [5].

3) Solar activity affects the flux of solar H Lyman-α that reaches Mars. Variations on this 11-year timescale are expected and seen throughout the MAVEN mission timeline [5]. Additional space weather events have been seen to trigger significant changes in the properties of D and H in the upper atmosphere of Mars, mainly through upper atmospheric heating [6].

In this presentation, the variations in D and H properties in the upper atmosphere of Mars, observed by MAVEN to date, are presented and put in context of variability of molecular water isotopologues lower in the atmosphere. Estimates of the escape rates are made. These results will be significant for complementary lower atmospheric studies by TGO and will improve our understanding of historic water escape at Mars.

References

[1] Jakosky, B. (2015). MAVEN explores the Martian upper atmosphere. *Science*, 350(6261), 643.

[2] Mayyasi, M., Clarke, J., Quénerais, E., Katushkina, O., Bhattacharyya, D., Chaufray, J.-Y., …Jakosky, B. (2017). IUVS echelle-mode observations of interplanetary hydrogen: Standard for calibration and reference for cavity variations between Earth and Mars during MAVEN cruise, J. Geophys. Res., 122, 2089–2105.

[3] Hunten, D. M. & McElroy, M. B. *J. Geophys. Res.*, 75, 5989–6001 (1970).

[4] Clarke, J. T., et al. (2017), Variability of D and H in the Martian upper atmosphere observed with the MAVEN IUVS echelle channel, *J. Geophys. Res.*, 122.

[5] Mayyasi, M., Clarke, J., Bhattacharyya, D., Deighan, J., Jain, S., Chaffin, M., … Jakosky, B. (2017), The variability of atmospheric deuterium brightness at Mars: Evidence for seasonal dependence., *J. Geophys. Res.*, 122.

[6] Mayyasi, M., J. Clarke, D. Bhattacharyya, A. Catalano, M., Benna, P. Mahaffy, …B. Jakosky (2018), Significant space weather impact on the escape of Hydrogen from Mars, *Geophys. Res. Lett.*, in press.

EPSC Abstracts
Vol. 12, EPSC2018-186, 2018
European Planetary Science Congress 2018

Global characteristics of gravity waves in the upper atmosphere of Mars as measured by MAVEN/NGIMS

Alex Siddle (1), Ingo Mueller-Wodarg (1), Roger Yelle (2) and Shane Stone (2)

(1) Blackett Laboratory, Imperial College London, Prince Consort Road, London SW7 2AZ, UK, (2) Lunar and Planetary Laboratory, University of Arizona, Tucson, Arizona 85721, USA

(a.siddle16@imperial.ac.uk)

Abstract

Gravity waves (GWs) are omni-present in stratified atmospheres such as Earth, Mars and Titan's [1][2][3]. These perturbations have been observed at Mars by previous spacecraft such as Mars Global Surveyor (MGS) and more recently the Mars Atmosphere and Volatile EvolutionN (MAVEN) mission [4][5][6].

GWs are generated from a diverse range of sources including flow over topography, atmospheric instabilities and volatile convection, however any process which perturbs the atmosphere could generate GWs. Many modelling studies have shown the significance of the effects of GWs for an accurate description of the atmosphere [7][8]. GWs carry energy and momentum as they propagate upwards and have been found to slow down or reverse mean flows in the upper atmosphere. The deposition of wave energy has the potential to either warm or cool the atmosphere, dependent on local atmosphere conditions [8].

We have performed a comprehensive study of gravity waves in Mars' upper atmosphere. Using in situ data from the Neutral Gas and Mass Spectrometer (NGIMS) onboard MAVEN we have been able to characterise waves from nearly 4000 orbits [9]. We use density and temperature profiles to extract waves. We interpret these waves as vertical structures and characterise them by their amplitude and wavelength. We compare our results to those found using data from MGS, Odyssey (ODY) and MAVEN [2][5][6]. By using solar zenith angle and Mars-Sun distance as proxies for temperature, we have investigated correlations between temperature and GW characteristics. Large variations in amplitude are observed over the sampled zenith angle range. No such trend is found for wavelengths. By comparing pre- and post-periapsis profiles, we find that the largest variations are found in the coolest regions of the atmosphere, such as on the nightside. We discuss these results in the context of future aerobraking missions.

References

[1] Fritts, D. C. (1984), Gravity wave saturation in the middle atmosphere: A review of theory and observations, Rev. Geophys., 22(3), 275–308

[2] Fritts, D. C., L. Wang, and R. H. Tolson (2006), Mean and gravity wave structures and variability in the Mars upper atmosphere inferred from Mars Global Surveyor and Mars Odyssey aerobraking densities, J. Geophys. Res., 111, A12304

[3] Mueller-Wodarg, I. C. F., R. V. Yelle, N. Borggren, and J. H. Waite Jr. (2006), Waves and horizontal structures in Titan's thermosphere, J. Geophys. Res., 111, A12315

[4] Keating, G., Bougher, S., Zurek, R., Tolson, R., Cancro, G., Noll, S. Babicke, J. (1998). The Structure of the Upper Atmosphere of Mars: In Situ Accelerometer Measurements from Mars Global Surveyor. Science, 279(5357), 1672-1676

[5] Creasey, J. E., J. M. Forbes, and G. M. Keating (2006), Density variability at scales typical of gravity waves observed in Mars' thermosphere by the MGS accelerometer, Geophys. Res. Lett., 33, L22814,

[6] Yiğit, E., S. L. England, G. Liu, A. S. Medvedev, P. R. Mahaffy, T. Kuroda, and B. M. Jakosky (2015), High - altitude gravity waves in the Martian thermosphere observed by MAVEN/NGIMS and modeled by a gravity wave scheme, Geophys. Res. Lett., 42, 8993–9000

[7] Medvedev, A. S., E. Yiğit, P. Hartogh, and E. Becker (2011), Influence of gravity waves on the Martian atmosphere: General circulation modeling, J. Geophys. Res., 116, E10004

[8] Medvedev, A. S., & Yiğit, E. (2012). Thermal effects of internal gravity waves in the Martian upper atmosphere. Geophysical Research Letters, 39(5).

[9] Mahaffy, P. R., Benna, M., King et al. (2015). The Neutral Gas and Ion Mass Spectrometer on the Mars Atmosphere and Volatile Evolution Mission. Space Science Reviews, 195(1-4), 49-73

EPSC Abstracts
Vol. 12, EPSC2018-187-2, 2018
European Planetary Science Congress 2018

Mars emissions from CO and CO_2^+: IUVS-MAVEN limb observations and model

J.-C. Gérard (1), L. Gkouvelis (1), B. Ritter (1), B. Hubert (1), S. Jain (2), N.M. Schneider (2), V.I. Shematovich (3) and D.V. Bisikalo (3)

(1) LPAP, Université de Liège, Belgium, (2) LASP, University of Colorado, Boulder, USA, (3) Institute of Astronomy, Moscow (jc.gerard@uliege.be)

Abstract

We analyzed limb observations of various dayglow emissions collected during about 3 years by the Imaging Ultraviolet Spectrograph (IUVS) instrument on board the Mars Atmosphere and Volatile Evolution mission (MAVEN) satellite orbiting Mars. These profiles have been analyzed in terms of latitude, season, local time, solar zenith angle and Martian year. They are compared with the altitude distribution and brightness expected by model simulations based on densities from Mars General Circulation models. To fit the observations scaling factors have to be applied to the GCM atmospheric densities. These are generally less then unity. In this study, we take advantage of the measurements by the EUV instrument on board MAVEN that allows monitoring of incoming solar flux reaching Mars every minute.

1. Introduction

Limb observation of airglow emissions is a standard technique to study the altitude profiles of the chemical elements in the Martian atmosphere and its thermal structure. Several previous missions have performed observations in the past (Mariners, Mars Express). Three years ago, the IUVS Ultraviolet spectrograph (McClintock et al. 2014) on board MAVEN started collecting thousands of airglow and auroral limb profiles in the range 120 to 340 nm. We now have analyzed more that three years of airglow observations and compared them to model simulations. The objective is to study the characteristics of the CO_2 and CO FUV emissions to describe the Martian upper atmospheric structure and its variations.

2. IUVS observations

The Imaging Ultraviolet Spectrometer is a remote sensing instrument on MAVEN, equipped with two ultraviolet channels: the MUV (middle ultraviolet) and FUV (far ultraviolet) detectors cover the 115-190 nm and 180-340 nm spectral ranges respectively. MAVEN has collected limb spectra over three years of airglow observations covering more than a full Martian year and various latitudes ranges per epoch.

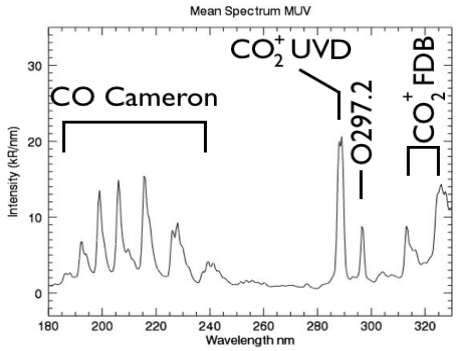

Figure 1: Sum of 210 FUV spectra collected between 110 and 130 km. The main dayglow emissions are identified between 180 and 330 nm. CO_2 is the main source constituent of all four emissions.

We have analyzed the data and generated mean altitudes profiles for many of the emission features, grouping them in epoch, seasonal and latitude ranges (Figure 2). An example of simultaneous limb scans of several emissions is shown in Figure 3. The limb brightness profile of each spectral feature was obtained by using a multiple linear regression method to fit each observed spectrum.

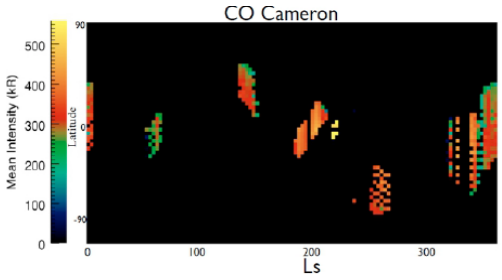

Figure 2: coverage of MAVEN dayglow observations during the first Martian year of the mission. The map shows the peak brightness of the CO Cameron emission in a 6°x6° bins.

3. Modelling

To model the dayglow emissions of the Martian atmosphere, we first construct neutral atmosphere distribution of the main constituents for different seasons, latitudes and local times based on the MCD model. Second, we use Monte Carlo simulations to calculate the photoelectron energy spectrum as a function of altitude for the latitude, solar longitude, local time and solar activity corresponding to the observations. Calculations of the collisional sources are based on the Direct Simulation Monte Carlo (DSMC) method that has been developed over the years (Shematovich et al. 2008; Gérard et al., 2008) to calculate the brightness profiles of emissions of the Earth, Jupiter, Saturn, Venus and Mars atmospheres. The energy spectrum of the photoelectrons calculated at fixed grid points is folded with relevant electron impact excitation cross sections to determine the corresponding collisional excitation rates. Finally, these sources are combined with directly solar-induced sources such as photodissociation to obtain the total volume production rates (Figure 3). In the case of the CO Cameron and CO_2^+ bands, the dominant sources are directly proportional to the CO_2 density. These emissions are therefore direct indicators of changes in thermospheric CO_2. To fit the observations, scaling factors have to be applied to the GCM atmospheric densities. These are generally less then unity.

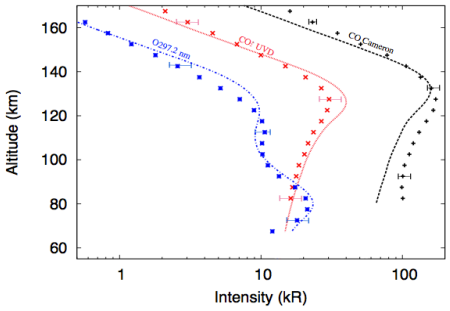

Figure 3: comparison between IUVS limb observations and model simulations for three airglow emissions. The best fit was obtained by scaling the CO_2 density by a factor of ~0.5.

4. Summary and Conclusions

A large number of limb profiles of CO and CO_2^+ dayglow emissions have been collected with the IUVS instrument on board MAVEN. They cover more than a Martian year and a wide range of latitudes, solar longitudes and local times. Comparisons with simulated limb profiles for conditions similar to the observations are presented. They provide information about the Martian atmospheric structure in a region that is difficult to probe with other techniques.

Acknowledgements. This research is supported by the PRODEX program of ESA, managed with the help of the Belgian Science Policy Office (BELSPO). Funding was also provided by BELSPO's SCOOP/BRAIN research project.

References

[1] Gérard, J.C. et al., PSS, 56, 542-552, 2008.

[2] McClintock, W.E. et al., Space Sci. Rev., 1-50,10-1007/s, 2014

[3] Shematovich, V.I. et al., J. Geophys. Res., 113, E02011, 2008.

EPSC Abstracts
Vol. 12, EPSC2018-275, 2018
European Planetary Science Congress 2018

Venus' winds measured with visible imaging-spectroscopy at the THEMIS observatory

Patrick Gaulme (1,2,3), François-Xavier Schmider (4), Thomas Widemann (5,6), Ivan Gonçalves (4), Arturo López Ariste (7) and Bernard Gelly (8)
(1) Max-Planck-Institut für Sonnensystemforschung, Justus-von-Liebig-Weg 3, 37077, Göttingen (gaulme@mps.mpg.de), (2) Department of Astronomy, New Mexico State University, P.O. Box 30001, MSC 4500, Las Cruces, NM 88003-8001, USA, (3) Physics Department, New Mexico Institute of Mining and Technology, 801 Leroy Place, Socorro, NM 87801, USA, (4) Laboratoire Lagrange, Université de Nice Sophia Antipolis, UMR 7293, Observatoire de la Côte d'Azur (OCA), Nice, France, (5) LESIA, Observatoire de Paris, PSL, CNRS, Sorbonne Université, U. Paris-Diderot, France, (6) DYPAC, Université Versailles-Saint-Quentin, Université Paris Saclay, France, (7) IRAP, Université de Toulouse, CNRS, CNES, UPS. 14, Av. E. Belin. 31400 Toulouse, France, (8) THEMIS Observatory, La Laguna, Tenerife, Spain

Abstract

The objective of the present work is to measure the global properties of Venus' atmospheric dynamics, through the obtention of a complete radial-velocity map of Venus at the altitude of the uppermost cloud layer. Our results are based on high-resolution spectroscopic observations of Venus performed in the visible domain with the long slit spectrometer of the solar telescope THEMIS (Spain). We present the first instantaneous "radial-velocity snapshot" of any planet of the solar system in the visible domain, i.e., a complete RV map of the planet obtained by stacking data on less than 10 % of its rotation period. From this, we measure the properties of the zonal and meridional winds, which we unambiguously detect. We identify a wind circulation pattern that significantly differs from what we know about Venus. The zonal wind displays a "hot spot" structure, featuring about 200 m s^{-1} at sunrise and 70 m s^{-1} at noon in the equatorial region. Regarding meridional winds, we detect an equator-to-pole meridional flow peaking at 45 m s^{-1} at mid latitudes, i.e., which is about twice as large as what was reported so far.

1. Context

Venus' atmosphere is well known for rotating in a retrograde direction (from east to west), contrarily to all other bodies in the solar system, with the notable exception of Saturn's moon Titan. First evidenced from the ground, the atmospheric super-rotation has been extensively studied both from space and ground-based telescopes (e.g., Gierasch et al. 1997). The cloud top region is important as it constrains the global mesospheric circulation in which zonal winds generally decrease with height while thermospheric sub-solar to anti-solar winds increase (e.g., Lellouch et al. 1997). It also shows important spatial and temporal variability (e.g., Sánchez-Lavega et al. 2008; Khatuntsev et al. 2013).

In 2007, a significant international effort was organized to support the atmospheric observations of Venus by ESA mission VEx (Lellouch & Witasse 2008). The objective was to measure the atmospheric circulation using different spectral ranges, to probe different altitudes in the Venus mesosphere. Significant results on the upper mesospheric dynamics were obtained using mid-infrared heterodyne spectroscopy (e.g., Sornig et al. 2012), millimeter and submillimeter wave spectroscopy (e.g., Moullet et al. 2012), and visible spectroscopy (e.g., Machado et al. 2017, and refs. therein).

Back in 2007, we proposed to use the THEMIS solar telescope to get Doppler maps of Venus by scanning the planet in the visible with the 100-arcsec long slit spectrometer MulTiRaies (MTR) at a resolution of 100,000. We present the extensive analysis of the observation campaign we led in September 2009.

2. Results

In this presentation, we present the first complete Doppler snapshot of a planet in the visible domain: the map obtained on September 14th, 2009 is the result of integrating eight hours of data, which represents about 10 % of the rotation period at the cloud-top altitude (Fig. 1). Despite poor atmospheric seeing conditions ($\approx$ 3 arcsec), we unambiguously detect a clear retrograde rotation and meridional component.

From a technical point of view, this paper makes use of an innovative and sophisticated method to measure and analyze the radial velocities of planetary atmosphere (Gaulme et al. 2018), which is has also been applied to Jupiter (see abstract by Gonçalves et al.). It involves the consideration of biases caused by atmospheric seeing on radial velocities, as well as the development of a dedicated MCMC routine to model the data.

The first main result confirms what was expected from both cloud-tracking and recent spectroscopic observations: solid body rotation alone is not sufficient to model observations, and equator-to-pole meridional circulation is needed. However, we find amplitudes of zonal and meridional winds to be larger that previously measured. It is hard to compare the zonal wind values because we identify a strong longitudinal and latitudinal variation, however, no observations have indicated winds as large as 200 m s^{-1} at the morning terminator, so far. As regards meridional winds, we find an amplitude about twice larger than expected (about 45 instead of 20 m s^{-1} at mid latitudes).

The second main result is a "hot-spot" structure of the atmospheric circulation (see Fig. 2) of the zonal component, which had never been suggested that clearly so far. Cloud tracking measurements and Doppler spectroscopic measurements indicated possible longitudinal variations of the wind as function of local time, with faster circulation towards the terminator (e.g., Khatuntsev et al. 2013). However, no such *hot-spot* pattern had been identified. We conclude the presentation on observational prospects with the new instrument project JOVIAL/JIVE, specially designed for measuring atmospheric dynamics of planets with radial velocities in the visible (Gonçalves et al. 2016).

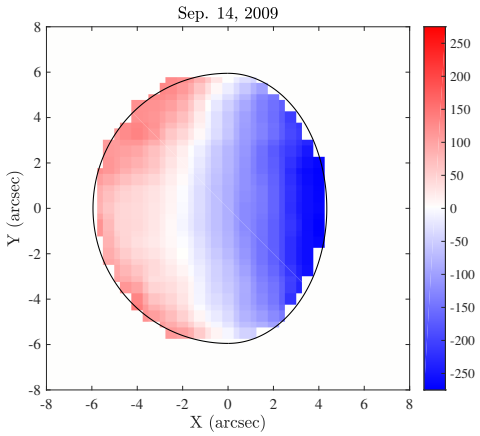

Figure 1: Radial velocity map obtained with the MTR/THEMIS long-slit spectrometer.

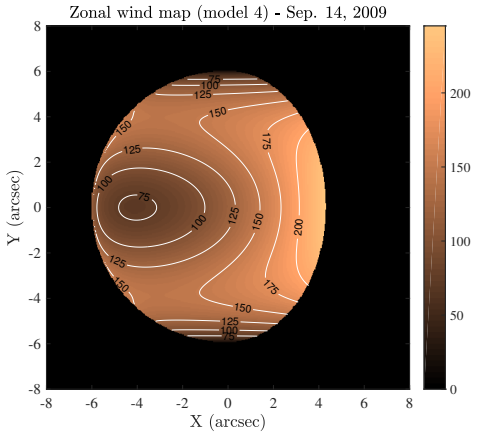

Figure 2: Map of zonal winds corresponding to the best-fit model of the data displayed in Fig. 1.

References

Gaulme, P., Schmider, F.-X., & Goncalves, I. 2018, ArXiv e-prints [[arXiv]1804.09445]

Gierasch, P. J., Goody, R. M., Young, R. E., et al. 1997, in Venus II: Geology, Geophysics, Atmosphere, and Solar Wind Environment, ed. S. W. Bougher, D. M. Hunten, & R. J. Phillips, 459

Gonçalves, I., Schmider, F.-X., Bresson, Y., et al. 2016, in Proc. of the SPIE, Vol. 9908, Ground-based and Airborne Instrumentation for Astronomy VI, 99083M

Khatuntsev, I. V., Patsaeva, M. V., Titov, D. V., et al. 2013, Icarus, 226, 140

Lellouch, E., Clancy, T., Crisp, D., et al. 1997, in Venus II: Geology, Geophysics, Atmosphere, and Solar Wind Environment, ed. S. W. Bougher, D. M. Hunten, & R. J. Phillips, 295

Lellouch, E. & Witasse, O. 2008, PSS, 56, 1317

Machado, P., Widemann, T., Peralta, J., et al. 2017, Icarus, 285, 8

Moullet, A., Lellouch, E., Moreno, R., Gurwell, M., & Sagawa, H. 2012, A&A, 546, A102

Sánchez-Lavega, A., Hueso, R., Piccioni, G., et al. 2008, GRL, 35, 13204

Sornig, M., Livengood, T. A., Sonnabend, G., Stupar, D., & Kroetz, P. 2012, Icarus, 217, 863

EPSC Abstracts
Vol. 12, EPSC2018-334, 2018
European Planetary Science Congress 2018

CO_2 variations in the Martian lower thermosphere from IUVS-MAVEN airglow observations.

L. Gkouvelis (1), J.-C. Gérard (1), B. Ritter (1), B. Hubert (1), S. Jain (2) and N.M Schneider (2)
(1) LPAP, Université de Liège, Belgium, (2) LASP, University of Colorado, Boulder, USA (l.gkouvelis@uliege.be)

Abstract

IUVS-MAVEN limb observations have been performed since 2014. We have analyzed almost four years of observations focusing on the O(^{1}S) 297.2 nm dayglow emission line. We have developed an automatic methodology to retrieve the CO_2 column densities near 80 km, a region difficult to probe by other techniques. We present nearly two Martian years of observations of pressure variations at different latitudes and comparisons with MCD model predictions. Generally, the best agreement is reached following scaling down of the MCD values from 0.3 to 0.8 to fit the observations. This result was previously expected on the basis of model comparisons with ultraviolet occultation measurements.

1. Introduction

The production of the O(^{1}S) atoms in the Martian dayglow was first modelled by Fox and Dalgarno (1979). They predicted a first peak around 130 km and the presence of a second, brighter maximum near 90 km resulting from dissociation of CO_2 by solar Lyman-α radiation. They explained the presence of the lower peak by the deeper penetration of this radiation into the Martian lower thermosphere. This is a consequence of the low value of the CO_2 absorption cross section at 121.6 nm, which is coupled with the high intensity of the solar Lyman-α flux reaching the planet. The lower peak was first observed by IUVS (Jain et al. 2015). It was later shown (Gérard et al., ESLAB 2018 Symposium) that the observations are fully compatible with photodissociation of CO_2 as the major source of O(^{1}S) atoms. These conditions make the lower peak a sensitive indicator of the CO_2 column density. In this work we quantify the changes of the lower peak characteristics from the set of MAVEN observations. This method makes it possible to extract the seasonal and latitude variations at the altitude level of the lower peak.

2. IUVS observations

The data used in this study have been downloaded from NASA's Planetary Data System (PDS) archives. Three different processing levels of the data are available. Level 1A data corresponds to the raw instrument readouts in data numbers per bin. Level 1B data provide calibrated instrument readouts in kR/nm and include background subtraction and ancillary data. Level 1C data includes calibrated brightness of individual emissions that has been reduced by isolating emission features and spatial binning to facilitate processing: The dayglow spectra include many different atomic and molecular emissions, including the spectral feature from oxygen at 297.2 nm. Each emission may be identified by its wavelength and its expected relative

intensity. The brightness of any atomic or molecular feature is determined by using a multiple linear regression method to fit the various components of each observed spectrum following convolution with the instrumental line spread function.

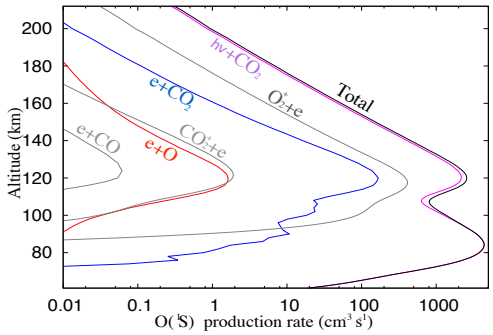

Figure 1: Production rate of $O(^1S)$ state. It is clearly seen that CO_2 photodissociation is the main excitation process below 200 km and the only one for the lower emission peak.

3. Methodology

Comparisons with our model calculations confirm that photodissociation of CO_2 is the major source of $O(^1S)$ atoms below 200 km and the largely dominant excitation process of the lower emission peak. Simulations have also indicated that the upper emission peak does not significantly influence the altitude and the intensity of the lower peak for observations of the limb profiles. A direct consequence is that the altitude of the lower peak of 297.2 nm dayglow is solely controlled by the overlying column density of CO_2, while the maximum brightness essentially depends on the flux of solar Lyman-α.This flux is directly measured on board MAVEN by the EUVM instrument.

Since the altitude of the lower peak directly depends on the overlying column of CO_2, its value may be used as an indicator of the seasonal/latitudinal variations of the thermospheric CO_2 distribution and therefore of the changes of altitude of the $\tau=1$ level. These altitude changes correspond to variations of the height of the isobars that are controlled by the seasonal and latitudinal pressure variations and the dust load in the lower atmosphere.

Acknowledgements. This research is supported by the PRODEX program of ESA, managed with the help of the Belgian Science Policy Office (BELSPO).

References

[1] Fox, J. L., & Dalgarno, A. (1979). Ionization, luminosity, and heating of the upper atmosphere of Mars. J. Geophys. Res., 84(A12), 7315-7333

[2] Jain, S. K., et al. (2015), The structure and variability of Mars upper atmosphere as seen in MAVEN/IUVS dayglow observations, Geophys. Res. Lett., 42, doi: 10.1002/2015GL065419.

EPSC Abstracts
Vol. 12, EPSC2018-379, 2018
European Planetary Science Congress 2018

Akatsuki and TNG/HARPS-N coordinated wind measurements of cloud top Venus' atmosphere

Ruben Gonçalves (1), Pedro Machado (1) Thomas Widemann (2), Javier Peralta (3), Shigeto Watanabe (4), Atsushi Yamazaki (3), Takehiko Satoh (3), Masahiro Takagi (5), Kazunori Ogohara (6), Yeon Joo Lee (3), Harutyunyan Avet (7), José Silva (1)
(1) Institute of Astrophysics and Space Sciences, Observatório Astronómico de Lisboa, Lisbon, Portugal
(2) LESIA - UMR CNRS 8019 - Laboratoire d'Études Spatiales et d'Instrumentation en Astrophysique, Observatoire de Paris, CNRS, UPMC, Université Paris-Diderot, Meudon, France
(3) Institute of Space and Astronautical Science, Japan Aerospace Exploration Agency (ISAS/JAXA), Japan
(4) Hokkaido Information University, Japan
(5) Faculty of Science, Kyoto Sangyo University, Kyoto, Japan
(6) School of Engineering, University of Shiga Prefecture, Japan
(7) Telescopio Nazionale Galileo (TNG) and Italian Instituto Nazionale di Astrofisica (INAF), Italia
(rgoncalves@oal.ul.pt)

Abstract

We present wind velocity results based in the measurements of the horizontal wind field at the cloud top level of the atmosphere of Venus, near 70 km altitude, in the visible range on the dayside. The cloud-tracking space observations were carried out, between 26-31 January 2017, by the "Ultra Violet Imager" (UVI) onboard Akatsuki's Venus Climate Orbiter (VCO), using the 365 nm filter, which tracks UV cloud features at about 68-71 km [1]. The cloud-tracking technique we used was evolved from a phase correlation method between images developed by Peralta et al. 2007 [2]. The use of UVI images to track cloud features from the unknown UV absorber has already provided important results in the constrain of zonal and meridional wind at cloud-top [3]. Venus Climate Orbiter "Akatsuki" is currently the only spacecraft operating around Venus. Due to its low inclination orbit (<10º), Akatsuki's images offer a great range in Venus' dayside, allowing us to track cloud features from 60º N to 70º S latitude and from 7:30 to 17:00 local time - this has enable a study of spatial and time variability of the wind. The ground observations probed the cloud top layer (70km altitude) using the Doppler velocimetry technique, enabling a cross-validation with Akatsuki cloud-tracking technique.

The ground observations were carried out, on the 28th and 29th of January 2017, at the 3.58-meter "Telescopio Nazionale Galileo" (TNG) using the "High Accuracy Radial velocity Planet Searcher" spectrograph (HARPS-N) in the visible range (0.38-6.9 µm). It was the first use of this high-resolution (R ≈115000) spectrograph to study the dynamics of a solar system atmosphere. The sequential technique of visible Doppler velocimetry is based on solar light scattered by cloud top particles in motion. This technique was developed over the last decade ([4], [5], [6]) and has proven to be a reference technique in the retrieval of instantaneous zonal and meridional winds [7]. In this work we successfully adapt this technique to the HARPS-N fiber-fed spectrograph with consistent results.

1. Introduction

Venus is covered by thick clouds, separated into three main decks: the lower (44-50 km), the middle (50-55 km), and the upper cloud deck (55-70 km). The cloud tops are located at altitudes of 67-71 km at the equator with a nearly constant altitude until 45-50º and a drop of altitude poleward of 50º, reaching about 61-63 km over both poles [1]. At UV wavelenghts, cloud features are originated by an yet unknown UV absorber which yields the highest contrasts on the cloud top. The wind flow on Venus within the cloud and haze layers is dominated by a zonal wind in the retrograde sense (East to West), that peaks at the top of the upper layer with equatorial zonal speeds higher than 100 ms^{-1} ([3] [6] [7]). The retrograde zonal superotation (RZS) is accompanied by a Hadley-type poleward meridional circulation which transports angular momentum from the equator to the poles. The retrograde zonal winds at the cloud tops circles the planet in 4.4 days, about 60 times faster than the solid globe (243 days), thus, the atmosphere is said to super rotate the planet. Both the source and maintenance of a superrotating atmosphere in a slow rotating planet constitute a long-standing problem in planetary atmospheric dynamics.

2. Figures

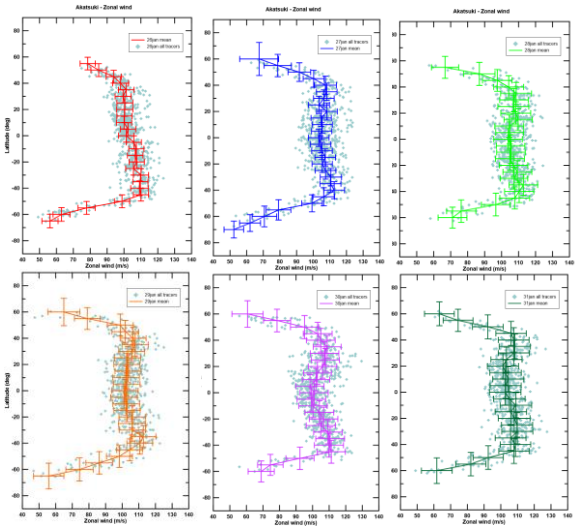

Figure 1: Daily zonal wind latitudinal profiles of Akatsuki/UVI results, for each day (26-31 January), weighted average with a binning of 5º latitude. Cloud tracers are represented as grey diamonds, while the colored solid line is the mean wind latitude and its respective error bars.

3. Summary and Conclusions

Due to the high-quality UVI images, it was possible to study wind spatial variability, with high consistency when compared with previous cloud top wind measurements from space observations.

HARPS-N high-quality spectra raised the level of precision and completeness of wind profile retrieved from cloud-top, demonstrating the high consistency and reliability of the Doppler velocimetry technique, using different telescopes, different instruments at different time frames.

The retrieval of Venus' cloud top wind from different observations, (both space and ground based) and different techniques (cloud-tracking and doppler velocimetry), is essential to (1) cross-validate different observations and techniques; (2) retrieve complimentary results (different geometry of observations, instantaneous/averaged velocities); (3) constrain coud-top dynamics and superrotational mechanisms.

Acknowledgements

We thank the Akatsuki team for support with coordinated observations. We gratefully acknowledge the collaboration of the TNG staff at La Palma (Canary Islands, Spain). We acknowledge support from Fundação para a Ciência e a Tecnologia, (fellowship ref. PD/BD/128019/2016) through national funds.

References

[1] Ignatiev, N.I. et al.: Altimetry of the Venus cloud tops from the Venus Express observations; Journal of Geophysical Research, vol. 114, E00B43, doi:10.1029/2008JE003320, 2009.

[2] Peralta J., Hueso R., Sánchez-Lavega A.: Cloud brightness distribution and turbulence in Venus using Galileo violet images; Icarus, vol. 188, p. 305-314, 2007

[3] Horinouchi T., Kouyama T., Lee Y.J., Murakami S., Ogohara K., Takagi M., Imamura T., Nakajima K., Peralta J., Yamazaki A.: Mean winds at the cloud top of Venus obtained from two-wavelength UV imaging by Akatsuki; Earth, Planets and Space, 70:10, 2018.

[4] Widemann T., Lellouch E., Donati J.F.: Venus Doppler winds at cloud tops observed with ESPaDOnS at CFHT; Planetary and Space Science, vol. 56, p. 1320-1334, 2008.

[5] Machado P., Luz D., Widemann T., Lellouch E., Witasse O.: Characterizing the atmospheric dynamics of Venus from ground-based Doppler velocimetry; Icarus, vol. 221, p. 248-261, 2012

[6] Machado P., Widemann T., Luz D., Peralta J.: Wind circulation regimes at Venus' cloud tops: Ground-based Doppler velocimetry using CFHT/ESPaDOnS and comparison with simultaneous cloud tracking measurements using VEx/VIRTIS in February 2011; Icarus, vol. 243, p. 249-263, 2014.

[7] Machado P., Widemann T., Peralta J., Gonçalves R., Donati J., Luz D.: Venus cloud-tracked and doppler velocimetry winds from CFHT/ESPaDOnS and Venus Express/VIRTIS in April 2014; Icarus, vol. 285, p. 8-26, 2017.

EPSC Abstracts
Vol. 12, EPSC2018-434, 2018
European Planetary Science Congress 2018

Impact of gradients at the Martian terminator on the retrieval of ozone from SPICAM/MEx

A. Piccialli (1), A.C. Vandaele (1), L. Trompet (1), L. Neary (1), S. Viscardy (1), F. Daerden (1), S. Robert (1), S. Aoki (1,2,3), Y. Willame (1), V. Wilquet (1), F. Lefèvre (4), A. Määttänen (4), and F. Montmessin (4)
(1) Planetary Aeronomy, Royal Belgian Institute for Space Aeronomy, 3 av. Circulaire, 1180 Brussels, Belgium; (2) Fonds National de la Recherche Scientifique, Brussels, Belgium, (3) Tohoku University, Japan, (4) LATMOS/IPSL, UVSQ Université Paris-Saclay, UPMC Univ. Paris 06, CNRS, Guyancourt, France.
(Email: arianna.piccialli@aeronomie.be, Twitter: @apic79)

1. Introduction

Rapid variations in species concentration at the terminator have the potential to cause asymmetries in the species distributions along the line of sight (LOS) of a solar occultation experiment. Ozone, in particular, displays steep gradients across the terminator of Mars due to photolysis [1]. Nowadays, most of the retrieval algorithms for solar and stellar occultations rely on the assumption of a spherically symmetrical atmosphere. However, photochemically induced variations near sunrise/sunset conditions need to be taken into account in the retrieval process in order to prevent inaccuracies.

Here, we investigated the impact of gradients along the LOS of the solar occultation experiment SPICAM for the retrieval of ozone under sunrise/sunset conditions. We used the diurnal variations in the ozone concentration obtained from photochemical model calculations together with an adapted radiative transfer code.

2. SPICAM solar occultations

SPICAM (SPectroscopie pour l'Investigation des Caractéristiques Atmosphériques de Mars), on board the ESA's spacecraft Mars Express, is a remote sensing spectrometer observing in the ultraviolet (118–320 nm) and in the near infrared (1–17 μm) [2]. In the solar occultation mode, the UV sensor is particularly well suited to measure the vertical profiles of O_3 and aerosols of the Martian atmosphere [3]. Figure 1 displays transmission spectra obtained at different altitudes for the observation 00633A02.

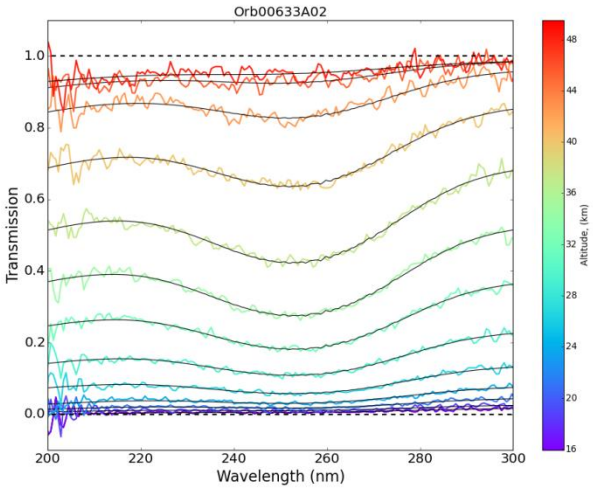

Figure 1: Example of SPICAM transmission spectra at different altitudes: (blue) low altitudes; (red) high altitudes.

We followed the same method described in [4] to check that the spectra are correctly calibrated and accurately normalized to the solar spectrum.

3. Retrieval technique

SPICAM-UV spectra are simulated using the line-by-line radiative transfer code ASIMUT-ALVL developed at IASB-BIRA [5]. ASIMUT has been modified in order to take into account the atmospheric composition and structure at the day-night terminator. Three different gradients along the LOS can be considered: temperature, total density gradients and the variations of the concentration of specific species. As input for ASIMUT, we used gradients predicted by the 3D GEM-Mars v4 Global Circulation Model (GCM) [6,7]. Figure 2 shows the diurnal cycle of ozone derived by GEM-Mars. Ozone

is more abundant during the night time, especially above 40-50 km. As the Sun rises, the destruction of O_3, although stronger in the high atmosphere, is observed at all altitudes.

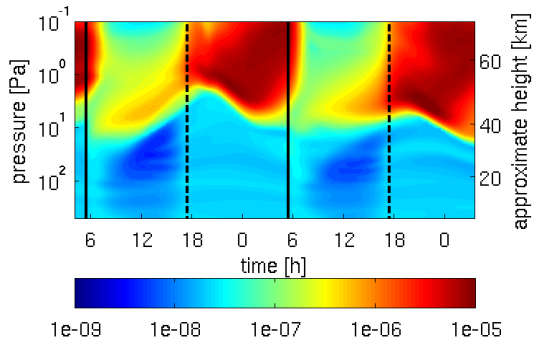

Figure 2: Diurnal cycle of ozone predicted by the 3D GEM-Mars v4 GCM.

4. Preliminary results

As preliminary study, we selected four occultations at sunrise and at sunset each. As first step, we retrieved O_3 profiles without taking in account gradients and we obtained results in agreement with previous studies. Then, we investigated the effects of ozone density gradients on the retrieval of ozone. The retrieved ozone profiles are lower compared to retrievals without gradients, even if differences are within the error bars. These effects will be analysed in more detail.

5. Future work

We will extend our analysis to the whole SPICAM-UV solar occultation dataset. The main objective is to investigate fully the impact of these gradients on ozone retrievals. We will compare our retrievals with those from a similar study carried out at LATMOS within the UPWARDS project. Results of this study will then be used for the analysis of the data expected from the NOMAD instrument on the ExoMars 2016 Trace Gas Orbiter.

Acknowledgements

The research leading to these results has received funding from the European Union's Horizon 2020 Programme (H2020-Compet-08-2014) under grant agreement UPWARDS-633127. SA has been supported by the FNRS "CRAMIC" project under grant agreement n° T.0171.16.

References

[1] Lefèvre, F., Bertaux, J.L., Clancy, R. T., Encrenaz, T., Fast, K., Forget, F., Lebonnois, S., Montmessin, F., Perrier, S., Aug. 2008. Heterogeneous chemistry in the atmosphere of Mars. Nature 454, 971–975.

[2] Bertaux, J., Korablev, O., Perrier, S., Quémerais, E., Montmessin, F., Leblanc, F., Lebonnois, S., Rannou, P., Lefévre, F., Forget, F., Fedorova, A., Dimarellis, E., Reberac, A., Fonteyn, D., Chaufray, J. Y., Guibert, S., 2006 SPICAM on Mars Express: Observing modes and overview of UV spectrometer data and scientific results. JGR (Planets) 111 (E10).

[3] Määttänen, A., Listowski, C., Montmessin, F., Maltagliati, L., Reberac, A., Joly, L., Bertaux, J.L., Apr. 2013. A complete climatology of the aerosol vertical distribution on Mars from MEx/SPICAM UV solar occultations. Icarus 223, 892–941.

[4] Trompet, L., Mahieux, A., Ristic, B., Robert, S., Wilquet, V., Thomas, I.R., Vandaele , A.C., Bertaux, J.L., 2016. Improved algorithm for the transmittance estimation of spectra obtained with SOIR/Venus Express. Applied Optics 55, 9275-9281.

[5] Vandaele, A.C., M. De Mazière, R. Drummond, A. Mahieux, E. Neefs, V. Wilquet, O. Korablev, A. Fedorova, D. Belyaev, F. Montmessin, and J.L. Bertaux, Composition of the Venus mesosphere measured by SOIR on board Venus Express. JGR, 2008. 113 doi:10.1029/2008JE003140.

[6] Daerden, F.; Whiteway, J. A.; Neary, L.; Komguem, L.; Lemmon, M. T.; Heavens, N. G.; Cantor, B. A.; Hébrard, E.; Smith, M. D. A solar escalator on Mars: Self-lifting of dust layers by radiative heating. GRL, 2015, 42, 18, 7319-7326.

[7] Neary, L., and F. Daerden (2018), The GEM-Mars general circulation model for Mars: Description and evaluation, Icarus 300, 458–476, doi:10.1016/j.icarus.2017.09.028

EPSC Abstracts
Vol. 12, EPSC2018-460, 2018
European Planetary Science Congress 2018

Simulation of CO and H_2O_2 on Mars

Frank Daerden (1), Lori Neary (1), Sébastien Viscardy (1), Antonio García Muñoz (2), R. Todd Clancy (3), Michael D. Smith (4) and Thérèse Encrenaz (5)
(1) Royal Belgian Institute for Space Aeronomy BIRA-IASB, Brussels, Belgium, (2) Zentrum für Astronomie und Astrophysik, Technische Universität Berlin, Berlin, Germany, (3) Space Science Institute, Boulder, Colorado, USA, (4) NASA Goddard Space Flight Center, Greenbelt, Maryland, USA, (5) LESIA, Observatoire de Paris, CNRS, UPMC, UPD, Meudon, France (Frank.Daerden@aeronomie.be)

Abstract

We present new results of the GEM-Mars General Circulation Model with interactive atmospheric chemistry [1]. The simulation of the vertically integrated column of carbon monoxide (CO) is compared to the most complete dataset to date, obtained from CRISM [2]. The general trends in the data are reproduced by the model while differences expose possible issues with atmospheric mixing in the model. The simulation of the vertically integrated column of hydrogen peroxide (H_2O_2) is compared to the complete set of available data [3] and provides an exceptionally good result, which illustrates that the water cycle and the Mars photochemistry are well implemented in the model. The abstract is accompanied by one that presents results for ozone (O_3) and oxygen dayglow ($O_2(a^1\Delta_g)$) (Neary et al., this session), and another one on the simulation of semiheavy water (HDO) (Daerden et al., ExoMars session).

1. Introduction

The atmospheric chemistry on Mars is dominated by CO_2 and H_2O and their photolysis products. The interaction between these products has been understood to be crucial in the stabilization of the Martian atmosphere [e.g. 4]. In this photochemical cycle, only a few species have been observed, and only for some of those, the spatiotemporal coverage is dense enough to confine seasonal trends: CO [e.g. 2], H_2O_2 [e.g. 3], O_3 [e.g. 5], and $O_2(a^1\Delta_g)$ airglow (e.g. [6]). These datasets provide important constraints for global model simulations of atmospheric chemistry.

2. Simulations

For the simulation of gas enrichment upon condensation of CO_2, a parameterization was developed that calculates the local enrichment factor from the amount of CO_2 ice condensing/evaporating. This led to a simulation of the polar argon enhancement that was in agreement with other models [1, 2]. The resulting seasonal trend of the vertically integrated abundance of CO was compared to the latest dataset retrieved from CRISM observations, comprising 5 Mars years of data [2]. The most important features are reproduced although some model-data differences remain, providing insight in the accuracy of model parameterizations.

The GEM-Mars chemistry was updated from previous versions, e.g. by including improved cross-sections for CO_2 and H_2O, especially in the 190 nm region, and by improving the calculation of photolysis rates taking into account the true direction of the sun. This led to a much improved simulation of H_2O_2, that is now consistent with all observational data (except for a few outliers).

Acknowledgements

Part of the research was performed as part of the “Excellence of Science” project “Evolution and Tracers of Habitability on Mars and the Earth” (FNRS 30442502).

References

[1] Neary, L., and F. Daerden (2018), Icarus, 300, 458–476, https://doi.org/10.1016/j.icarus.2017.09.028
[2] Smith, M., F. Daerden, L. Neary and S. Khayat (2018), Icarus, 301, 117–131, https://doi.org/10.1016/j.icarus.2017.09.027
[3] Encrenaz, T., et al. (2015), Astron. Astrophys. 578, A127, doi:10.1051/0004-6361/201425448.
[4] Lefèvre, F., et al. (2004), J. Geophys. Res., 109, E07004, doi:10.1029/2004JE002268.
[5] Clancy, R. T., et al. (2016), Icarus, 266, 112–133. doi:10.1016/j.icarus.2015.11.016
[6] Guslyakova, S., et al. (2016), Planet. Space Sci. 122, 1–12. doi: 10.1016/j.pss.2015.12.006.

EPSC Abstracts
Vol. 12, EPSC2018-477, 2018
European Planetary Science Congress 2018

Impact of gravity waves on the middle atmosphere of Mars studied combining Global Climate modelling and Mars Climate Sounder observations

G. Gilli (1,2), F. Forget (2), A. Spiga (2), T. Navarro (3), L. Montabone (3,2)
(1) Instituto de Astrofisica e Ciências do Espaço (IA), Lisbon, Portugal, (2) Laboratoire de Météorologie Dynamique (LMD), Paris, France, (3) Department of Earth, Planetary, and Space Sciences, University of California, Los Angeles, USA (3) Space Science Institute (SSI), Boulder, CO, USA. (ggilli@oal.ul.pt)

Abstract

We implemented a stochastic parameterization of non-orographic gravity waves (GW) into the Laboratoire de Météorologie Dynamique (LMD) Mars General Circulation Model (LMD-MGCM), following an innovative approach as described in [1]. The source is assumed to be located above typical convective cells ($\approx$ 250 Pa) and the impact of GW on the circulation and the predicted thermal structure above 50 km is analyzed. We focus on the comparison between model simulations and observations by the Mars Climate Sounder (MCS) on board Mars Reconnaissance Orbiter [2] during Martian Year (MY) 29. The inclusion of the parametrized gravity waves significantly improve the accuracy of the LMD-MGCM in comparison with the observations, thus providing a plausible explanation to the systematic biases previously identified between 1 and 0.01 Pa (around 50-80 km), locally reaching 10 to 20 K. The corresponding changes in mean zonal wind velocity reach 100 m/s in proximity of the equatorial easterly jet.

1. Introduction

Gravity waves (GWs) are frequently detected in terrestrial planet atmospheres and they are supposed to play a dominant role in their large-scale circulation and variability. Small scale variability, in the form of perturbations of density and temperature have systematically been observed in the upper atmosphere of Mars whenever in situ data have been obtained [3, 5, 4] and attributed to GWs. In particular, non-orographic (i.e non-zero phase velocity) GW are supposed to be emitted above the convective layer and propagate upwards, providing a significant source of momentum and energy, thus affecting the transport of heat and constituents. The role of mesoscale GW is also supposed to be crucial for local CO_2 condensation, responsible of the formation of mesospheric CO_2 clouds observed by Mars Express between 60 and 80 km altitude [6]. Thermal effects of gravity waves has been proposed to explain some of the puzzling model-observation discrepancy identified in the Martian atmosphere temperatures between 100 and 140 km [7]

c [m/s]	k_h [km]	F^0 kg m^{-1} s^{-2}	S_c
[1 - 30]	[10 - 300]	[0 - 10^{-4}]	1

Table 1: Baseline wave characteristics in the GW scheme implemented in this work: c the absolute phase speed, k_h the horizontal wavelength amplitude, F^0 the vertical momentum (EP-flux) at the source ($\approx$ 8 km), S_c the saturation parameter. Values in the bracket indicate the extremes of the probability distribution used in the "best-case" simulations.

2. This work

One of the main goals of this study is to understand the role of non-orographic GW on the global circulation and the thermal structure of the Martian middle atmosphere (50-100 km altitude). What is the magnitude of GW-induced drag on the winds? Can GW explain the remaining discrepancy between the MCS observations and the GCM simulations? If so, what is their impact on the predicted winds? With these purposes in mind we use the LMD-MGCM, a finite-difference model based on the discretization of the horizontal domain fields on a latitude-longitude grid [8], being 64 longitude x 48 latitudes (3.75° x 5.62°) the horizontal resolution used in this work. We have employed the latest version of the model which includes several recent improvements [9] in addition to the implementation of a non-orographic GW parameterization follow-

ing the formalism developed for the Earth GCM fully described in [1]. We focus here on the comparison between model simulations and observations by the Mars Climate Sounder (MCS) on board MRO [2] during the MY29. MCS represents the best existing systematic measurements of the Martian mesosphere up to 80 km. Discrepancies between data and model, notably the incorrect representation of thermal tide wave in the vertical, such as those found with the MCS observations [9, 10], indicated that some key process(es) are missing in our model.

2.1 Non-orographic GW parameterization

The GW scheme is based on a stochastic approach, in which a finite number M of waves with characteristics chosen randomly, but within a fixed probability distribution, are launched upwards at each time-step from a few random location to simulate they global effect. We assumed that the GW source is placed above typical convective cells (i.e around 8 km, depending on the topography). This allows to treat a large number of waves at a given time t by adding the effect of those M waves to that of the waves launched at previous steps, to compute the tendencies. A range of plausible values, and for different representations of the mean flow thermal forcing, have been considered (Gilli et al. 2018, in preparation).

3. Impact of GW mean flow forcing parameters

The main tunable GW parameters used in our scheme are listed in Table 1. The GW induced drag drives changes of the wind (e.g. deceleration/acceleration of jet streams) and consequently produces thermal structure variations via adiabatic heating/cooling rates associated with the altered circulation. An example of sensitivity tests, performed to evaluate the impact of GW mean flow forcing to thermal tides is shown in Figure 1. Those tests also help to select the baseline parameters by MCS-MGCM comparison. As shown in the Figure: 1) the maximum day-night difference value in Panel C ("best-case") is around 20 K, comparable with observed values, and more interestingly 2) the peak altitude of the tides is shifted down, and 3) its amplitude is also more realistic (between 22°S and 22°N latitudes, as observed) The impact of induced GW drag on the jet streams for all martian seasons will be also shown and discussed.

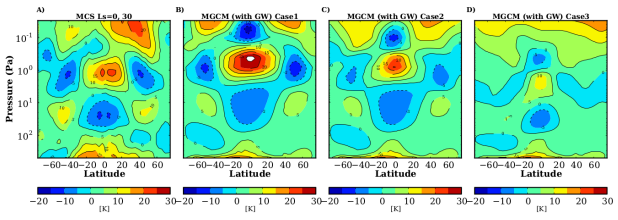

Figure 1: Example of observed and simulated day-night temperature differences (in K), between dayside (15 LT) and nightside (3 LT), during L_s= 0°-30°N. Panel A: MCS measurements. Panels B, C and D: selection of model simulations. Panels C represents the "best-case" run (Table 1). Panels B and D show two tests, where the upper value of the probability distribution for the EP-flux at the source is reduced and increased by one order of magnitude, respectively.

Acknowledgements

GG was supported by FCT (Portugal) through national funds and from FEDER through COMPETE2020 by grants UID/FIS/04434/2013, POCI-01-0145-FEDER-007672, PTDC/FIS-AST/1526/2014 and POCI-01-0145-FEDER-016886

References

[1] Lott, F., and L. Guez (2013), , J. Geophys. Res. (Atmospheres), *118*, 8897–8909.

[2] McCleese et al. 2010, J. Geophys. Res. (Planets), *115*(E14), E12016

[3] Fritts et al. 2006, J. of Geophys.l Res. (Space Physics), *111*, A12304,

[4] Terada et al. 2017, J. of Geophys. Res. (Space Physics), *122*, 2374–2397

[5] Yiğit et al. 2015, Geophys. Res. Letter, *42*, 8993–9000

[6] Spiga et al. 2012, Geophy. Res. Letters, *39*, L02201

[7] Medvedev et al. 2015, J. Geophys. Res. (Planets), *120*, 913–927,

[8] Forget et al. 1999, J. Geophys. Res., *104*, 24,155–24,176.

[9] Forget et al. 2017, in *The Mars Atmosphere: Modelling and observation*, edited by F. Forget and M. Millour, p. 1113.

[10] Navarro et al. 2017, *Earth and Space Science*, *4*(12), 690–722,

EPSC Abstracts
Vol. 12, EPSC2018-480, 2018
European Planetary Science Congress 2018

Simulation of Ozone and Oxygen Airglow on Mars

Lori Neary (1), Frank Daerden (1), Sébastien Viscardy (1), Antonio García-Muñoz (2), R. Todd Clancy (3), Michael D. Smith (4) and Anna Fedorova (5)
(1) Royal Belgian Institute for Space Aeronomy BIRA-IASB, Brussels, Belgium, (2) Zentrum für Astronomie und Astrophysik, Technische Universität Berlin, Berlin, Germany, (3) Space Science Institute, Boulder, Colorado, USA, (4) NASA Goddard Space Flight Center, Greenbelt, Maryland, USA, (5) Space Research Institute RAS, Moscow, Russia (Lori.Neary@aeronomie.be)

Abstract

We present new results of the GEM-Mars General Circulation Model with interactive atmospheric chemistry [1], comparing the simulation of the vertically integrated column of ozone (O_3) to observations from the MARs Color Imager (MARCI) [2] on Mars Reconnaissance Orbiter (MRO). We also compare the vertically integrated oxygen dayglow emission ($O_2(a^1\Delta_g)$) at 1.27 µm with measurements taken with the Mars Express SPICAM instrument [3]. The seasonal cycles of total column O_3 and dayglow emission are generally reproduced except for a few differences, highlighting possible processes that are not well represented in the model.

This abstract complements that of Daerden et al. (this session) where results for carbon monoxide and hydrogen peroxide are presented. Also related, we refer to the abstract on the use of the GEM-Mars ozone gradients at the terminator in the retrieval of ozone from SPICAM (Piccialli et al., this session).

1. Introduction

Ozone in the Mars atmosphere is closely related to the abundance of water vapour as one of its main destruction mechanisms is through reactions with the products of H_2O photo-dissociation (H, OH, HO_2 = HO_x). One of the main features of the seasonal cycle of O_3 is the enhancement in the polar winter regions where there is a lack of photolysis and of HO_x species.

Closely related to ozone is the 1.27 µm $O_2(a^1\Delta_g)$ dayglow emission. $O_2(a^1\Delta_g)$ is produced by the photolysis of ozone as well as the three-body reaction of $2O(^3P)$ and CO_2. It can then be quenched by CO_2 or produce an emission at 1.27 µm.

Observations of these two quantities provide important constraints for the global model simulations of atmospheric chemistry.

2. Simulations

Several modifications have been implemented relating to GEM-Mars chemistry, including an update to the cross-sections for CO_2 and H_2O around 190 nm. In addition, the on-line calculation of photolysis rates has been improved to take into account the true line-of-sight of the sun.

Based on the suggestion by [2], the rate for the quenching reaction for $O_2(a^1\Delta_g)$ has been reduced to a value of 0.25×10^{-20} $cm^3 s^{-1}$ from that given in [4].

Acknowledgements

Part of the research was performed as part of the "Excellence of Science" project "Evolution and Tracers of Habitability on Mars and the Earth" (FNRS 30442502). This project also acknowledges funding by the Belgian Science Policy Office (BELSPO), with the financial and contractual coordination by the ESA Prodex Office (PEA 4000103401, 4000121493).

References

[1] Neary L. and F. Daerden (2018), Icarus, 300, 458-476, doi:10.1016/j.icarus.2017.09.28.

[2] Clancy, R. T., et al. (2016), Icarus, 266, 112-133, doi:10.1016/j.icarus.2015.11.016.

[3] Guslyakova, S., et al., (2016), Planet. Space Sci., 122, 1-12, doi:10.1016/j.pss.2015.12.006.

[4] García-Muñoz, A., et al., (2005), Icarus, 176, 75-95, doi:10.1016/j.icarus.2005.01.006.

EPSC Abstracts
Vol. 12, EPSC2018-496, 2018
European Planetary Science Congress 2018

Temperature variability in the Martian thermosphere

Francisco González-Galindo (1), M.A. López-Valverde (1), M. García-Comas (1), F. Forget (2), and E. Millour (2)
(1) Instituto de Astrofísica de Andalucía-CSIC, Granada, Spain (2) Laboratoire de Météorologie Dynamique, IPSL/CNRS, Paris, France (ggalindo@iaa.es)

Abstract

We use a ground-to-exosphere Mars Global Climate Model to characterize the variability of the temperatures in the upper atmosphere of Mars at different temporal and geographical scales. A strong solar cycle variability is found in the upper thermosphere, but dependent on the latitude and season. Non-migrating tides induce a significant longitudinal variability.

1 Introduction

The Martian thermosphere-ionosphere is a very variable region strongly coupled to the lower atmosphere and to the solar activity [1]. It is also a transition region between the gravitationally bound lower atmosphere and the escaping exosphere, and the thermospheric variability has a significant effect over the atmospheric escape rate [2]. From a practical perspective, the upper atmosphere of Mars is the region where aerobraking maneuvers take place upon spacecrafts' orbit insertion. These operations are critically affected by variations in the atmospheric density. A good characterization of the temperature and density structure and of the variability of the upper atmosphere is thus mandatory both for better understanding the past evolution of Mars and for planning future space missions.

Despite the significant improvement in our knowledge of the Martian thermosphere in the last 20 years, and in particular since the arrival of MAVEN, we are still far from having a measured temperature climatology with a complete seasonal and latitudinal coverage, similar to those existing for the lower and middle atmosphere. Global Climate Models (GCMs) contribute to provide a more complete understanding on the picture, by helping in the interpretation of the existing measurements and by completing their coverage. Here we use a ground-to-exosphere GCM to study the variability of the thermosphere.

2 Model

We use in this work the ground-to-exosphere LMD-Mars GCM (LMD-MGCM) [4]. This model can simulate the temperature, dynamics and composition of the neutral and ionized Martian upper atmosphere, taking into account the observed day-to-day variability of the UV solar flux and of the dust load in the lower atmosphere. The version of the model used here does not include the effects of non-orographic gravity waves, which are known to affect the dynamical and thermal state of the mesosphere-thermosphere [5]. The simulations discussed here cover 10 complete Martian Years and almost 2 complete solar cycles. Selected model outputs are included in the latest version of the Mars Climate Database (MCD).

3 Selected results

The model predicts a linear dependence of the exobase temperatures with the solar activity (Fig. 1), but with important variations at different latitudes and seasons. The mesopause temperatures, on the other hand, present a small response to solar variability.

Regarding the LT variability, while minimum temperatures at the exobase are usually obtained before dawn, the LT of maximum temperature is not fixed but depends on season and latitude.

A significant longitudinal variability is predicted by the model, produced by non-migrating tides.

We will also show comparisons with observational datasets, as the SPICAM stellar occultation temperature profiles [3] and with new results from a recent reanalysis of Mars Express datasets in the UV and in the IR.

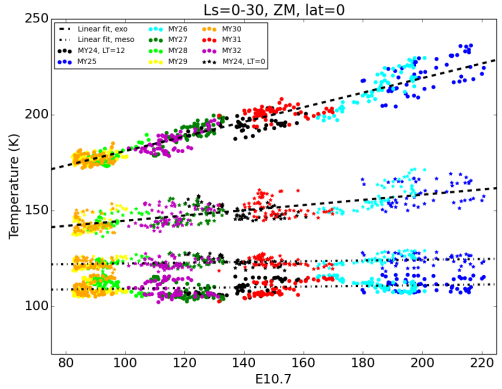

Figure 1: Solar cycle variability of the exobase (top lines) and mesopause (bottom lines) for the Ls=0-30 season and the equator. We show temperatures at LT=12 (circles) and LT=0 (stars). Different colors indicate temperatures obtained at different simulated Mars Years

Acknowledgements

This work was supported by the European Union's Horizon 2020 Programme under grant agreement UPWARDS-633127 and by the Spanish National Research Council under "intramural" project CSIC 201450E022.

References

[1] Bougher, S.W. et al.: Upper neutral atmosphere and ionosphere, in The atmosphere and climate of Mars, Cambridge Univ. Press, 2017.

[2] Chaufray, J.-Y. et al.: Variability of the hydrogen in the martian upper atmosphere as simulated by a 3D atmosphere-exosphere coupling, Icarus, Vol. 245, p. 282-294, 2015.

[3] Forget, F., et al.: Density and temperatures of the upper Martian atmosphere measured by stellar occultations with Mars Express SPICAM, J. Geophys. Res., Vol. 114, E01004, 2009.

[4] González-Galindo, F. et al.: Variability of the Martian thermosphere during eight Martian years as simulated by a ground-to-exosphere global circulation model, J. Geophys. Res., Vol. 120, pp. 2020-2035, 2015.

[5] Medvedev, A. et al.: Cooling of the Martian thermosphere by CO2 radiation and gravity waves: An intercomparison study with two general circulation models, J. Geophys. Res., Vol. 120, pp. 913-927, 2015.

EPSC Abstracts
Vol. 12, EPSC2018-564, 2018
European Planetary Science Congress 2018

Analysis of Recalibrated Phoenix Relative Humidity Sensor Data

E. Fischer, G. M. Martínez and N. O. Rennó
Department of Climate and Space Sciences and Engineering, University of Michigan, Ann Arbor, MI, USA
(erikfis@umich.edu)

1. Introduction

The Phoenix Lander mission carried the Thermal and Electrical Conductivity Probe (TECP) to investigate heat and water exchange between the surface and the atmosphere close to the Martian North Pole. One of its sensors is a capacitive relative humidity (RH) sensor, the first to measure humidity at the Martian surface [4]. Due to preflight calibration uncertainties, only unprocessed sensor output data was available in NASA's Planetary Data System (PDS) until recent efforts in improving the calibration, which corrected for low temperature inaccuracies by using three new calibration points obtained from in-flight data [5]. We have further improved the RH sensor's calibration in the entire range of temperature and RH observed on Mars, with focus on the warmest and driest conditions achieved during daytime, using a novel technique that involves testing a spare engineering unit of the TECP at Martian conditions in our environmental chamber. Here we give an overview of our methodology and results and discuss recent improvements of the recalibration and sensitivity studies.

2. Preflight Calibration

Values of TECP board temperature (T_b), frost point temperature (T_f) and resulting raw output of the RH sensor (*DNRH*) that were covered in the pre-flight calibration only partially overlap the environmental conditions at the Phoenix landing site (Fig. 1, red and gray points). This resulted in large uncertainties in the calibration of the RH values, especially around noon (when T_b is high), and dawn (when T_b is low). An updated calibration function added three additional data points at very low temperatures (<200 K) while assuming a saturated atmosphere, resulting in new high-level RH values presented in [5]. Nonetheless, large parts of the observed in-situ conditions, particularly the warmest and driest conditions achieved during daytime, remained sparsely covered by the calibration.

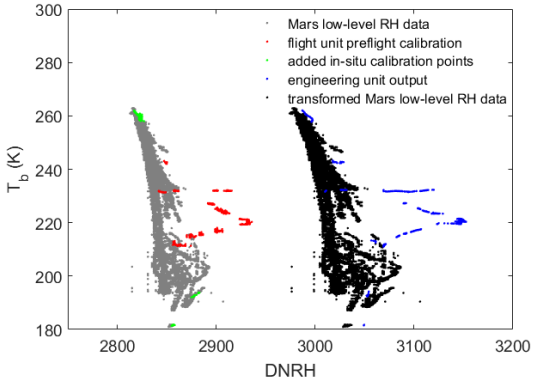

Figure 1: The TECP preflight calibration (red) only partially overlaps the recorded RH measurements at the Phoenix landing site (gray). We use the output of a TECP engineering unit (blue) at the same environmental conditions as the preflight calibration (red) and at additional known landing site conditions (green) to transform the insitu measurements (gray) into the dynamic range of the engineering unit (black). We then cover this entire range of T and RH conditions (black) to calibrate the engineering unit and find a recalibration for the flight unit.

3. A Novel Recalibration Method

We use a spare engineering unit of the TECP in combination with a reference hygrometer in our environmental chamber to significantly augment the calibration data set and to improve the calibration function. Being able to accurately simulate the entire range of polar Martian environmental conditions allows us to produce high level RH data from the existing raw output of the TECP flight unit [1]. First, to ensure comparability of the TECP engineering unit output (Fig. 1, blue) with that of the flight unit (Fig. 1, red), we obtain a "translation function" $DNRH_{eu} = g(DNRH_{fu}, T_b)$ by covering the preflight flight unit calibration with the engineering unit. To improve the accuracy of this function we use additional in-situ measurements at the lowest and highest end of the T_b range (Fig. 1, green). At the lower end we can safely

assume saturated RH conditions based on independent and contemporaneous data sets [3], whereas at the higher end we assume maximum water vapor pressure (e) values between 1 and 10 Pa based on satellite retrievals of atmospheric water content and numerical modeling [2]. Second, we cover the entire range of transformed environmental conditions (black) to find a new calibration function for the engineering unit $T_f = f(DNRH_{eu}, T_b)$, which is then used to calculate high-level RH data for the flight unit.

4. Recalibration Results and Comparison with Previous Data

Our recalibration function yields the most accurate results when a maximum water vapor pressure (e) of 2 Pa is assumed. Results of our recalibration are shown in Fig. 2. Sensitivity studies of this assumption between 1 and 10 Pa show resulting maximum errors of 30%. Values of e increase during roughly the first half of the mission, until around sol 80 and then decrease. This trend and the range of values obtained are consistent with independent estimations of e from satellite [2]. The recalibrated relative humidity at 2 m above the surface based on Phoenix MET data shows saturated conditions at nighttime after sol ~80 (Fig. 2, middle), consistent with independent observations of near-surface fog [3]. Fig. 2 (bottom) shows a comparison of the data obtained by our recalibration compared to previous calibrations [4,5]. Even though our recalibration shows nighttime values similar to those currently available in the PDS [5], daytime values differ by an order of magnitude (regardless the e assumption at the warmest conditions). Our daytime values resemble those of the first calibration.

Acknowledgements

Funding for this project was provided by NASA Mars Data Analysis Program: Award #NNX15AM53G.

References

[1] Fischer, E. *et al.*: Formation and persistence of brine on Mars: experimental simulations throughout the diurnal cycle at the Phoenix landing site, *Astrobiology 16*, 12, 2016.

[2] Tamppari, L. K. *et al.*: Phoenix and MRO coordinated atmospheric measurements, *J. Geophys. Res. 115*, E00E17, 2010.

[3] Whiteway, J. A. *et al.*: Mars Water-Ice Clouds and Precipitation, Science *325*, 68, 2009.

[4] Zent, A. P. *et al.*: Initial results from the thermal and electrical conductivity probe (TECP) on Phoenix, *J. Geophys. Res. Planets 115*, E3, 2010.

[5] Zent, A. P. *et al.*: A revised calibration function and results for the Phoenix mission TECP relative humidity sensor, *J. Geophys. Res. Planets 121*, 626-651, 2016.

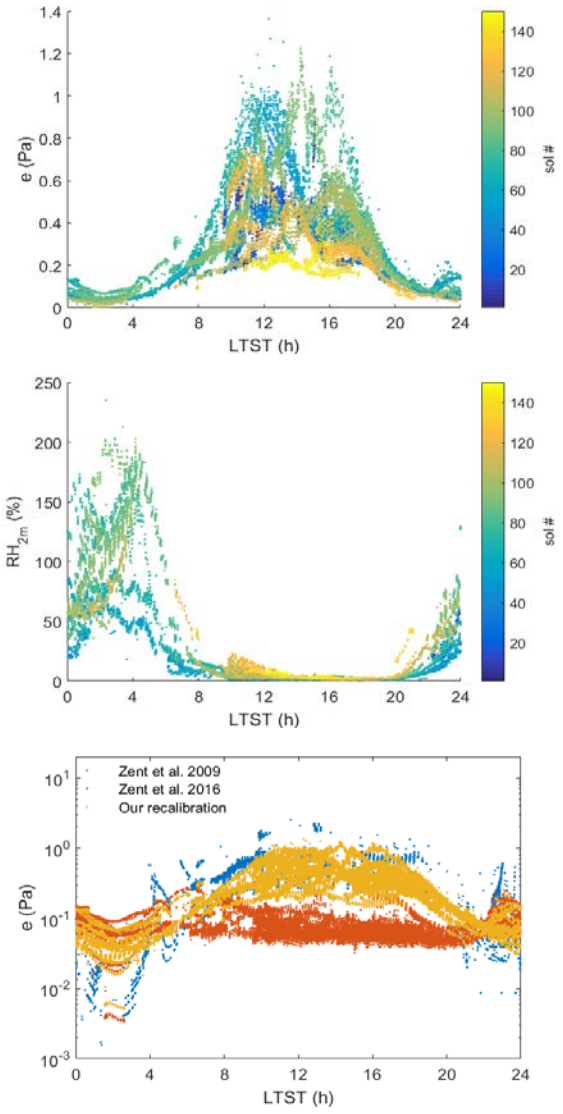

Figure 2: The recalibrated TECP RH sensor measurements color-coded by sol number in terms of water vapor pressure (top) and relative humidity at 2 m height (middle) over local time and comparison with past calibrations (bottom).

EPSC Abstracts
Vol. 12, EPSC2018-570, 2018
European Planetary Science Congress 2018

Local-time dependence of the zonal wave number spectra derived from the Venus cloud-top Temperature observed by Akatsuki LIR

T. Fukuhara (1), A. Nagata (1), M. Taguchi (1), T. Imamura (2) and LIR project team
(1) Rikkyo University, Japan, (2) The University of Tokyo, Japan

Abstract

Zonal wavenumber spectra of the temperature deviation at the equatorial region of Venus derived from the close-up observations by LIR onboard Akatsuki has been represented. The result indicates that the spectral peak appears at ~0.002 km^{-1} in local time (LT) of 14:00-18:00, and at ~0.005 km^{-1} in LT ~23:00. The peak at LT 14:00-18:00 would be attributed by the stationary gravity wave which was discovered by LIR initial observation. The peak at 23:00 has never been discussed in previous observations. It may be caused by the convection generated at the cloud layer, which is predicted by the numerical study in Imamura et al., 2014.

1. Introduction

The Long-wave infrared camera (LIR) on board Akatsuki detects thermal infrared radiation at wavelengths of 8–12 μm and maps brightness temperature of the cloud-top level (65 km) of Venus. LIR has mainly obtained Venus disk images with more than 50,000 km distance along Akatsuki's elliptical orbit. More than 10,000 of images have been acquired by LIR since December 2015. Meanwhile, more than 500 sheets of close-up images, that cover most of local time at equatorial region, have been obtained since September 2016 (Fukuhara et al., 2017a, EPS). These images with high spatial resolution provide us the horizontal temperature distribution at mesoscales (20–1000 km).

2. Data analysis

Close-up images which have been acquired less than 50,000 km of distance have been chosen from all LIR observation, and zonal mean temperatures and deviations were derived from each image in latitude from 30 to -30 degree with each 5 degree steps. Zonal wavenumber spectra of the temperature deviation were obtained in each image with 5 degrees step of latitude. The local time variation of the zonal wave number spectra on the equator is shown in Fig.1.

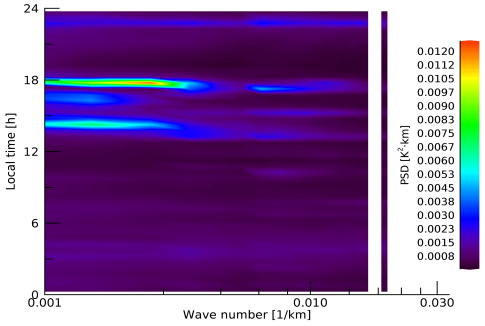

3. Result and Discussion

Fig.1 shows that obvious temperature deviations appear in LT 14:00–18:00, which have the spectral peak at ~0.002 km^{-1} (wavelengths of 500 km). The local time of the temperature deviations correspond with that of the stationary gravity wave appearing in the initial observation of LIR (Fukuhara et al., 2017b, Nature Geo). On the other hand, another temperature deviation is seen in LT ~23:00, and the spectral peak corresponds with ~0.005 km^{-1} (wavelengths of 150 km). The deviation has never been discussed based on previous observations. The previous numerical study (Imamura et al., 2014,

Icarus) has predicted that temperature deviation at the cloud-top level can cause upward propagation of the gravity wave, which is generated by the convection at the cloud layer in the night-side of the equatorial region. Our result can support existence of such upward propagation of the gravity wave in the cloud level of Venus.

References

[1] Fukuhara, T., et al., EPS, 69:141 DOI 10.1186/s40623-017-0727-y, 2017a.

[2] Fukuhara, T., et al., Nature Geo., Nat Geosci. doi:10.1038/NGEO2873, 2017b.

[3] Imamura, T., et al., 2014, Icarus, 228,181-188

EPSC Abstracts
Vol. 12, EPSC2018-595, 2018
European Planetary Science Congress 2018

O_2 distributions and related chemistry on Mars: Potential scientific targets for the future Mars terahertz sensor missions

Takeshi Kuroda (1,2), Richard Larsson (1,3), Hideo Sagawa (4), Shohei Aoki (5), Yasuko Kasai (1), Hiroyuki Maezawa (6) and Yasumasa Kasaba (2)
(1) National Institute of Information and Communications Technology, Koganei, Japan (tkuroda@nict.go.jp), (2) Department of Geophysics, Tohoku University, Sendai, Japan, (3) Max Planck Institute for Solar System Research, Göttingen, Germany, (4) Kyoto Sangyo University, Kyoto, Japan, (5) The Royal Belgian Institute for Space Aeronomy, Brussels, Belgium, (6) Osaka Prefecture University, Sakai, Japan.

The importance of O_2 (molecular oxygen) for the atmospheric chemistry on Mars had been overlooked historically, because it has been thought to exist horizontally and vertically constant (~1400 ppmv) and impossible to observe from ground-based telescopes due to the deep absorption of the terrestrial O_2. However, the recent sub-millimeter spectroscopic observation using the Herschel Space Observatory suggested the possibility of higher concentration of O_2 near the Martian surface based on which detected the non-uniform vertical distribution of O_2 in global-mean abundance [1], and, since then, we have started to investigate the importance of O_2 for the atmospheric environment of Mars.

The abundance of O_2 is chemically related to the existences of O_3, H_2O, HO_2, H_2O_2, CO and methane. Simulated results by a Mars global climate model (MGCM) including a chemical suite (Mars Climate Database v5.3) [2,3] did not show the specific vertical variances of O_2 abundance except the winter polar regions where the composition changes due to the condensation of CO_2 (Figure 1). It means that current MGCMs may lack the processes which cause the vertical gradient in the O_2 abundance that suggested by the Herschel observation: e.g., unusual chemical reactions inside local dust storms and/or other surface activities including biological and geological ones.

Terahertz sensors which are planned to be onboard future satellite missions may observe the abundances of O_2 and chemically-related molecules (O_3, H_2O, H_2O_2) (Figure 2), and would be suitable for the first specific observational investigations of O_2 distributions and its formation/loss processes on Mars. In this presentation we show test experiments of O_2 distributions using our high-resolution MGCM (DRAMATIC) with water cycle [4] and a chemical module, and discuss the potential scientific interests for future terahertz observations from Mars landers/orbiters.

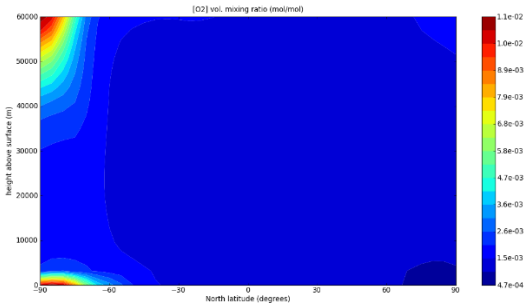

Figure 1: Zonal-mean O_2 volume mixing ratio at Ls=90° in the Mars Climate Database v5.3.

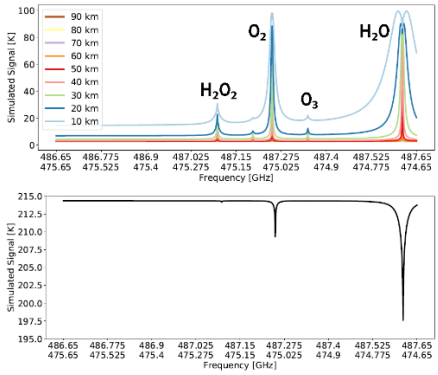

Figure 2: Simulated limb (upper) and nadir (lower) spectra of a planned terahertz sensor on Mars [5].

References

[1] Hartogh et al., Astron. Astrophys. 521, L49, 2010.
[2] Forget et al., J. Geophys. Res. 104, 24155-24176, 1999.
[3] Millour et al., EPSC2015-438, 2015.
[4] Kuroda, Sixth international workshop on the Mars atmosphere: modelling and observations, 2017.
[5] Larsson et al., Geosci. Instrum. Method. Data Syst. Discuss., in review, 2017.

EPSC Abstracts
Vol. 12, EPSC2018-596, 2018
European Planetary Science Congress 2018

Tagging dust and water in the NASA Ames Mars GCM: a new global vision of the Martian climate

Tanguy Bertrand, Melinda A. Kahre, R. John Wilson, and Alexandre. Kling
NASA Ames Research Center, Moffett Field, CA 94035, USA (tanguy.bertrand@nasa.gov).

Abstract

Many fundamentally issues remain unsolved regarding the current dust and water cycles on Mars. In particular: *What are the role and impact of the different reservoirs of dust and water on the cycles? What controls and triggers the regional and global dust storms? Where and how is dust lifted and transported in the atmosphere? What is the current global dust and water budget and how has it evolved over time and space?* In order to provide new insights on these questions, we implemented the so-called tagging method in the NASA Ames Mars Global Climate Model (MGCM) [1]. Below we describe this method and some of its promising applications.

1. The tagging method

The MGCM simulates the atmospheric transport of dust particles, water vapor and water ice. The tagging method "tags" or "labels" these transported constituents according to a chosen criterion (Figure 1). As an example, if dust particles are the tagged constituent (« dust tagging ») and the criterion is its geographic origin (e.g., the low thermal inertia regions), this means that during the entire simulation, we keep track of the dust that originated in the selected regions of Mars. Each tag is transported by the model as a tracer and behaves like the constituents they follow, but is completely passive and does not alter the predictions.

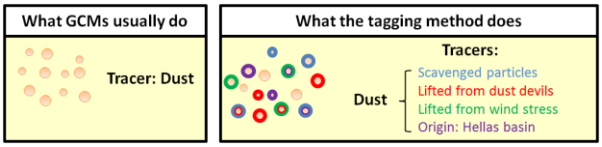

Figure 1: Illustration of the tagging method for the dust tracer. Instead of one unique tracer describing the dust population, the tagging method produces many tracers allowing us to keep track of its history.

This technique enables us to track not only the origin of a given atmospheric constituent, but also the physical processes it goes through (e.g., scavenging, ice cloud, storm, frost, etc.), or the different environments it has encountered since its emission (crater, mountains, dusty atmosphere, poles, etc.).
This powerful method, never tested on Mars, was first implemented in the NASA/GISS GCM [2] to identify the origin of the precipitation in various regions of the Earth, and is now widely used for detailed studies of the Earth water cycle.

2. Possible applications

The tagging method has been implemented, tested, and validated. We are currently exploring the possible applications, summarized in Table 1. At the conference, we aim to show the results concerning the first three applications (A1-A3), which are focused on the dust cycle.

2.1 Application A1

We tag dust depending on its geographic origin. We divide the Martian surface into different geographic areas, including the main regions of dust lifting [3][4] and the high/low albedo and thermal inertia regions [5]. By running different simulations with finite sources [6,7], we also investigate the role and contribution of each reservoir on the dust cycle and quantify their dust exchanges. We are also able to isolate the contribution of each region to the formation of global dust storms, providing insight into the main pathways dust particles take during the formation of a global dust storm. In addition, the simulations reveal the regions where dust is deposited after the decay of such a storm. On a multidecadal time scale, the simulations using this tagging method also constrain the mass balance and equilibrium state of the dust cycle.

Table 1: Envisioned applications

	TAG	Criterion	Objectives
A1	Dust	Geographic origin of lifting	Investigate the role of the reservoirs on the dust cycle and quantify the dust exchanges, considering finite/infinite sources
A2	Dust	Local time of lifting	Investigate the diurnal dependence of lifting and transport
A3	Dust	Scavenged by water ice	Estimate the global impact of scavenging on the current and past Martian climate, in particular during high obliquity periods
A4	Dust	Lifting scheme	Quantify the contributions of dust lifted by dust devils activity and surface wind stress when both schemes are active
A5	H_2O ice	N. polar cap and outliers	Assess/compare the impact of the water ice reservoir located in the N. polar cap and in the outliers on the climate
A6	Dust + H_2O ice	Altitude	Follow where high altitude aerosols tend to be transported

2.2 Application A2

By tagging dust depending on the local time it has been lifted and lofted in the atmosphere, we investigate how the diurnal cycle affects the dust lifting and transport. With this method, we provide insight into the contribution of upslope and downslope winds on the dust cycle.

2.3 Application A3

We tag dust particles that have been scavenged by water ice clouds. This enables us to assess the global impact of scavenging on the current and past Martian climate, in particular during the high obliquity periods where this process is thought to have been more efficient than it is today.

2.4 Other Applications

By tagging dust depending on the type of lifting, we can also quantify the contributions of dust lifted by dust devils activity and surface wind stress when both schemes are active, and determine where each type of dust tends to accumulate and influence the surface reservoirs (A4). By tagging water depending on its sublimation source, the northern polar cap or its outliers, we can assess the impact of both reservoirs on the current climate, and investigate their exchange of ice and global budget. This study can also be applied to past climates, where other reservoirs of water ice may be stable (A5). By tagging the aerosols depending on the altitude they reach, we can probe where the different levels tend to transport the aerosols (A6).

3. Summary and Conclusions

The potential of the dust, water and water ice tagging method in the GCMs opens the door to many powerful results regarding the long-term evolution of the dust and water cycles. We expect this method to fill many gaps in the understanding of the current and past Martian climate and provide insights on the development of global dust storms, the influence of the scavenging of dust particles during both the present-day and past climates, the exchanges between the different dust and water reservoirs and the long-term mass balance and equilibrium state of the cycles.

Acknowledgements

T. B. was supported for this research by an appointment to the National Aeronautics and Space Administration (NASA) Post-doctoral Program at the Ames Research Center administered by Universities Space Research Association (USRA) through a contract with NASA.

References

[1] Kahre, M. A., et al.: Coupling the Mars dust and water cycles: The importance of radiative-dynamic feedbacks during northern hemisphere summer, Icarus, 260:477, 2015.

[2] Koster, R., J., et al.: Global sources of local precipitation as determined by the Nasa/Giss GCM, GRL, 13:121, 1986.

[3] Basu, S., et al.: Simulation of the Martian dust cycle with the GFDL Mars GCM, JGR, 109:E11, 2004.

[4] Kahre, M. A., et al.: Modeling the Martian dust cycle and surface dust reservoirs with the NASA Ames general circulation model, JGR, 111, 2006.

[5] Ruff, S. W., Christensen, P. R.: Bright and dark regions on Mars: Particle size and mineralogical characteristics based on Thermal Emission Spectrometer data, JGR (Planets), 107:E12, 2002.

[6] Newman, C. E. et al.: The impact of surface dust source exhaustion on the martian dust cycle, dust storms and interannual variability, as simulated by the MarsWRF General Circulation Model, Icarus 257:47, 2015.

[7] M. A. Kahre, et al.: Investigations of the variability of dust particle sizes in the martian atmosphere using the NASA Ames General Circulation Model, Icarus 195:576, 2008.

EPSC Abstracts
Vol. 12, EPSC2018-600, 2018
European Planetary Science Congress 2018

High resolution 3D global climate modelling of Pluto's atmosphere to interpret New Horizons observations

Tanguy Bertrand (1,2), François Forget (2)
(1) NASA Ames Research Center, Moffett Field, CA 94035, USA (2) Laboratoire de Météorologie Dynamique, IPSL, Sorbonne Universités, UPMC Univ Paris 06, CNRS, 4 place Jussieu, 75005 Paris, France. (tanguy.bertrand@nasa.gov).

1. Introduction

In July 2015, our vision of Pluto changed as the New Horizons spacecraft flew by Pluto and revealed an active frozen world, with unprecedented landscapes in the Solar System [1]. Its surface is notably covered with frosts and spectacular glaciers, including a kilometers-thick icecap of nitrogen ice, mixed with methane and CO [1][2]. Surprisingly, this half-heart shaped icecap did not form at the poles and at high elevation, like Antarctica on the Earth. It is located near the equator, at the bottom of a vast basin called Sputnik Planitia. New Horizons also detected methane ice almost everywhere in the northern hemisphere, with different brightness and textures: bright deposits at high latitudes and darker deposits in the equatorial regions [2][3]. The atmosphere of Pluto was also astonishing. New Horizons determined the surface pressure and the atmospheric temperature profile at two opposite locations, including one in Sputnik Planitia [4]. The two profiles were found to differ, which was not expected. Also, by observing Pluto in backlight, a magnificent organic haze was revealed, with a maximal extent at the North Pole [5].

Here we used high resolution simulations performed with the LMD Global Climate Model (GCM) of Pluto's atmosphere to simulate the Pluto climate system in 2015 and interpret New Horizons observations. Below we detail the modeling strategy and the results that we will present at the conference.

2. The LMD Pluto GCM

The Pluto 3D GCM is described in details in [6]. It takes into account the sublimation and condensation cycles of N_2, CH_4, and CO [6], the cloud formation, the atmospheric circulation and turbulence, the radiative transfer, the organic haze formation [7], as well as many other physical processes.

However it simulates the atmosphere of Pluto over only thirty terrestrial years. In order to ensure our simulations, sensitive to our initial conditions and our surface parameters (e.g. albedo, emissivity, thermal inertia), correctly describe reality, we initialize the GCM with a set of subsurface temperatures and ice distribution, which converged toward steady state after millions of years simulated with a fast 2D version of the model [8][9]. This 2D model also enables us to identify "realistic" simulations which differ by their spatial distribution in 2015 but remain consistent with the evolution of the surface pressure [10] and the amount of atmospheric methane observed on Pluto [11].

3. Results

We perform a comprehensive characterization of Pluto's atmosphere in 2015 using these best-case simulations. Wind regimes and near surface winds can be compared to wind streaks and dunes orientation on Pluto, while the simulated waves and thermal structure can be compared to the New Horizons occultations measurements [4].

We discuss the sensitivity of the general circulation to the distribution of the nitrogen ice on the surface. Our latest results suggest that Pluto's atmosphere undergoes a retrograde rotation, a unique circulation regime in the Solar System (except maybe on Triton), induced by the condensation-sublimation of nitrogen in the Sputnik Planitia basin. In Sputnik Planitia, the near-surface winds favor a deposition of haze particles in the northern and western part of the ice cap, which helps to interpret the different colors observed.

The GCM also shows that several atmospheric phenomena are at the origin of the cold boundary layer observed deep in the Sputnik Planitia basin: the sublimation of cold nitrogen, katabatic winds bringing cold air in the basin, and the formation of a

western boundary current transporting cold air from the northern to the southern part of Sputnik Planitia (Figure 1). This allows us to understand the near-surface differences observed between the entry and exit temperature profiles, measured by REX on-board New Horizons. However it does not reproduce the differences observed between 6 and 30 km above the mean surface.

Our work confirms that despite a frozen surface and a tenuous atmosphere, Pluto's climate is remarkably active. The nitrogen icecap within Sputnik Plantia is the heart of this climate system since it regulates the general circulation.

Figure 1: Map of the horizontal winds at 1 km above the local surface, obtained from a GCM simulation at the date of July 14, 2015 (the local time at longitude 180° is 2:00pm). At the center of the figure, within the bright half-heart shaped Sputnik Planitia ice sheet, we obtain a western boundary courant crossing the basin from the north to the south. These winds, induced by the sublimation of nitrogen in the northern latitudes of the basin and the Coriolis force, transport cold nitrogen air toward the southern latitudes of the basin.

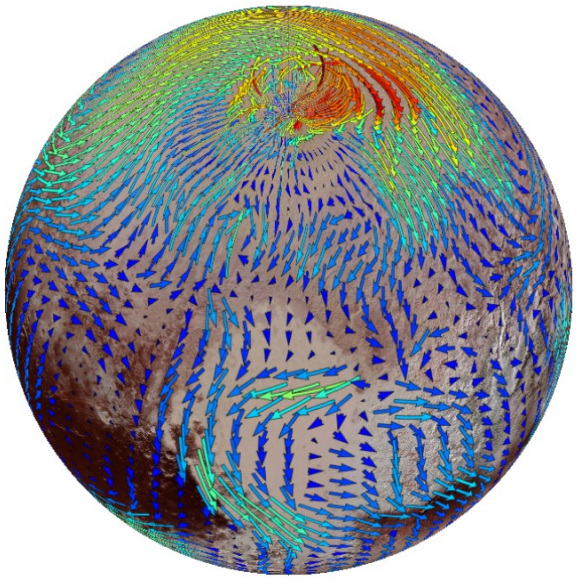

Acknowledgements

T. B. was supported for this research by an appointment to the National Aeronautics and Space Administration (NASA) Post-doctoral Program at the Ames Research Center administered by Universities Space Research Association (USRA) through a contract with NASA.

References

[1] Stern, A., et al.: The Pluto system: Initial results from its exploration by New Horizons, Science, 350:1815, 2015.

[2] Grundy, W. M., et al.: Surface compositions across Pluto and Charon, Science, 351 :aad9189, 2016a.

[3] Schmitt, B, et al.: Physical state and distribution of materials at the surface of Pluto from New Horizons LEISA imaging spectrometer, Icarus, 287 :229–260, 2017.

[4] Hinson, D. P., et al.: Radio occultation measurements of Pluto's neutral atmosphere with New Horizons, Icarus, 290 :96–111, 2017.

[5] Gladstone, R., et al.: The atmosphere of Pluto as observed by New Horizons, Science, 351:8866, 2016.

[6] Forget, F., Bertrand, T., Vangvichith, M., Leconte, J., Millour, E., and Lellouch, E.: A post-new horizons global climate model of Pluto including the N2, CH4 and CO cycles, Icarus, 287 :54–71, 2017.

[7] Bertrand, T. and Forget, F.: 3D modeling of organic haze in Pluto's atmosphere, Icarus, 287:72, 2017.

[8] Bertrand, T. and Forget, F.: Observed glacier and volatile distribution on Pluto from atmosphere–topography processes, Nature, 987:42, 2016.

[9] Bertrand, T., et al.: The nitrogen cycles on Pluto over seasonal and astronomical timescales, Icarus, 309:277, 2018.

[10] Sicardy, B., et al.: Pluto's Atmosphere from the 2015 June 29 Ground-based Stellar Occultation at the Time of the New Horizons Flyby. Astrophys. J.l, 819 :L38, 2015.

[11] Lellouch, E., et al.: Exploring the spatial, temporal, and vertical distribution of methane in Pluto's atmosphere, Icarus, 246 :268–278, 2016a.

EPSC Abstracts
Vol. 12, EPSC2018-604, 2018
European Planetary Science Congress 2018

Non-thermal escape rates of light species from Mars using MAVEN in-situ measurements

Marko Gacesa(1), Robert J. Lillis(1), Justin Deighan(2), Meredith Elrod(3), Jane L. Fox(4), and the MAVEN NGIMS team
(1) Space Sciences Laboratory, University of California, Berkeley, CA, USA; (2) Laboratory for Atmosphere and Space Physics, University of Colorado Boulder, Boulder, CO, USA; (3) Goddard Space Flight Center, NASA, Greenbelt, MD, USA; (4) Wright State University, Dayton, OH, USA

Abstract

We present a theoretical analysis of non-thermal escape rates of molecular hydrogen and other light species from Mars induced by collisions with superthermal oxygen atoms produced either photochemically or by precipitating energetic neutral particles (ENAs). The hot oxygen production rates were derived from MAVEN density and temperature in-situ measurements taken over last 36 months and used to calculate collisional escape rates of light atmospheric species. The energy transfer in collisions is described using either extensive quantum-mechanical calculations of state-to-state elastic, inelastic, and reactive cross sections[1] or model momentum transport cross sections[2]. We find that D/H escape ratio may be modified by up to 15% by this non-thermal process. The described collisional ejection mechanism is theoretically estimated to be able to eject atmospheric species up to mass 30 *u*, including H_2O and OH[3], possibly affecting primordial water loss from Mars. Based on in-situ data, seasonal variation of non-thermal escape is discussed.

1. Introduction

Dissociative recombination (DR) of photoionized O_2^+ with electrons in the upper atmosphere of Mars produces translationally superthermal O atoms capable of overcoming martian gravitational potential and escaping into space. This process is known as photochemical escape and found to be one of the major escape mechanisms presently active on Mars. In addition to escaping, superthermal O atoms can collide with thermal atmospheric atoms and molecules and transfer sufficient kinetic energy to eject them to space. This non-thermal escape mechanism is significant for the species heavier than atomic hydrogen, and more efficient than Jeans escape for light atmospheric species heavier than deuterium. For example, the non-thermal escape rate of HD molecules from Mars was estimated to be about 25 times greater than their Jeans escape rate[4]. The collisionally ejected molecules will be preferentially excited to higher rotational and/or vibrational states.

The Mars Atmosphere and Volatile EvolutioN Mission (MAVEN), launched in 2014 as a part of NASA's Mars Scout program, is the first mission that can perform in-situ measurements of physical quantities necessary to derive photochemical escape fluxes on orbit-to-orbit basis [5]. Specifically, MAVEN measurements constrain photochemical oxygen escape from Mars in three separate ways: Hot oxygen production rates are calculated from measured electron temperatures and densities (from the Langmuir Probe and Waves (LPW) experiment) and ion temperatures and densities from the SupraThermal And Thermal Ion Composition (STATIC) and Neutral Gas and Ion Mass Spectrometer (NGIMS), while escape probability are calculated with neutral densities measured by NGIMS instrument. We have constructed average and seasonal escape fluxes of hot O from the Martian atmosphere based on more than 36 months of data from the listed instruments. The altitude profiles of hot O escape rates were to determine the altitude profiles of non-thermal escape rates of light neutrals (with focus on H_2, HD, He, OH and H_2O) driven by collisions with superthermal O atoms and their impact on the total escape fluxes. The determined average and seasonal dayside escape fluxes of hot O were found to be broadly consistent with pre-MAVEN predictions. The non-thermal escape rates of H_2 and HD induced by collisions with hot O were found to exceed the pre-MAVEN predictions and to exhibit potentially observable seasonal variations (Fig. 1), while preliminary results for other light species show similar trends.

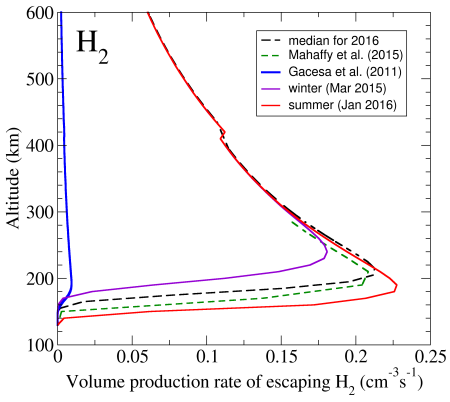

Figure 1: Sample altitude profiles of volume production rate of escaping H_2 molecules ejected by collisions with photochemically produced superthermal O atoms. Our preliminary results, based on MAVEN in-situ seasonal temperature and density measurements, are shown for selected orbits during a martian summer (red curve), martian winter (purple curve), and a single deep-dip (orbit #1064) [6] (dashed green). A pre-MAVEN estimate of non-thermal escape rate of H_2 for assumed low solar activity [4] is also shown (blue). Note the seasonal differences in altitudes for the maximal rates.

2. Results and discussion

Our preliminary estimates of collisionally induced non-thermal escape rates of H_2, HD, He, and OH, based on MAVEN in-situ measurements, are nearly an order of magnitude larger than pre-MAVEN theoretical estimates based on theoretical atmospheric density and temperature profiles [2, 3, 4]. Major factors influencing the results are differences in assumed vs measured atmospheric density and temperature profiles on Mars, as well as improved cross sections used in the study. We found that differences in momentum transfer cross sections (previous works used mass-scaling of O+Ar cross sections to model unknown cross sections) account for 30-50% difference in results, indicating their importance. The results also show significant variations between seasons. The work to fully understand the seasonal and diurnal variations is in progress and likely requires 3D models of escape. Our results indicate that non-thermal escape of D, as HD and possibly OD and HDO, may contribute up to 15% of the total D loss from Mars. Similarly, non-thermal escape likely plays a more significant role in helium isotope (^{3}He vs ^{4}He) fractionation.

The work to compare the measured contributions of ENAs to simulated superthermal oxygen altitude profiles is in progress. Here, as for the photochemically produced superthermal oxygen, we expect the measured atmospheric densities and temperatures to affect the non-thermal escape rates, possibly resulting in similar enhancements in escape rates of ejected light species.

Acknowledgements

We acknowledge V. Kharchenko and N. Lewkow for providing their computer code for Monte Carlo simulation of the incoming fluxes of hot ENAs on Mars. MG was partially supported by an appointment to the NASA Postdoctoral Fellowship Program at the NASA Ames Research Center, administered by USRA under contract with NASA.

References

[1] Gacesa, M., Kharchenko, V., Quantum reactive scattering of O(^{3}P)+ H_2 at collision energies up to 4.4 eV, J. Chem. Phys. 141 (16), 164324 (2014)

[2] Lewkow, N. R. and Kharchenko, V.: Precipitation of energetic neutral atoms and induced non-thermal escape fluxes from the martian atmosphere, Astrophys. J. 790, 98 (2014).

[3] Gacesa, M., Lewkow, N. R., Kharchenko, V., Non-thermal production and escape of OH from the upper atmosphere of Mars, Icarus 284, 90 (2017).

[4] Gacesa, M., Zhang, P., Kharchenko, V., Non-thermal escape of molecular hydrogen from Mars, Geophys. Res. Lett. 39, L10203 (2012)

[5] Lillis, R. J. et al., Photochemical escape of oxygen from Mars: First results from MAVEN in situ data, J. Geophys. Res. 122 (3), 3815 (2017)

[6] Mahaffy, P. R. et al.: Structure and composition of the neutral upper atmosphere of Mars from the MAVEN NGIMS investigation, Geophys. Res. Lett. 42, 8951 (2015)

EPSC Abstracts
Vol. 12, EPSC2018-636, 2018
European Planetary Science Congress 2018

Atomic oxygen in the Martian thermosphere traced by the 130.4 and 135.6 nm emission lines with MAVEN/IUVS

Birgit Ritter[1,2], Jean-Claude Gérard[1], Leonardos Gkouvelis[1], Benoit Hubert[1], Sonal Jain[3] and Nick Schneider[3]
(1) LPAP, University of Liège, Liège, Belgium, (2) Royal Observatory of Belgium, Brussels, Belgium, (3) LASP, University of Colorado, USA (b.ritter@uliege.be)

Abstract

We analyze limb observations of dayglow emissions from atomic oxygen in the upper Martian atmosphere. The data has been collected during the last almost four years by the Imaging Ultraviolet Spectrograph (IUVS) instrument on board the Mars Atmosphere and Volatile EvolutioN mission (MAVEN) spacecraft. Mean profiles for specific solar longitude, latitude and solar zenith angle ranges are created. We then use atmospheres from the Mars General Circulation models and in situ solar flux data from the MAVEN Extreme Ultraviolet Monitor (EUVM) to perform Monte Carlo and radiative transfer modeling for comparison with the observations. In order to match the results and to eventually retrieve oxygen densities, scaling factors are applied to the GCM atmospheric densities. We will present preliminary results of this analysis.

1. Introduction

Limb observation of airglow emissions is a standard technique to study the altitude profiles of the chemical elements in the Martian atmosphere and its thermal structure. Several previous missions have performed observations in the past (Mariners, Mars Express). In 2014, the Imaging Ultraviolet Spectrometer (IUVS, McClintock et al., 2014) on board MAVEN started collecting thousands of airglow and auroral limb profiles in the range 120 to 340 nm.
While below 200 km CO_2 is the dominating neutral species in the Martian atmosphere, above and up to lower exosphere atomic oxygen is more abundant. Atomic oxygen is produced by photodissociation of CO_2 and airglow transitions from the O(^{1}S) (297.2 nm), O(^{3}S) (130.2-4-6 nm triplet), and O(^{5}S) (135.6-8 nm doublet) excited states fall into the spectral detection range of IUVS.
Resonance scattering from solar emission is by far the dominant source for the excitation of the 130.4 nm triplet and electron impact on atomic oxygen and CO_2 – resulting in dissociation of the molecule – contribute less than ten percent to the emission. Photodissociation of CO_2 can be neglected. This line triplet is optically thick, hence its intensity does not give direct indication of the oxygen abundance and radiative transfer codes are needed to understand the observations. Differently, the 135.6 nm doublet of atomic oxygen is an optically thin line emission and results mostly from electron impact on oxygen and on CO_2. Even though its intensity is therefore proportional to the oxygen density, interaction cross-sections leading to the O(^{5}S) excited state are much less known than for the ones leading to the O(^{3}S) excited state. Studying both emissions lines in parallel will therefore provide more robust results than treating these features separately.

We now have analyzed samples from more than three years of airglow observations and compared them to model simulations. The objective is to study the characteristics of the oxygen FUV emissions at 130.4 and 135.6 nm in order to describe the Martian upper atmospheric oxygen density.

2. Methodology

MAVEN observations

The Imaging Ultraviolet Spectrometer (IUVS) on board MAVEN is capable of observing the Martian upper atmosphere within a total spectral range of 115-340 nm. It operates in limb, coronal scan, and disc mode, respectively. By now the observations cover more than a full Martian year and provide an unprecedented data set, covering various latitude ranges per epoch. We analyze periapse limb observations of the Martian thermosphere with tangent point altitudes between 80 and 200 km. In order to do so, we use processed data provided by the NASA Planetary Data System (PDS) to generate mean altitude profiles for small ranges of season,

latitude and solar zenith angle.
Figure 1 shows an example of limb profiles of the 130.4 nm and the 135.6 nm lines.

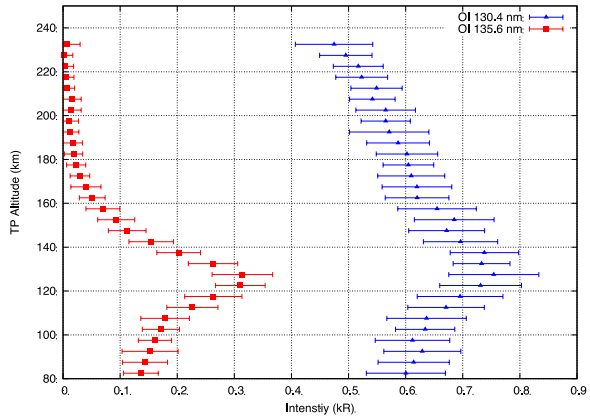

Figure 1: Averaged sum of more than 70 limb profiles in dependence of the tangent point (TP) altitude. Blue triangles show the 130.4 nm and red squares show 135.6 nm oxygen intensities. The horizontal bars indicate the 1-σ variability of the mean limb intensity at the respective altitude level.

The Extreme Ultraviolet Monitor (EUVM, Eparvier et al., 2015) on board MAVEN measures continuously the solar EUV flux. Data and extrapolated model data are available on the NASA PDS. We generate an average solar flux spectrum corresponding to the selected limb profiles as input for the models.

Modelling

We use model neutral atmospheres provided by Mars Climate Database that provide the respective altitude distribution of the main neutral constituents in dependence of season, local time, latitude and solar activity. Using the EUVM data as the solar driver, we employ Monte Carlo simulation for the calculation of the photoelectron spectrum as a function of altitude. Calculations of the collisional sources are based on the Direct Simulation Monte Carlo (DSMC) method that has been developed over the years (Shematovich et al. 2008; Gérard et al., 2008) to calculate the brightness profiles of emissions of the Earth, Jupiter, Saturn, Venus and Mars atmospheres. Collisional (photoelectron impact) (as well as photodissociation) excitation rates are calculated to provide the total volume production rates. For the 130.4 nm triplet we combine these results additionally with calculations for the resonance scattering of the solar 130.4 nm triplet. The solar line intensity is again taken from the EUVM and its line shape from Gladstone (1992). We employ the REDISTER radiative transfer code from Gladstone (1985) to calculate the effects of multiple scattering including frequency redistribution, which allows photons to escape an optically thick atmosphere by scattering in frequency from the core of the line into the optically thin line wings. Additionally, absorption due to CO_2 is taken into account, which influences not only the observed 130.4 nm intensity, but also the altitude of the intensity peak in the limb profile.

3. Summary

We present preliminary results of a parallel study of the 130.4 nm and 135.6 nm atomic oxygen dayglow emissions from the Martian thermosphere. We use MAVEN/IUVS limb profile observations, in situ solar flux measurements by MAVEN/EUVM, and Monte Carlo and radiative transfer modelling on neutral model atmospheres whose composition distribution matches the respective season, latitude, solar zenith angel and solar activity of the observational samples.

Acknowledgements

This research was partly funded by the PRODEX program managed by the European Space Agency with help of the Belgian Science Policy Office (BELSPO) and by BELSPO's SCOOP/BRAIN research contract.

References

[1] Eparvier, F. G. et al. 2015. Space Science Reviews, 195(1-4), 293-301.
[2] Gérard, J.C. et al., 2008, PSS, 56, 542-552.
[3] Gladstone, G.R., 1985. J. Quant. Spectrosc. Radiat. Trans. 33, 453–458.
[4] Gladstone, G.R., 1992. J. Geophys. Res. 97, 19125–19519.
[5] McClintock, W.E. et al., 2014, Space Sci. Rev., 1-50,10-1007/s.
[6] Shematovich, V.I. et al., 2008, J. Geophys. Res., 113, E02011.

EPSC Abstracts
Vol. 12, EPSC2018-648, 2018
European Planetary Science Congress 2018

Photochemical model of the Martian atmosphere to investigate the fate of trace gases

P. Witek (1), P. Wajer (1), M. Banaszkiewicz (1), W. Kofman (1,2), L. Czechowski (3) and A. Pommerol (4)

(1) Space Research Centre PAS, Warsaw, Poland (wajer@cbk.waw.pl), (2) Institut de Planetologie et d'Astrophysique de Grenoble CNRS/UJF, Grenoble, France, (3) Institute of Geophysics, Faculty of Physics, University of Warsaw, (4) Physics Institute, Space Research and Planetary Sciences - University of Bern, Bern, Switzerland.

Abstract

The European-Russian ExoMars Trace Gas Orbiter (TGO) is now on its scientific orbit. The orbiter has started to return new data on abundance of trace gases as well as colour and stereo images of the surface, that are useful in characterizing the sources and sinks of some atmospheric gases. One of the most interesting subjects of investigation is appearance and disappearance of large quantities of methane (CH_4) on Mars on short timescales. Our model of Martian atmospheric photochemistry, chemistry and transport is developed to analyse the data sent back by the probe. All constituents of the atmosphere are subjected to solar radiation and react with each other, in presence of the atmospheric aerosols. This leads to several hundred reactions that change the abundance of different species. We model these reactions in single-column model coupled with model of the subsurface, to properly simulate the release, transport and loss of trace gases. The molecules can react with each other, be exchanged between the layers of the atmosphere and may be lost to reactions with aerosols and surface, or escape into space.

1. Introduction

Changes in the abundance of trace gases in the atmosphere indicate active processes on a planet. In the last 15 years Earth-based observatories, Mars Express Orbiter and MSL Curiosity rover detected appearance of methane in the Martian atmosphere [1] [2][3]. The data show high variability, suggesting occasional release of gas and removal on timescales much shorter than expected from photochemistry alone. The sources of this gas are of special interest because they may signify recently active hydrothermal, volcanic or biological processes. The variability currently lacks undisputable explanation, and sinks capable of reducing the concentration to the background level on the scale of several months are not known.

The release of other trace gases together with methane may be an indicator of its origin. If methane is accompanied by sulphur dioxide, it suggests the release of volcanic gases. A likely source of methane on Mars is hydrothermal alteration of silicates (serpentinization) in the subsurface, and biological origin through methanogenesis (whether by extant or extinct microorganisms) is not excluded. Methane can also be released from methane hydrates in the permafrost, where it could have been trapped after formation in the past. [1]

Recent tumbling experiments have shown that wind erosion of quartz and basalt grains in the absence of oxygen activates the surface and leads to production of reactive species [4][5]. The ubiquity of dust on Mars makes this possibly important sink for methane, which can be lost due to formation of strong covalent bonds between silicon and methyl group [4]. Heterogeneous reactions on dust and ice aerosols in the Martian atmosphere have been previously suggested to be important for loss of some species [6].

High precision measurements of trace gases, now possible with instruments such as NOMAD and ACS on board ExoMars TGO, will determine the amount of various trace gases, including detection or at least placing strong constraints on abundance of species that have been predicted to be present, but not yet detected in the Martian atmosphere (e.g. SO_2) [7][8].

2. Research methodology

We develop a single-column model of the Martian atmosphere to compute its steady-state chemical composition. Starting there, we will study the release, propagation and loss of trace gases such as methane and other hydrocarbons, and sulphur and chlorine

species. To model the transport we solve one-dimensional time-dependent equations:

$$\frac{\partial n_i}{\partial t} = \frac{-\partial \Phi_i}{\partial z} + P_i - n_i L_i \qquad (1)$$

Where n_i is the concentration of i-th molecule (cm^{-3}), Φ_i is the vertical flux of molecules ($cm^{-2}s^{-1}$), z is the altitude, P_i is the production rate (cm^{-3} s^{-1}), and L_i is the loss rate (s^{-1}).

We model molecular and turbulent diffusion of the molecules and changes of their concentration resulting from interaction with each other and solar radiation. We simulate changes in the concentration resulting from chemical reactions, including some important heterogeneous ones. We use two-stream approximation of the radiative transfer equation. The overall photon flux is the sum of the direct and scattered parts. We simulate temporal variability of the incoming radiation, absorption and Rayleigh scattering by gas molecules and scattering on aerosol particles such as dust or ice crystals.

Our photochemical model requires upper and lower boundary conditions for each molecule. We include the loss of some molecules to space at the upper boundary, especially for the lightest species such as H or H_2 [9]. The lower boundary conditions are more complex. The molecules may react with chemically active surface and in some cases (like methane) may be released from the subsurface. This requires knowledge and proper modelling of the processes in the subsurface.

Separate numerical model is developed to simulate the processes in the Martian subsurface such as diffusion through porous rocks, adsorption and desorption, and others. The model will be coupled with the main photochemical model of the atmosphere.

We plan to use images obtained by the Colour and Stereo Surface Imaging System (CaSSIS) on board the ExoMars TGO [10] to put proper lower boundary conditions on our atmospheric model and numerical model of the subsurface. For example colour images obtained by CaSSIS should give us information on mineralogy of the surface in places where the methane release is most likely.

3. Summary and Conclusions

With the sophisticated instruments on board the Trace Gas Orbiter studying Martian atmosphere and surface, an adequate model of transport and changes of the concentration of the trace gases is needed. We develop a complex chemical and photochemical model to simulate the transport and fate of the gas species that are known to be present or expected to be detected in the Martian atmosphere. The behaviour of elusive trace gases such as CH_4 holds information on past and present activity and habitability of Mars. The results of our simulations will be confronted with measurements to assess the importance of various considered mechanisms of loss.

Acknowledgements

This research is grounded on the involvement of the Space Research Centre (SRC) in ESA's ExoMars TGO mission. The power supply unit for the ExoMars camera, CaSSIS was built in the SRC (in the project “Zasilacz Cassis/Cassis Power Supply Unit”, Um. 4000111561, funded by the European Space Agency) and the CaSSIS Science Team includes members in SRC.

References

[1] Atreya, Sushil K., Paul R. Mahaffy, and Ah-San Wong. "Methane and related trace species on Mars: Origin, loss, implications for life, and habitability." Planetary and Space Science 55.3 (2007): 358-369.

[2] Mumma, Michael J., et al. "Strong release of methane on Mars in northern summer 2003." Science 323.5917 (2009): 1041-1045.

[3] Webster, Christopher R., et al. "Mars methane detection and variability at Gale crater." Science 347.6220 (2015): 415-417.

[4] Jensen, Svend J. Knak, et al. "A sink for methane on Mars? The answer is blowing in the wind." Icarus 236 (2014): 24-27.

[5] Bak, Ebbe N., et al. "Silicates Eroded under Simulated Martian Conditions Effectively Kill Bacteria—A Challenge for Life on Mars." Frontiers in microbiology 8 (2017): 1709.

[6] Lefèvre, Franck, et al. "Heterogeneous chemistry in the atmosphere of Mars." Nature 454.7207 (2008): 971.

[7] Korablev, O. I., et al. "ACS experiment for atmospheric studies on “ExoMars-2016” Orbiter." Solar System Research 49.7 (2015): 529-537.

[8] Vandaele, Ann Carine, et al. "Science objectives and performances of NOMAD, a spectrometer suite for the ExoMars TGO mission." Planetary and Space Science 119 (2015): 233-249.

[9] Zahnle, Kevin, et al. "Photochemical instability of the ancient Martian atmosphere." Journal of Geophysical Research: Planets 113.E11 (2008).

[10] Thomas, Nicolas, et al. "The colour and stereo surface imaging system (CaSSIS) for the ExoMars Trace Gas orbiter." Space science reviews 212.3-4 (2017): 1897-1944.

EPSC Abstracts
Vol. 12, EPSC2018-680, 2018
European Planetary Science Congress 2018

Gravity wave drag parameterization for the new generation of Mars Global Circulation Models

Alexandre Kling (1,2), Melinda Kahre (1), John Wilson (1) Amanda Bretch (1) and James Murphy (3)
(1) Nasa Ames Research Center, Moffet Field, CA, USA (2) Bay Area Environmental Research Institute, Moffet Field, CA, USA (3) New Mexico State University, NM, USA (alexandre.m.kling@nasa.gov)

Abstract

We investigate the prevailing role of the sub-grid scale parametrization for the gravity wave drag in the Martian atmosphere using the NASA Ames Legacy General Circulation Model and the high performance Geophysical Fluid Dynamics Laboratory (GFDL)'s FV3 dynamical core running at high (sub-degree) resolution.

1. Introduction

Gravity waves are vertically propagating waves that can propagate over tens of kilometers, break, and deposit momentum that changes the mean atmospheric flow afar from their sources. Gravity waves can be orographic, that is, excited by the topography, or non-orographic when the source of the perturbation is dynamic (e.g. convection, front systems). On Mars, orographic gravity waves, in particular, have been studied with Global Circulation Model (GCMs). They are known to have a significant influence on the Hadley circulation and to dynamically alter the thermal structure of the atmosphere in the polar regions [2]; [4]

Oftentimes with GCMs, the horizontal scales of the topographic features that are exciting the orographic gravity waves are smaller than the grid spacing of the model. Therefore, these waves can not be adequately resolved within a numerical simulation and must be parameterized as a sub-grid scale process.

2. Method

We port the implementation of the Palmer et al. gravity wave drag scheme [6] for the NASA Ames Legacy GCM to the GFDL's FV3 dynamical core. The implementation includes wavelength-dependant thermal damping rates from Eckermann et al. [3] and also requires some degree of tuning to correctly match orbiter observations. The NASA Legacy Ames GCM uses a baseline resolution of 5 degree in latitude by 6 degree in longitude and 24 vertical levels. Within the FV3 framework though, sub-degree horizontal resolution is obtained and additional vertical layers are added in a computationally efficient manner. Therefore, the model now reaches a resolution where some of the topography features and dynamics that are exciting the gravity waves start to be resolved explicitly. Simulations are run at different horizontal resolutions, vertical resolutions and the tuning of the scheme is adapted consequently to investigate the impact of the spatial discretization on the waves' propagation and breaking.

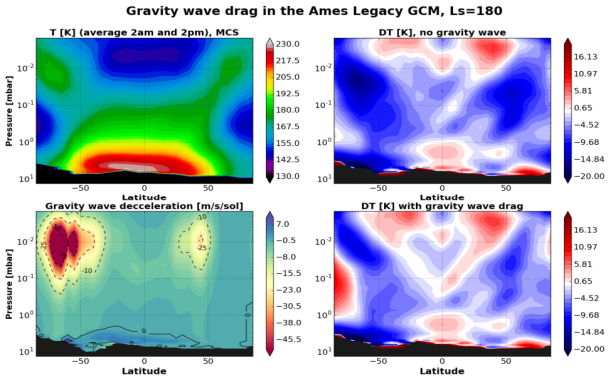

Figure 1: (Top left) MCS temperature retrievals. (Top right) Temperature difference GCM-MCS with no gravity wave. (Bottom left) Deceleration on the mean flow induced by the gravity wave drag. (Bottom right) Temperature difference GCM-MCS with gravity waves. The fields are zonally -averaged and the solar longitude is 180.

3. Preliminary Results

Figure 1 shows predictions for the temperature structure of the atmosphere from the NASA Ames Legacy GCM without (top right), and with (bottom right) sub-grid scale orographic gravity wave drag. The results are presented as difference plots with Mars Climate Sounder (MCS) temperature retrievals (top left) at a solar longitude of Ls =180. With gravity wave drag, the deceleration applied to the mean flow (bottom left) induce warming above the 1 mbar level at high latitudes.

4. Summary and ongoing work

The orographic gravity wave scheme improves the temperature structure of the atmosphere in the polar regions. [2] We are currently attempting to characterize the sensitivity of the spatial discretization for the tuning of the Palmer et al. [6] gravity wave drag scheme using FV3's high resolution capabilities. We also intent to test other gravity wave schemes, namely the orographic scheme from Garner et al. [5], and the non-orographic scheme from by Alexander and Dunkerton [1] which have been used in the GFDL terrestrial model.

References

[1] Alexander, M. J. and Dunkerton, T.J: A Spectral Parameterization of Mean-Flow Forcing due to Breaking Gravity Waves, Journal of the Atmospheric Sciences 56 (24), p4167-4182 (1999)

[2] Collins, M. et al : Gravity wave drag in a global circulation model of the Martian atmosphere: Parameterisation and validation, Advances in Space Research, 19, Issue 8, p1245-1254. (1997)

[3] Eckermann D., S. et al : Scale-Dependent Infrared Radiative Damping Rates on Mars and Their Role in the Deposition of Gravity-Wave Momentum Flux, Icarus 211, p429-442, (2011)

[4] Forget, F et al: Improved general circulation models of the Martian atmosphere from the surface to above 80 km, J. Geophys. Res., 104 (E10), p24155-24175, (1999)

[5] Garner, S. T: A Topographic Drag Closure Built on an Analytical Base Flux. Journal of the Atmospheric Sciences 62, p2302-2315 (2005)

[6] Palmer, T. N et al: Alleviation of a systematic westerly bias in general circulation and numerical weather prediction models through an orographic gravity wave drag parametrization. Q.J.R. Meteorol. Soc., 112: 1001-1039. (1986),

EPSC Abstracts
Vol. 12, EPSC2018-689, 2018
European Planetary Science Congress 2018

Looking for the sources of methane on Mars: statistical analysis of GCM simulations

Sébastien Viscardy (1), Frank Daerden (1), Lori Neary (1), Marco Giuranna (2), Giuseppe Etiope (3,4,2), Dorothy Oehler (5)
(1) Royal Belgian Institute for Space Aeronomy, Brussels, Belgium, (2) Istituto di Astrofisica e Planetologia Spaziali, Rome, Italy, (3) Istituto Nazionale di Geofisica e Vulcanologia, Rome, Italy (4) Faculty of Environmental Science and Engineering, Babes-Bolyai University, Cluj-Napoca, Romania (5) Planetary Science Institute, Tucson, Arizona, USA (sebastien.viscardy@aeronomie.be)

Abstract

Recent modeling studies looking for the source of atmospheric methane detected on Mars have consisted of looking for a single emission scenario that would be in agreement with the observations. We here propose a new strategy based on a large statistical sample of possible release scenarios, with the aim of determining the best source region *in terms of probability*.

1. Introduction

Several observations of methane on Mars have been reported over the last 15 years [1 and references therein]. Given its short photochemical lifetime in the Martian atmosphere, the presence of methane points to recent activity. Looking for the potential gas sources on Mars is thus a crucial step toward a better understanding of the origin of the released gas.

Several model studies [e.g. 2, 3] demonstrated the capabilities of GCMs to understand processes forming atmospheric plumes of methane from local outgassing events, such as the plume observed in 2003 by Earth-based telescopes [4]. Nevertheless, those investigations are largely inconclusive because many combinations of release locations and release scenarios can explain observations. Indeed, such problems are weakly constrained given the sparsity of observational data. In addition, the use of release patterns (either instantaneous or continuous) in previous studies has not been supported by methane emissions on Earth. Emission patterns (strength and duration) of methane releases are known from various types of terrestrial analogs, including faulted areas, springs, mud volcanoes, and areas with diffuse low levels of gas release called microseepage [5]. This information from terrestrial analogs can provide guidance for GCM simulations, so that values used are within reason for the geological systems on Mars in the vicinity of any methane detections.

2. Statistical analysis of release experiments

In this context, instead of supporting the available CH_4 observations with one consistent numerical experiment, we developed an innovative statistical approach considering a large number of realistic release scenarios and applied a statistical analysis to this sample. Such a study is made possible taking advantage of the additivity of tracers. Methane emission events can be viewed as a sequence of stochastic gas fluxes generated by combining tracers released successively and scaled randomly in order to mimic the time variability of typical methane seepage observed on Earth. Hence, a probability can be attributed to the given emission site in terms of the ratio between the number of scenarios consistent with the observations and the size of the statistically representative sample. As a result, comparing the probabilities associated with all potential emission sites within a predetermined region indicates the most plausible sites from the standpoint of the atmospheric circulation.

3. Application to the long high-CH_4 sequence recorded by Curiosity

In Mars year 32, the tunable laser spectrometer (TLS) of the Sample Analysis at Mars (SAM) instrument suite on the Curiosity rover recorded at Gale crater 4 successive high-CH_4 abundances spread over 60 sols [1]. This emission event will be considered in order to illustrate the capabilities of the new statistical approach. Simulations performed using the GEM-Mars GCM [6], a model already applied to study the time evolution of the gas in the atmosphere after surface release [7], will be used to form a large

sample of release scenarios that will be constrained by the available CH_4 observations in order to determine the most likely source regions around Gale crater. In addition, a detailed analysis of geological features observed in the investigated area will be conducted [8]. Combining the results of the modeling and geological analyses will allow us to narrow the range of potential regions from which the detected methane originated.

Acknowledgements

The research was performed as part of the "Excellence of Science" project "Evolution and Tracers of Habitability on Mars and the Earth" (FNRS 30442502). This project also acknowledges funding by the Belgian Science Policy Office (BELSPO), with the financial and contractual coordination by the ESA Prodex Office (PEA 4000103401, 4000121493).

References

[1] Webster, C. R. *et al.*, Mars methane detection and variability at Gale crater, Science, Vol. 347, pp. 415-417, 2015.

[2] Holmes, J. A., Lewis, S. R. and Patel, M. R. : Analysing the consistency of martian methane observations by investigation of global methane transport, Icarus, Vol. 257, pp.23-32, 2015.

[3] Mischna, M. A. *et al.*: Atmospheric modeling of Mars methane surface releases, Planet. Space Sci., Vol. 59, pp. 227-237, 2011.

[4] Mumma, M. J. *et al.*: Strong Release of Methane on Mars in Northern Summer 2003, Science, Vol. 323, pp. 1041-1045, 2009.

[5] Etiope, G.: Natural gas seepage. The Earth's hydrocarbon degassing, Springer, Cham, Switzerland, 2015.

[6] Neary, L. and Daerden, F: The GEM-Mars general circulation model for Mars: Description and evaluation, Icarus, Vol. 300, pp. 478-476, 2018.

[7] Viscardy, S., Daerden, F. and Neary, L.: Formation of layers of methane in the atmosphere of Mars after surface release, Geophys. Res. Lett., Vol. 43, pp. 1868-1875, 2016.

[8] Oehler, D. and Etiope, G.: Methane seepage on Mars: where to look and why. Astrobiology, Vol. 17, pp. 1233-1264, 2017.

EPSC Abstracts
Vol. 12, EPSC2018-694, 2018
European Planetary Science Congress 2018

Atmospheric escape at early Mars and its constraints on the evolution of the Martian atmosphere

Manuel Scherf (1), Sergey Dyadechkin (1), Ute Amerstorfer (1), Helmut Lammer (1), Maxim Khodachenko (1,2), Herbert Lichtenegger (1), Esa Kallio (3), Markku Alho (3), Igor Alexeev (2), David Parunakian (2), Raven Adam (4), Elena Belenkaya (2), Hannes Groeller (5), Colin Johnstone (6), and Manuel Guedel (6)
(1) Space Research Institute, Austrian Academy of Sciences, Graz, Austria (manuel.scherf@oeaw.ac.at), (2) Skobeltsyn Institute of Nuclear Physics, Moscow State University, Moscow, Russian Federation, (3) Aalto University, School of Electrical Engineering, Department of Electronics and Nanoengineering, Espoo, Finland, (4) Institute of Physics, University of Graz, Graz, Austria, (5) Lunar and Planetary Laboratory, University of Arizona, Tucson, AZ, USA, (6) Department of Astrophysics, University of Vienna, Vienna, Austria

Abstract

It is assumed that the Martian atmosphere was much denser in the past than it is today. However, how and when the Martian atmosphere changed to the present time tenuous and dry atmosphere is still one of the fundamental science questions in Martian research. To gain a better understanding of this key question, we studied how the early Martian atmosphere responded to different EUV fluxes from the young Sun and how this influenced the loss of carbon and oxygen. Since Mars had an intrinsic magnetic field early on, i.e. until ~4.1 billion years ago (Ga), its paleo-magnetosphere also has to be considered during the first few million years to reconstruct the atmospheric escape over the history of the planet. Thus, we simulated the ancient Martian intrinsic magnetic field with an adapted version of the Paraboloid Magnetospheric Model (PMM) and included the magnetosphere into our escape simulations. In addition, we will also address the escape of argon over the planet's history.

1. Loss of oxygen and carbon over time

We study the escape of suprathermal oxygen and carbon from the Martian atmosphere for four points in time in its history corresponding to 1, 3, 10, and 20 times the present solar EUV flux with a Monte-Carlo model. Different source reactions of hot oxygen and carbon atoms in the thermosphere and their changing importance with the EUV flux are discussed.

For the same EUV fluxes and solar wind parameters, we also investigate on how ionized atmospheric oxygen and carbon atoms are picked up by the solar wind convection electric field. Analysis was made by a 3D kinetic hybrid model which treats ions as particles and electrons as a massless charge neutralizing fluid. The hybrid simulation allows studying self-consistently the motion of ions in the Martian environment and together with the suprathermal escape rates from our Monte Carlo simulations we can thus estimate the total atmospheric escape rate during the Martian history.

Before ~4.1 Ga, we also consider the ancient intrinsic Martian magnetic field, and thus simulated the paleo-magnetosphere with an adapted version of the Paraboloid Magnetospheric Model (PMM) for Mars, which was then included into the hybrid model for the 20 EUV case.

2. Evolution of the Martian atmosphere

Finally, we discuss different magma ocean related and volcanic CO_2 outgassing scenarios and their interplay with thermal and non-thermal loss processes, as well as the influence of the paleo-magnetosphere on the early atmospheric escape. Our results show that Mars could not have had a dense atmosphere at the end of the Noachian eon, since such an atmosphere would not have been able to escape until today. However, Mars could have had a dense atmosphere early on in the pre-Noachian eon.

An important insight into this early environment can also be gained by the strong isotopic fractionation of 36Ar/38Ar in the present-day Martian atmosphere, which suggests that a significant atmospheric amount should have been escaped in the early past. However, the fractionation of argon and other noble gases such as neon is strongly dependent on the environmental conditions, in particular on temperature and altitude

of the exobase, which is in turn highly sensitive to the EUV flux of the early Sun.

Acknowledgements

H. Lammer, S. Dyadechkin, M. L. Khodachenko, M. Scherf, C. Johnstone and M. Guedel acknowledge support by the Austrian Science Fund (FWF): S11604-N16, S11606-N16, and S11607-N16. U.V. Amerstorfer and H. Lichtenegger are supported by the Austrian Science Fund (FWF): P24247-N16. I. Alexeev, M. Khodachenko, E. Belenkaya and D. Parunakian acknowledge the support of the Ministry of Education and Science of the Russian Federation Grant RFMEFI61617X0084.

EPSC Abstracts
Vol. 12, EPSC2018-697, 2018
European Planetary Science Congress 2018

An analytical climate model to reproduce first order, yearly-averaged, climatology on early Mars: implications for the ancient lakes in Gale crater

Alexandre Kling (1,2) Robert Haberle (1)
(1)Planetary Systems Branch, NASA Ames Research Center, Moffett Field, CA, USA
(2) Bay Area Environmental Research Institute, Moffett Field, CA, USA (alexandre.m.kling@nasa.gov)

Abstract

We provide an analytical "toy" model to reproduce the first order, yearly-averaged, latitudinal distribution of surface temperatures for Mars under different surface pressure, luminosity, eccentricity and obliquity. The model is intended to be used as a complementary tool to include the effect of meridional heat transport for one dimensional radiative studies (i.e. investing greenhouse warming for early Mars).

1. Introduction

Sedimentary deposits characterized by the Mars Science Laboratory *Curiosity* rover provide evidence that Gale crater, Mars intermittently hosted a fluvio-lacustrine environment during the Hesperian (∼3.8Gya). [1] However, no theory has been able to provide a robust and self-consistent way to maintain global mean temperature above the freezing point due to the low solar energy input available at that time (e.g. warming by CO_2 clouds [2], water ice clouds [3], dust [4], impacts [5], volcanism [6], reduced atmospheres [7]; [8], carbonate-silicate cycles [9]). While it has been challenging to raise the *global mean* temperature above the freezing point [10], it is possible that *equatorial* temperatures could have reached 273K. We address this possibility using an analytical, latitudinally-resolved climate model.

2. Model

We adapt one of the earlier methods originally developed to study the Earth climate [11] and use the analytical formulations for the annual mean insolation provided by [12]. We show that the yearly-averaged surface temperature is:

$$\overline{T_s}(x) = \frac{\varphi_0}{4\sqrt{1-e^2}}\left(\frac{Sa_0}{B}\right) - \frac{A}{B} + \frac{\varphi_0}{4\sqrt{1-e^2}}\left(\frac{Sa_2\ p_2(x)}{6D+B} + \frac{Sa_4\ p_4(x)}{20D+B}\right) \quad (1)$$

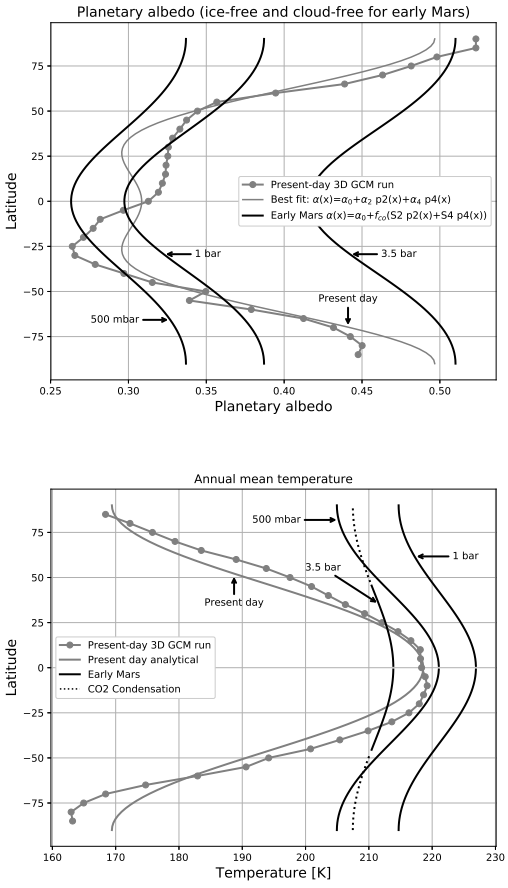

Figure 1: (Top) Zonally-averaged planetary albedo from the GCM (grey markers), best fit for present day Mars (grey line) and albedo distribution used for the early Mars predictions (black lines). (Bottom) Comparison of the mean annual temperature predicted by the NASA-Ames GCM (grey markers) with the analytical model calculation for present-day Mars (grey line), and analytical predictions for early Mars for different surface pressures (black lines).

with x the sine of the latitude, φ_0 the solar constant at Mars (e.g. $\frac{1370}{1.52^2}$ $W.m^{-2}$ for present day), e the eccentricity, D the diffusivity of the atmosphere in unit of $[W/m^2/K]$, A and B the outgoing longwave radiation (OLR) parameters such as $OLR = A + B\ T$. $p_n(x)$ are the Legendre polynomes and Sa_n the net solar insolation parameters, defined as:

$$\begin{cases} p_2(x) = \left(3x^2 - 1\right)/2 \\ p_4(x) = \left(35x^4 - 30x^2 + 3\right)/8 \\ S_{a0} = \frac{1}{5}S_2\alpha_2 + \frac{1}{9}S_4\alpha_4 + \alpha_0 \\ S_{a2} = S_2\alpha_0 + \frac{2}{7}S_2\alpha_2 + \frac{2}{7}S_2a4 + \frac{2}{7}S_4\alpha_2 + \frac{100}{693}S_4\alpha_4 + \alpha_2 \\ S_{a4} = \frac{18}{35}S_2\alpha_2 + \frac{20}{77}S_2\alpha_4 + S_4\alpha_0 + \frac{20}{77}S_4\alpha_2 + \frac{162}{1001}S_4\alpha_4 + \alpha_4 \\ S_2 = -\frac{5}{8}p_2(cos(\beta)) \\ S_4 = -\frac{9}{64}p_4(cos(\beta)) \end{cases} \quad (2)$$

where β is the obliquity, S_n the annually-averaged direct solar insolation parameters and α_n the coefficients used to parametrize the annually-averaged co-albedo as

$$\overline{\alpha}(x) = \alpha_0 + \alpha_2\ p_2(x) + \alpha_4\ p_4(x) \quad (3)$$

For present-day Mars we provide a direct fit to the NASA Ames General Circulation model (GCM) for the co-albedo: α_0=0.67, α_2=-0.095, α_4=-0.072. For early Mars, we propose to use $\alpha_0 = 1 - a_0$, $\alpha_2 = -f_a \times S_2$ and $\alpha_4 = -f_a \times S_4$ with a_0 a global mean value for the planetary albedo and f_a a parameter used to simulate the dependence of the albedo on the solar zenith angle. The albedo a_0, as well as the parameters f_a, A, and B are estimated using the NASA Ames radiative transfer code for a pure CO_2 atmosphere. Suggested values for these coefficients for present-day Mars and for 500mbar, 1 bar and 3.5bar ancient atmospheres are given in Table 1

3. Results

Figure 1 (bottom) shows that, given its simplicity, the analytical climate model (grey line) reproduces reasonably well the annually-averaged surface temperature from the GCM for present-day Mars (grey markers). For the 500 mbar atmosphere and for the 1 bar atmosphere, greenhouse warming and rather low values for the planetary albedo (see Figure 1 (top)) lead to surface temperatures warmer than present-day, despites a reduced solar luminosity (black lines in Figure 1 (bottom)). However, further increasing the surface pressure to 3.5 bar ultimately results in lower surface temperatures due to the increase in atmospheric scattering. The 3.5 bar case drops bellow the condensation temperature of CO_2 at high latitudes (dotted lines in Figure 1 (bottom)) so this solution is not stable against atmospheric collapse.

Pressure [mbar]	D	OLR=$A + B\ T$		Albedo	
		A	B	a_0	f_a
7	0.02	-212	1.54	(see text)	
500	0.46	-134	0.99	0.29	-0.111
1000	0.70	-72	0.66	0.33	-0.135
3500	1.28	13	0.23	0.45	-0.142

Table 1: Estimates for the diffusivity, outgoing longwave radiation at the top of the atmosphere, and planetary albedo as a function of the surface pressure

4. Summary and conclusions

The simple analytical climate model demonstrates that there is no obvious combination of orbital parameters nor greenhouse scenarios that would lead to annually-averaged surface temperature above 273K at the equator. This raises the possibility that the lacustrine environment at Gale crater may have subsisted during the Hesperian in the form of ice-covered lakes.

References

[1] J. P. Grotzinger *et al.*, "Deposition, exhumation, and paleoclimate of an ancient lake deposit, gale crater, mars," *Science*, vol. 350, Oct 2015.

[2] F. Forget *et al.*, "Modelling of the early martian climate under a denser co_2 atmosphere: temperatures and co_2 ice clouds," *Icarus*, vol. 222, pp. 81–99, 2013.

[3] R. Wordsworth *et al.*, "Global modelling of the early martian climate under a denser co2 atmosphere: Water cycle and ice evolution," *Icarus*, vol. 222, pp. 1–19, 2013.

[4] M. A. Kahre *et al.*, "The early maritian atmsophere: Investigating the role of the dust cycle in the possible maintenance of two stable climate states," *Journal of Geophysical Research: Planets*, vol. 118, pp. 1388–1396, 2013.

[5] T. L. Segura *et al.*, "An impact-induced, stable, runaway climate on mars," *Icarus*, vol. 220, pp. 144–148, July 2012.

[6] I. Havely and J. W. I. Head, "Episodic warming of early mars by punctuated volcanism," *Nature Geoscience*, vol. 7, pp. 865–868, 2014.

[7] R. M. Ramirez *et al.*, "Warming early mars with co2 and h2," *Nature Geoscience*, vol. 7, pp. 59–63, 2014.

[8] R. Wordsworth, Y. Kalugina, S. Lokshtanov, A. Vigasin, B. Ehlmann, J. Head, C. Sanders, and H. Wang, "Transient reducing greenhouse warming on early mars," *Geophysical Research Letters*, vol. 44, no. 2, pp. 665–671, 2017, 2016GL071766. [Online]. Available: http://dx.doi.org/10.1002/2016GL071766

[9] N. E. Batalha *et al.*, "Climate cycling on early mars caused by the carbonate-silicate cycle," *Earth and Planetary Science Letters*, vol. 455, pp. 7–13, 2016.

[10] J. F. Kasting, "co_2 condensation and the climate of early mars," *Icarus*, vol. 94, pp. 1–13, 1991.

[11] G. R. North, "Analytical Solution to a Simple Climate Model with Diffusive Heat Transport." *Journal of Atmospheric Sciences*, vol. 32, pp. 1301–1307, Jul. 1975.

[12] A. Nadeau and R. McGehee, "A simple formula for a planet's mean annual insolation by latitude," *Icarus*, vol. 291, pp. 46 – 50, 2017.

EPSC Abstracts
Vol. 12, EPSC2018-708, 2018
European Planetary Science Congress 2018

Creating *a priori* atmospheres from GEM-Mars GCM for the investigation of Mars

Justin Erwin (1), Lori Neary (1), Frank Daerden (1), Sébastien Viscardy (1), Shohei Aoki (1,2,3), Séverine Robert (1), Ann Carine Vandaele (1)
(1) Royal Belgian Institute for Space Aeronomy (BIRA-IASB), Brussels, Belgium, (2) Fonds National de la Recherche Scientifique, Belgium, (3) Tohoku University, Japan. (jt.erwin@aeronomie.be)

Abstract

We present a set of *a priori* atmospheric number densities for the atmosphere of Mars derived from the GEM-Mars GCM. The latitude, time of day, and season are binned in a way relevant to the Martian atmosphere and the nature of the retrieval geometries expected. We explore different statistical bin definitions, ways to incorporate the surface height (which vary much more on Mars than on Earth) and areoid, and the correct way to incorporate the mean and variance under the Bayesian framework used in the retrievals (i.e. Rodgers' methods [1]).

1. Bayesian Retrievals

Most of current retrieval algorithms, such as those based on Optimal Estimation Method [2, 3], do need a priori information on the variables to be retrieved. For example, BIRA-IASB will be using the in house developed ASIMUT program [4] to perform the spectroscopic retrievals of molecular and aerosol number densities. One aspect of these methods is the incorporations on *a priori* constraints of a mean and variance number densities profiles for each atmospheric species, including molecules and aerosols. For our purposes, we choose to construct a set of *a priori* states from the GEM-Mars GCM, developed at BIRA-IASB, since we can have full coverage geographical and temporally (time of day and year).

GEM-Mars is a General Circulation Model for the atmosphere of Mars with online atmospheric chemistry. The model is operated on a grid with a horizontal resolution of 4°x4° and with 103 vertical levels reaching from the surface to ~150 km. It calculates atmospheric heating and cooling rates by solar and IR radiation through atmospheric CO and dust and ice particles and solves the primitive equations of atmospheric dynamics. Geophysical boundary conditions are taken from observations. Physical parameterizations in the model include an interactive condensation/surface pressure cycle, a fully interactive water cycle including cloud radiative feedbacks, a thermal soil model including subsurface ice, interactive dust lifting schemes for saltation and dust devils, turbulent transport in the atmospheric surface layer and convective transport inside the planetary boundary layer (PBL), subgrid scale vertical mixing in the free troposphere, a low level blocking scheme, gravity wave drag, molecular diffusion, non-condensable gas enrichment, and atmospheric chemistry. A detailed description of the model, its formulation, grid, dynamical core and physical parameterizations, together with extensive validation against multiple datasets, was given in [5], and further details can be found in [6, 7, 8].

2. Methods

The data set from GEM Mars used in the construction of the *a priori* is comprised of 48 time steps per day, 36 days per year (every 10° L_s). Every day of the year is available, but the above subset is already 500GB, and is should provide sufficient enough coverage to be representative of the Martian atmosphere. Various combination of bins in L_s (e.g. seasons), Latitude (e.g. North-, South-, Mid-latitudes, etc), and Time of Day (e.g. Day, Night, Dusk, Dawn, etc.) are made available for individual applications.

The GEM-Mars uses a surface height at each grid point that is an averaged surface height derived from the well accepted MOLA data set [9], although the solutions themselves are given in terms of height above the surface. By adding the surface height before averaging, the altitude grid is given relative to the areoid. We compare three different options how to do this:

1. Interpolate onto a common grid.

2. Average into vertical bins, with each altitude given equal weight.

3. Average into vertical bins, with weighting proportional to altitude grid resolution.

Each of the above options has its trade-offs, which we will discuss in reference to the retrievals.

When reporting the mean and average, it is convenient to compute in terms of mixing ratio, because it is generally not exponential with altitude like number density. ASIMUT's forward model is to simulate spectra using the number density, which is computed using the mean mixing ratio times some representative total number density. But the variance of the mixing ratio under-represents the variance in the number density, especially for the the main constituents. We compute the relative standard deviation of the number density for each species, and use this with the mean mixing ratio for the species and a total atmosphere number density (which is derived separately, see our other presentation on *Interpolated Atmospheres*).

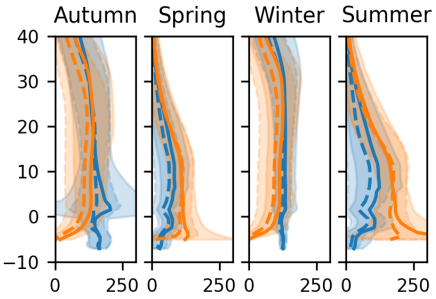

Figure 1: Example mean water vapor mixing with shaded standard deviation (in PPMV) versus z (in km). Northern hemisphere is blue, southern hemisphere is orange.

3. Summary and Conclusions

The *a priori* atmospheres derived from the GEM-Mars model will be used during the retrievals of NOMAD observations will be computed using ASIMUT. Our decision to incorporate the surface height and average each profiles into vertical bins with weighting proportional the altitude resolution (option 2c above) means that the altitude scale is relative to the areoid so that we can compare pressure levels easily across the planet. We decrease our bias towards the near surface atmosphere, which means the retrievals will be less constrained by the *a priori* in the lower atmosphere and more constrained by the data itself.

Acknowledgements

This project acknowledges funding by the Belgian Science Policy Office (BELSPO), with the financial and contractual coordination by the ESA Prodex Office (PEA 4000121493), and by the FNRS CRAMIC project under grant number T.0171.16. The research was performed as part of the "Excellence of Science" project "Evolution and Tracers of Habitability on Mars and the Earth" (FNRS 30442502).

References

[1] Rodgers, C. D., Inverse Methods for Atmospheric Sounding: Theory and Practice, World Sci., Rivers Edge, N. J., 2000.

[2] Rodgers, C.D., Characterization and Error Analysis of Profiles Retrieved From Remote Sounding Measurements. J. Geophys. Res., 1990. 95(D5): p. 5587-5595.

[3] Connor, B. and C. Rodgers. A comparison of retrieval methods: optimal estimation, onion-peeling and a combination of the two. in RSRM 87. 1989. Advances in Remote Sensing retrieval methods, A. DEEPAK Publishing.

[4] Vandaele, A. C., Kruglanski, M., De Mazière, M., Modeling and retrieval of atmospheric spectra using ASIMUT. Proceedings of the First Atmospheric Science Conference, ESRIN, Frascati, Italy, 2006.

[5] Neary, L., and F. Daerden (2018), The GEM-Mars General Circulation Model for Mars: Description and Evaluation, Icarus, 300, 458-476, https://doi.org/10.1016/j.icarus.2017.09.028

[6] Daerden, F., J. A. Whiteway, L. Neary, L. Komguem, M. T. Lemmon, N. G. Heavens, B. A. Cantor, E. Hébrard, and M. D. Smith (2015), A solar escalator on Mars: Self-lifting of dust layers by radiative heating. Geophys. Res. Lett., 42, 73197326.doi:10.1002/2015GL064892

[7] Viscardy, S., F. Daerden, and L. Neary (2016), Formation of layers of methane in the atmosphere of Mars after surface release, Geophys. Res. Lett., 43, 5, 1868-1875, doi:10.1002/2015GL067443.

[8] Smith, M., F. Daerden, L. Neary and S. Khayat (2018), The climatology of carbon monoxide and water vapor on Mars as observed by CRISM and modeled by the GEM-Mars general circulation model, Icarus, 301, 117-131, https://doi.org/10.1016/j.icarus.2017.09.027

[9] Smith, D. E., et al. (1999). The Global Topography of Mars and Implications for Surface Evolution, Science, 284 (5419), 1495–503, doi:10.1126/science.284.5419.1495.

EPSC Abstracts
Vol. 12, EPSC2018-717, 2018
European Planetary Science Congress 2018

Creating high-spatial resolution atmospheric profiles from the GEM-Mars GCM for the investigation of Mars

Justin Erwin, Lori Neary, Frank Daerden, Sébastien Viscardy, Ann Carine Vandaele
Royal Belgian Institute for Space Aeronomy (BIRA-IASB), Brussels, Belgium, (jt.erwin@aeronomie.be)

Abstract

It is necessary for GCMs to operate on a coarse resolution grid, especially when simulating an entire planet for long durations. But there are many circumstances when one desires the solution at much higher resolutions. In this work, we present our methods to interpolate the GEM-Mars GCM solution to higher resolutions in Latitude and Longitude, as well as time of day and time of year. A principle motivation of this work it to provide high-resolution approximations of the Martian atmosphere to be used during spectroscopic retrieval for the investigation of Mars.

1. GEM-Mars

GEM-Mars is a General Circulation Model for the atmosphere of Mars with online atmospheric chemistry. The model is operated on a grid with a horizontal resolution of 4°x4° and with 103 vertical levels reaching from the surface to ~150 km. It calculates atmospheric heating and cooling rates by solar and IR radiation through atmospheric CO and dust and ice particles and solves the primitive equations of atmospheric dynamics. Geophysical boundary conditions are taken from observations. Physical parameterizations in the model include an interactive condensation/surface pressure cycle, a fully interactive water cycle including cloud radiative feedbacks, a thermal soil model including subsurface ice, interactive dust lifting schemes for saltation and dust devils, turbulent transport in the atmospheric surface layer and convective transport inside the planetary boundary layer (PBL), subgrid scale vertical mixing in the free troposphere, a low level blocking scheme, gravity wave drag, molecular diffusion, non-condensable gas enrichment, and atmospheric chemistry. A detailed description of the model, its formulation, grid, dynamical core and physical parameterizations, together with extensive validation against multiple datasets, was given in [4], and further details can be found in [5, 6, 7].

2. Methods

BIRA-IASB will be using the in house developed ASIMUT program [1] to perform the spectroscopic retrievals of molecular and aerosol number densities based on the Optimal Estimation Methods [2, 3]. In addition to using mean atmospheric compositions as *a priori* constraints (see presentation by Erwin et al. on "Creating *a prior* atmospheres from GEM-Mars"), the retrieval process requires vertical temperature and pressure profiles on which to compute cross sections. For each observation, we need to compute vertical profiles which corresponds to the geographical and temporal circumstances of each observation.

2.1. Geographic Interpolation

The data set from GEM Mars used in the construction of the interpolated atmospheres is comprised of 48 time steps per day, 36 days per year (every 10° L_s). Every day of the year is available, but the above subset is already 500GB, and is should be sufficiently representative of the Martian atmosphere.

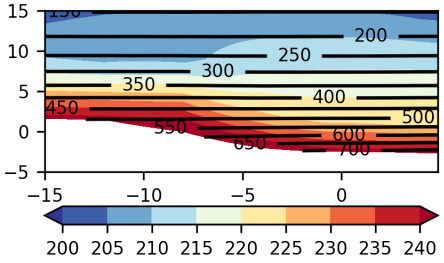

Figure 1: Gale crater using geographic interpolation. Temperature is colored contours (in Kelvin) and pressure levels are the contour lines (in Pascal).

For a particular Latitude and Longitude, a bi-linear spherical interpolation is performed to interpolate the bounding GCM grid points to the particular value.

Next, for a particular L_s and Local Solar Time (LST), we must interpolate in time using the time steps in a day, and days in L_s. First, we use a 4 point Lagrange interpolation in LST for each day. Second, we use a 4 point Lagrange interpolation in L_s (effectively using 16 points in a split, 2D interpolation).

2.2. Surface Height Correction

The interpolation from GEM produces a linear variation in surface height between GEM-Mars grid points. The surface of Mars has much more structure over this range, and we can use the MOLA data set [8] to get an improved value for the surface height. Yet, a simple offset or extrapolation using this new height would incorrectly interpret the upper or lower atmosphere.

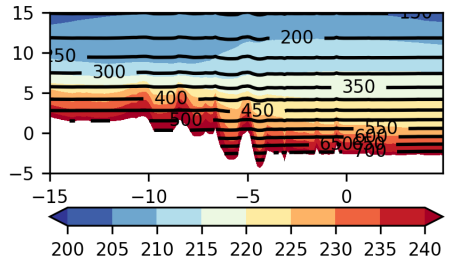

Figure 2: Gale crater with surface height correction.

Instead, we use a pressure scaling similar to the one discussed with in the MCD User's Guide [9]. Potentially, this correctly estimates the surface pressure, near surface structure, and upper atmosphere pressure relative to the areoid.

An additional step is to adjust the near surface pressure to adapt for the change in surface height. One option is to use the adiabatic lapse rate to adapt for the change in altitude, or we can instead use an averaged temperature profile (i.e. the *a priori* atmosphere) to interpret a change in temperature.

3. Summary and Conclusions

The interpolation detail in this work can be used to interpolate the GEM-Mars GCM solutions to any geometric or temporal parameters, extending the usefulness of the model. Correcting the surface height and pressure scaling produce a desirable vertical profile that ASIMUT can use to compute spectra.

Acknowledgements

This project acknowledges funding by the Belgian Science Policy Office (BELSPO), with the financial and contractual coordination by the ESA Prodex Office (PEA 4000121493). The research was performed as part of the "Excellence of Science" project "Evolution and Tracers of Habitability on Mars and the Earth" (FNRS 30442502).

References

[1] Vandaele, A. C., Kruglanski, M., De Mazière, M., Modeling and retrieval of atmospheric spectra using ASIMUT. Proceedings of the First Atmospheric Science Conference, ESRIN, Frascati, Italy, 2006.

[2] Rodgers, C.D., Characterization and Error Analysis of Profiles Retrieved From Remote Sounding Measurements. J. Geophys. Res., 1990. 95(D5): p. 5587-5595.

[3] Rodgers, C. D., Inverse Methods for Atmospheric Sounding: Theory and Practice, World Sci., Rivers Edge, N. J., 2000.

[4] Neary, L., and F. Daerden (2018), The GEM-Mars General Circulation Model for Mars: Description and Evaluation, Icarus, 300, 458-476, https://doi.org/10.1016/j.icarus.2017.09.028

[5] Daerden, F., J. A. Whiteway, L. Neary, L. Komguem, M. T. Lemmon, N. G. Heavens, B. A. Cantor, E. Hébrard, and M. D. Smith (2015), A solar escalator on Mars: Self-lifting of dust layers by radiative heating. Geophys. Res. Lett., 42, 73197326.doi:10.1002/2015GL064892

[6] Viscardy, S., F. Daerden, and L. Neary (2016), Formation of layers of methane in the atmosphere of Mars after surface release, Geophys. Res. Lett., 43, 5, 1868-1875, doi:10.1002/2015GL067443.

[7] Smith, M., F. Daerden, L. Neary and S. Khayat (2018), The climatology of carbon monoxide and water vapor on Mars as observed by CRISM and modeled by the GEM-Mars general circulation model, Icarus, 301, 117-131, https://doi.org/10.1016/j.icarus.2017.09.027

[8] Smith, D. E., et al. (1999). The Global Topography of Mars and Implications for Surface Evolution, Science, 284 (5419), 1495–503, doi:10.1126/science.284.5419.1495.

[9] Millour, E., Forget, F., Lewis, S. R. (2015), Mars Climate Database v5.2 User Manual, `http://www-mars.lmd.jussieu.fr/mars/info_web/user_manual_5.2.pdf`.

EPSC Abstracts
Vol. 12, EPSC2018-734, 2018
European Planetary Science Congress 2018

Study of the deuterium Lyman-alpha emission observed with the "low resolution mode"of MAVEN/IUVS

J-Y. Chaufray[1], M. Mayyasi[2], M.Chaffin[3], J. Clarke[2], J. Deighan[3], S. Jain[3] , D. Bhattacharyya[2], N. Schneider[3] and B. Jakosky[3], [1]LATMOS/IPSL (chaufray@latmos.ipsl.fr), CNRS, UPMC, UVSQ, [2]Center for Space Physics, Boston University, [3]LASP, University of Colorado

Abstract

We studied a set of observations of the Lyman-α profile by MAVEN/IUVS using the low resolution mode. The brightness profile in the lower corona, especially the bright limb, is best reproduced with a deuterium population during the southern summer as expected from the high resolution echelle mode observations. Therefore it is possible to derive information on the atomic deuterium density at this season not only from the echelle mode but also from the coarser spectral resolution.

1. Introduction

The recent observations performed with the "echelle mode" by the Imaging Ultraviolet Spectrograph (IUVS) aboard the Mars Atmosphere and Volatile EvolutioN (MAVEN) mission indicated large deuterium brightness near Ls=270° [1]. The deuterium brightness observed at the beginning of the mission, when Mars was close to its perihelion show brightness ~ 1 kR much larger than the first deuterium detection from Earth ~ 20-50 R [2]. During this period, especially near the terminator, the Lyman-α emission observed at 121.6 nm with the "low resolution mode" present some vertical profiles that were not reproducible with models that simulated only the emission from the thermal hydrogen population [3], that are expected to dominate at the observed altitudes. In this study we investigate the possible contribution of the deuterium Lyman-α emission to explain the vertical brightness profile in these observations.

2. Observations

A vertical average of few individual profiles of the emission at 121.6 nm observed by both "low resolution mode" and the echelle mode for a very close geometry of limb observations near the terminator on the end of December 2016 (Ls ~ 285-290) is displayed on Fig. 1. This profile indicates that the strong bright limb near ~ 120 km observed with the "low resolution mode" is mainly due to the deuterium emission and consistent with the observations obtained with the echelle mode.

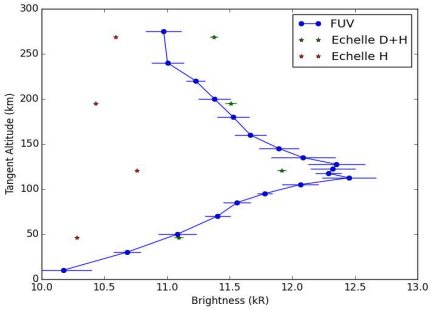

Fig. 1 Comparison between the Lyman-α average profile observed by the "low resolution mode" (blue line) and the average H (red dots) and H+D brightness profile (green dots) obtained at the same time and with similar geometry with the echelle mode.

Such bright limbs are observed systematically at other periods, where no limb observations with the echelle mode are available (from Dec 2014 to March 2015) and are not attributed to proton aurora that are observed only sporadically and characterized by short time scale increases of the brightness [4].

At other periods (for example July 2015), the deuterium emission observed with the echelle mode was much weaker [1]. The vertical profiles of the 121.6 nm brightness observed during this period with the "low resolution mode" do not present a

substantially bright limb (Fig. 2), showing correlation between the presence of a bright limb observed with the "low resolution mode" and the detection of a substantial deuterium emission with the echelle mode.

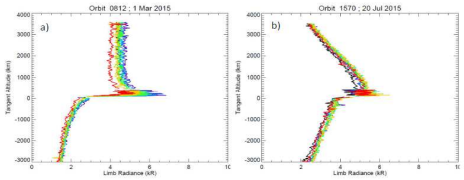

Fig. 2 Vertical profile of the 121.6 nm emission observed from the full outbound observations (disk and coronal scans) by IUVS for orbit 812. Each color represents the profile for one spatial bin. 1b) Same as figure 1a but for an orbit where no strong deuterium emission was detected with the echelle mode. The profile between 100 and 800 km is flat and doesn't present a bright limb.

3. Modeling

Hydrogen produced by the photodissociation of water vapor at ~80 km has been recently suggested to be an important source of atomic hydrogen in the Martian thermosphere near southern summer [5]. In that case, the hydrogen density profile should differ from the density profile simulated from the ionospheric H_2 + CO_2^+ only, due to a lower altitude of production. We will also present the effect on the derived D and H density profiles.

A model including both the H and D Lyman-α emissions provides a better fit to the observations in the lower corona below 500 km, as shown in Fig. 3. The relative D and H brightnesses are in reasonable agreement with the echelle brightnesses from the average profile (Fig. 1).

Therefore, it is possible to use the "low resolution mode" observations to complete the derivation of the D and H density profile near Ls= 270°.

The D and H density derived from the low resolution mode of IUVS observations and the local time variations will be presented.

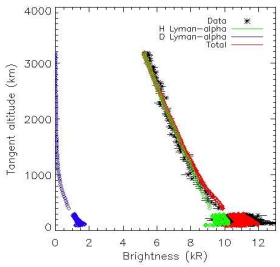

Fig. 3 Example of observed Lyman-α profile during orbit 4352 (Ls =286°, SZA ~ 84-90°) and the derived best fit, for an exospheric temperature of 200 K and an arbitrary interplanetary background of 500R.

References:

[1] Clarke J.T., Mayyasi, M., Batthacharyya, D., Schneider, N.M., McClintock, W.E., Deighan, J., Stewart, A.I.F, Chaffin, M.S., Jain, S., Stiepen, A., Crismani, M., Holsclaw, G.M., Montmessin, F., Jakosky, B.M., Variability of D and H in the Martian upper atmosphere observed with the MAVEN IUVS echelle mode, *J. Geopys. Res.*, 122 ; 2336-2344, 2017 [2] Krasnopolsky, V., Mumma, M. J., Gladstone G.R., Detection of atomic deuterium in the upper atmosphere of Mars, 1998, *Science*, 280, 1576 , [3] Chaffin, M., Chaufray, J-Y., Deighan, J., Schneider, N.M., McClintock, W.E., Thiemann, E., Clarke, J.T., Holsclaw, G.M., Jain, S., Crismani, M., Montmessin, F., Eparvier, F.G., Chamberlain, P.C., Jakosky; B. (2015), Three dimensional structure in the Mars H corona revealed by IUVS on MAVEN, *Geophys Res. Lett*, 42, 9001-9008, [4] Deighan et al., (2017), *Int Mars Aeronomy conf.*, Boulder. ; [5] Chaffin, M., Deighan, J., Schneider, N.M., Stewart, A.I.F, elevated atmospheric escape of atomic hydrogen from Mars induced by high altitude water (2017), *Nat Geosci*, 10, 174-178

Ackowledgements:

J-Y Chaufray is supported by CNES

EPSC Abstracts
Vol. 12, EPSC2018-777, 2018
European Planetary Science Congress 2018

Migration of intermediately-sized particles across the Martian surface

Mark Paton (1), Hannu Savijärvi (2) and Ari-Matti Harri (1)
(1) Finnish Meteorological Institute, Helsinki, Finland, (2) University of Helsinki, Finland (mark.paton@fmi.fi)

Abstract

Investigations of the sedimentary processes on Mars are often related to the saltation of sand particles or the long-term suspension of dust particles or a combination of both. A small proportion of particles on Mars will have an intermediate size between sand and dust close to the saltation/suspension transition region. The repeated ejection and suspension of such particles into Planetary Boundary Layer over long periods of time may then produce the accumulation of particles in specific regions on Mars that could be verified by observations. Such regions, if they exist could then help us understand the past and present Martian climate.

To investgate the transport of the particles we use a trajectory model combined with wind field data imported from the Mars Climate Database to visualise the transport of material across the surface of Mars. The result is similar to adding tracers into a numerical weather model but without having to run the whole simulation. The technique described here produces useful results very quickly and allows physically based modelling of the particle trajectories.

1. Introduction

Detailed observations of the Martian sedimentary cycle on Mars by orbital and landed spacecraft suggest a surprisingly active sedimentary cycle [1,2]. For example high resolution images from orbit have observed mobile sand dunes. Visually tracking of mobile particles in Gale Crater by Curiosity has been used to observe wind activity [3].

2. Background

A trajectory model, such as previously used to model the descent of spacecraft in a windy Martian atmosphere [4], can be used to realistically model the motion of objects in the PBL. Global wind fields are available from the Mars Climate Database (MCD) as shown in figure 1.

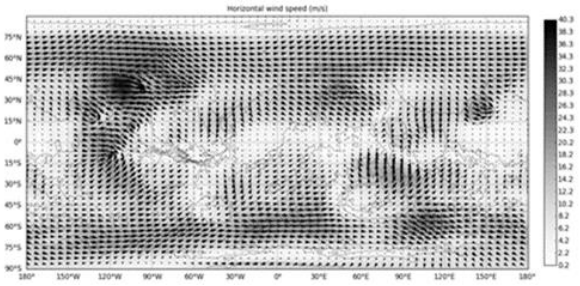

Figure 1: An example of a MCD wind field used for the trajectory calculations. It is not obvious the path, a wind blown particle released at an arbitrary location, would take by just looking at the wind data.

3. Investigation methodology

A spacecraft Entry, Descent and Landing trajectory model is used to calculate the horizontal transport and dispersion of particles in the size range of 20 to 100 μm, i.e. corresponding to the saltation/suspension transition particle size, by Planetary Boundary Layer (PBL) winds. Horizontal winds are imported into the model from the Mars Climate Database. The time of day is fixed for all longitudes.

Particles spread across the globe are then ‘released’ simultaneously in the modelled atmosphere. The particles are suspended for one Martian hour before falling to the surface. The wind field is not, at the moment, dynamically updated as time progresses. The following Martian day the particles are suspended at the same time as the previous day. Their trajectories, starting from the previous day’s location, are then calculated. Particles are initially released at longitudes and latitudes covering the entire Martian globe.

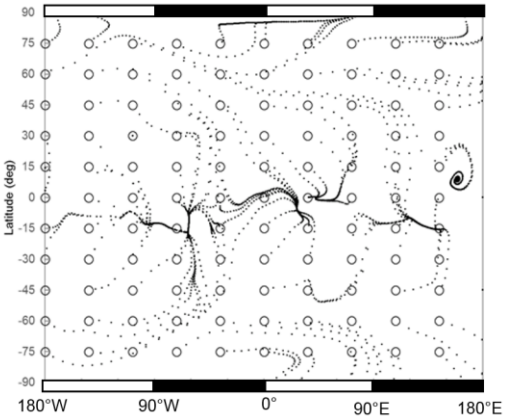

Figure 2: Paths of particles blown by winds at an altitude of between 10 and 500 m. There are 10000 ejection-descent events for each of the 110 particles modelled. During each event the particle is suspended in the atmosphere for one hour. The particle locations are plotted every 100 iterations of the trajectory model. Longitude is plotted along the x-axis. All atmospheric properties are kept constant except the wind during the model runs.

4. Summary

Maps of the paths taken by intermediately-sized particles across the Martian surface can be generated such as shown in figure 2. The maps are calculated by successfully combining the trajectory model in [4] with wind fields imported from the Mars Climate Database.

Some interesting observations so far:

- The PBL winds, in the model, blow material from the mid-latitudes to just south of the equator.
- The accumulation of PBL blown material coincides to the northern boundary of the belt of low albedo material around Mars.
- At high latitudes material in the model is blown towards towards the poles.
- There depleted zones around the mid-latitudes in the modelling results.

References

[1] Kok, J., Planetary science: Martian sand blowing in the wind, Nature, Vol. 485, pp. 312-313, 2012.

[2] Sullivan, R. and Kok, J. F., Aeolian saltation on Mars at low wind speeds, Journal of Geophysical Research: Planets, Vol. 122, pp. 2111-2143, 2017.

[3] Baker, M. M., Newman, C. E. N., Lapotre M. G. A., Sullivan, R., Bridges, N. T., and Lewis, K. W., Coarse sediment transport in the modern Martian environment, Journal of Geophysical Research: Planets, doi: 10.1002/2017je005513, 2018

[4] Paton, M. D., Harri, A. -M., and Savijärvi, H., Measurement of Martian boundary layer winds by the displacement of jettisoned lander hardware, Icarus, Vol. 309, pp. 345-362, 2018.

EPSC Abstracts
Vol. 12, EPSC2018-810, 2018
European Planetary Science Congress 2018

Venus' Meridional wind flow from: Akatsuki/UVI, Venus Express/VIRTIS, TNG/HARPS-N and CFHT/ESPaDOnS

Pedro Machado (1), T. Widemann (2), J. Peralta (3), R. Gonçalves (1), M. Takagi (4), A. Harutyunyan (5), Y. J. Lee (3), G. Gilli (1), S. Watanabe (6), T. Satoh (3), K. Ogohara (7) and A. Yamazaki(3)
(1) Institute of Astrophysics and Space Sciences, Lisboa, Portugal, (2) LESIA-Laboratoire d'Etudes Spatiales et d'Instrumentation en Astrophysique, Observatoire de Paris, France, (3) Institute of Space and Astronautical Science - Japan Aerospace Exploration Agency (JAXA), Japan, (4) Faculty of Science, Kyoto Sangyo University, Kyoto, Japan, (5) Telescopio Nazionale Galileo, TNG, and Italian Instituto Nazionale di Astrofisica (INAF), (6) Hokkaido Information University, Japan, (7) School of Engineering, University of Shiga Prefecture, Japan

Abstract

We will present meridional wind flow results in both Venus hemispheres. We will present, and compare, meridional wind measurements obtained from Akatsuki's space probe (JAXA) observations, namely observations taken with the UVI instrument, and simultaneous coordinated observations obtained with HARPS-N at *Telescopio Nazionale Galileo* (TNG) in January 2017. We will also compare this new results with meridional wind flow results from previous runs using space-based observations from Venus Express (ESA) with the instrument VIRTIS-M, and ground-based observations at Canada-France-Hawaii Telescope (CFHT) with the high-resolution spectrograph ESPaDOnS (Machado et al. 2014; 2017). Our previous sets of coordinated observations at Venus cloud-tops were based in two complementary techniques: Ground-based Doppler velocimetry and cloud-tracked winds using VEx/VIRTIS-M imaging at 0.38 μm. Cloud-tracked winds trace the true atmospheric motion also responsible for the Doppler-Fizeau shift of the solar radiation on the dayside by super-rotating moving cloud-tops with respect to both the Sun and the observer (Machado et al., 2014; 2017). Based on this complementarity, we performed a new coordinated campaign in January 2017, where HARPS-N (TNG) was used for the first time in order to perform atmospheric studies in a Solar System's planet, these observations where combined with simultaneous Akatsuki/UVI space-based observations. The ground-based observations undertaken at HARPS-N/TNG (La Palma) allowed us to obtain very high-resolution spectra (R$\sim$ 115 000) and retrieve Doppler wind measurements on the dayside of Venus' cloud tops. The observational results will be compared with the ground-to-thermosphere 3D model developed at the Laboratoire de Meteorologie Dynamique in Paris (Gilli et al. 2017).

1. Meridional wind at cloud tops

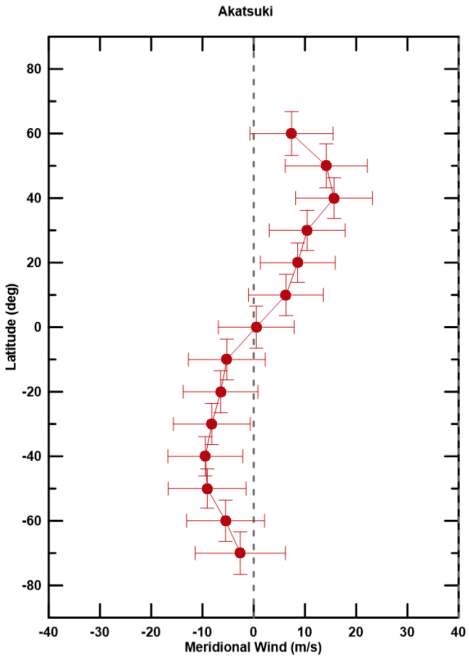

Figure 1: Mean meridional wind latitudinal profile from Akatsuki/UVI results. Weighted average of all the latitudinal profiles of all days, with a binning of 5 degrees latitude

From space, clouds features were tracked on image pairs obtained by the Akatsuki UVI operating in the

ultraviolet range (365 nm filter) and with a temporal interval of 2 hours. Ultraviolet images show the highest contrast features and the UV tracers are roughly located at about 65-70 km above the surface [1] Venus Express cloud top wind measurements based on tracking using images taken with the VIRTIS instrument [3, 9] followed the same method as the one described for retrieving cloud-tracked winds based on Akatsuki's observations. Along the observations with the high-resolution spectrograph HARPS-N the angular diameter of Venus was 14,98" (FOV of HARPS-N is 1"), the complete optical spectrum, from 383 to 690 nm, is collected over 40 spectral orders in a single exposure at a resolution of about 115,000, and with ESPaDOnS at CFHT, the complete optical spectrum, from 370 to 1050 nm, was collected also over 40 spectral orders in a single exposure at a resolution of about 80,000. In the single scattering approximation, the Doppler shift measured in solar light scattered on Venus dayside is the result of two instantaneous motions: (1) a motion between the Sun and Venus upper clouds particles, which scatter incoming radiation in all directions including the observer's [4, 5, 6]; this Doppler velocity is minimal near Venus sub-solar point; (2) a motion between the observer and Venus clouds, resulting from the topocentric velocity of Venus cloud particles in the observer's frame; this effect is minimal near Venus sub-terrestrial point. The Doppler shift related to horizontal motions parallel to equator vanishes at the half phase angle meridian (HPA), where both terms cancel each other [5, 6] and we took advantage of the fact that it is not possible to measure the zonal wind along the HPA in order to measure the meridional wind flow along this meridian [5, 6].

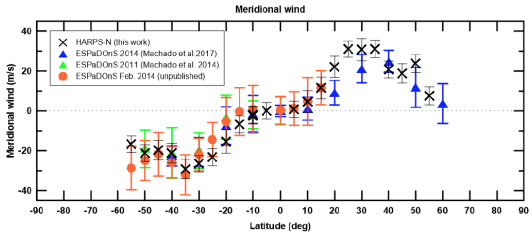

Figure 2: Comparison of meridional wind results retrieved from different observations and telescopes/ instruments, using the Doppler velocimetry technique. The legend of the figure refers the instrument used, date of observations and respective scientific article.

The analysis and results show (1) additional confirmation of the the coherence, and complementarity, in the results provided by these techniques, on both spatial and temporal time scales of the two methods; (2) first-time estimation of the meridional component of the wind in other planet using the Doppler velocimetry technique, with evidence of a symmetrical, poleward meridional Hadley flow in both hemispheres.

Acknowledgements

We gratefully acknowledge the collaboration of the Akatsuki team, of the TNG staff at La Palma (Canary Islands, Spain). We thank the VIRTIS/Venus Express team for support with coordinated observations. This work was supported by FCT (ref. UID/FIS/04434/2013) through national funds and by FEDER through COMPETE2020 (ref. POCI-01-0145-FEDER-007672).

References

[1] Esposito, L. et al., Venus III, Bougher, Hunten and Philips Eds., Sp. Sci. Ser., Arizona U. Press, pp. 415, 1997.

[2] Gilli G. et al. 2017, Icarus, Vol. 281, pp. 55-72.

[3] Hueso, R., Peralta, J., Sànchez-Lavega, A., Icarus, Vol. 217, pp. 585-598, 2012.

[4] Machado, P., Luz, D. Widemann, T., Lellouch, E., Witasse, O, Icarus, Vol. 221, pp. 248-261, 2012.

[5] Machado, P., Widemann, T., Luz, D., Peralta, J., Icarus, 2014.

[6] Machado, P., Widemann, T., Luz, D., Peralta, J., Icarus, 2017.

[7] Peralta, J., Hueso, R. and Sanchez-Lavega, A., Icarus, Vol. 190, pp. 469, 2007.

[8] Rossow, W. B., Del Genio, A. D. and Eichler, T., Journal of Atmospheric Sciences, Vol. 47, pp. 2053, 1990.

[9] Sanchez-Lavega et al., Geophys. Res. Lett., Vol. 35, L13204, 2008.

[10] Tavenner, T. et al., Planetary Space Sciences, Vol. 56, pp. 1435, 2008.

[11] Widemann, T. et al., Planetary and Space Science, Vol. 55, pp. 1741-1756, 2007.

[12] Widemann, T. et al., Planetary and Space Science, Vol. 56, pp. 1320-1334, 2008.

[13] Young, E. et al., Bull. Am. Ast. Soc., Vol. 40, pp. 513, 2008.

EPSC Abstracts
Vol. 12, EPSC2018-811, 2018
European Planetary Science Congress 2018

Martian CO and wind measurements from ALMA observations

Séverine Robert (1), Hideo Sagawa (2), Ann Carine Vandaele (1) and Shohei Aoki (1, 3, 4)
(1) Royal Belgian Institute for Space Aeronomy, BIRA-IASB, Belgium, (2) Kyoto Sangyo University, Japan, (3) Fonds National de la Recherche Scientifique, FRS-FNRS, Belgium, (4) Tohoku University, Japan, (severine.robert@aeronomie.be)

Abstract

The Earth-based Atacama Large Millimeter/Submillimeter Array (ALMA) telescope is a state-of-the-art interferometer in the sub-mm spectral range, which combines unprecedented spatial resolution and high sensitivity[1]. It is well suited to acquire global measurements of the thermal emission from planetary atmospheres, and its high-spectral resolution allows to measure the Doppler shifts of molecular lines due to wind velocity. Observations of the martian disk were done in May 2014 at the ALMA Observatory. The objective of the observations was to map the full disk at frequencies enabling the detection of CO, HDO and H_2O_2 absorption lines. As CO is optically thick, the temperature profiles may be derived, which is of great interest, as temperature profiles and wind fields in the Martian atmosphere are still incompletely mapped at the planetary scale. To perform this investigation, ASIMUT-ALVL, the BIRA-IASB Radiative Transfer code was used. The reduction and calibration of the interferometric data will be presented. We will also describe the modifications we did to the code and the sensitivity studies we performed beforehand. Hopefully, the global distributions of the thermal and dynamical structure of the atmosphere will be discussed.

1. ALMA observations

As summarized in Table 2, four spectral windows at the frequencies of 335 and 345 GHz (which fall in the ALMA Band-7 receiver) were selected. The heterodyne receivers of ALMA enable the frequency resolution as high as 122 kHz (corresponding to $\sim$ 100 m/s in velocity), which should allow to measure the Doppler - wind shift. An overview of the observations is presented in Table 1 and Table 2. The values given in Table 2 are identical for both observations presented in Table 1.

[1] http://www.almaobservatory.org/en/home/

Table 1: Overview of the observations.

	01 May 2014 4:40	18 May 2014 4:59
MY	32	32
L_S	123.9°	132.1°
Diameter of Mars	14.54"	14.53"
Angular resolution	0.65" (20x20)	1.09" (13x13)
Integration time (min)	44	20
Number of antennas	34	34
Maximum baseline length (m)	558	650

Table 2: Overview of the observations' frequencies

Nb.	Spectral range (GHz)	Resolution (kHz)	Target Species
0	345.31-346.25	969	CO wide range
1	345.67-345.90	122	CO line center
2	335.16-335.63	282	HDO
3	335.08-336.02	969	HDO + H_2O_2

The measured data (i.e. visibilities) were calibrated for the phase fluctuation and flux amplitude. The spectral bandpass characteristics were also corrected. Once the visibilities were calibrated, the radio images (spectral image cubes) were synthesized using the CLEAN procedure. This procedure removes the artefact emission features due to an imperfect visibility sampling on (u,v) spatial frequency domain. Fig. 1 shows the continuum emission image before and after the CLEAN procedure. The image is reconstructed as a 512 x 512

pixel image with a pixel scale of 0.1 arcsec.

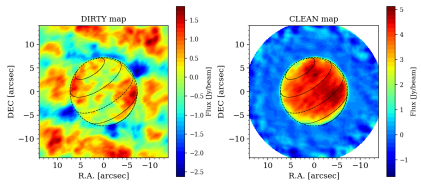

Figure 1: Mars continuum emission map at 335 GHz observed with ALMA. The dirty map (left) is an image which includes a false emission pattern due to imperfect visibility sampling. By applying the CLEAN procedure, the false emission pattern is deconvolved from the image, and finally the clean map is restored (right).

2. ASIMUT-ALVL, the BIRA-IASB Radiative Transfer Model

The BIRA-IASB radiative transfer and retrieval code, ASIMUT-ALVL[1], was used to analyse the data. The ALMA data analysis necessitated some new implementations in the code. In particular the multiple lines of sight (LOS) to be considered due to the size of the beam were not yet considered in ASIMUT. For the data obtained on 1st May, the synthesis beam (i.e. spatial resolution) is an elliptical 2d gaussian function with major and minor axis of 0.65 and 0.42 arcsec respectively. The observed spectral feature is then the result of the incoming radiation from a localized region of the mapped source. This effect is taken into account by considering the weighting function represented on Figure 2.

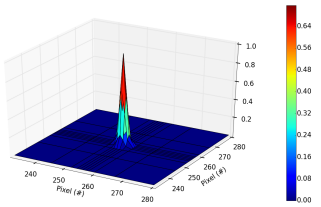

Figure 2: The different contributions are modelled by a two-dimensional gaussian function of Full Width at Half Maximum (FWHM) of the angular resolution and extended on 3 times the FWHM in each direction.

Retrieving the wind velocities implies the retrieval of a spectral shift in the planetary absorption line, here the 3-2 line centered at 345.795 GHz of ^{12}CO in the vibrational ground state. The CO line spectroscopic parameters were extracted from the latest version of HITRAN [2, 3], taking into account that the main buffer gas in the Martian atmosphere is CO_2. The shift retrieval method was modified in ASIMUT. Instead of being done by a simple fit approach, the Jacobians were introduced. This enables us to obtain vertical information, if the information level in the spectrum is sufficient.

3. Current status of the analyis

The update of ASIMUT-ALVL forward model enabled to simulate an appropriate continuum emission brightness temperature map as observed by ALMA. This model map can be used as an input for the "self-calibration" of the measured visibility, which possibly improves the image synthesis quality. After such a reconsideration on the visibility data reduction, the retrieval of wind and temperatures profiles will be tested.

Acknowledgements

This work is performed in the frame of the AMAVERO project, a bilateral agreement between Japan and Belgium. The authors wish to thank their funding agency, namely the Japan Society for the Promotion of Science (JSPS) and the Fonds de la recherche scientifique (FRS-FNRS).

References

[1] Vandaele, A.C., Kruglanski, M., and De Mazière, M.: Modeling and retrieval of Atmospheric spectra using ASIMUT, Proc. of the First 'Atmospheric Science Conference' (ESA SP-628), 8–12 May 2006, Frascati, Italy, 2006.

[2] Gordon, I.E., Rothman, L.S., Hill, C., et al.: The HITRAN2016 molecular spectroscopic database, J. Quant. Spectrosc. Radiat. Transf., Vol. 203, pp. 3-69, 2017.

[3] Li, G., Gordon, I.E., Rothman, L.S., Tan, Y., Hu, S.-M., Kassi, S., Campargue, A. and Medvedev, E.S.: Rovibrational line lists for nine isotopologues of the CO molecule in the X $^1\Sigma^+$ ground electronic state, The Astrophysical Journal Supplement Series, Vol. 216(15), pp. 1-18, 2015.

EPSC Abstracts
Vol. 12, EPSC2018-847, 2018
European Planetary Science Congress 2018

Impact of the refinement of the vertical resolution on the simulation of the water cycle by the martian LMD Global Climate Model

Margaux Vals , François Forget, Aymeric Spiga, Ehouarn Millour
Laboratoire de Météorologie Dynamique, Paris, France (margaux.vals@lmd.jussieu.fr)

Abstract

We study the impact of the refinement of the vertical resolution of the martian LMD GCM on the representation of the water cycle. Results highlight the need of a refined coupling of physical processes in the microphysics of water ice clouds.

1. Introduction

The martian atmosphere hosts a complex water cycle, which is mainly controlled by strong seasonal variations and plays a key role in the radiative transfer. The Martian Global Climate Model (GCM, see [1]) of the LMD (Laboratoire de Météorologie Dynamique) reproduces the main features of the water cycle, such as the sublimation and condensation of the water ice taking place on the surface, but also in the atmosphere, as water ice clouds. The representation of radiatively active water ice clouds has particularly been improved by recent implementations of detailed cloud microphysics ([3], [4]). These comprise the nucleation on dust particles, ice particle growth and scavenging of dust particles due to the condensation of ice. Nevertheless, some differences with the observations are persistent. Among these, the systematic temperature inversions observed within night-time clouds [2], such as a lack of water ice clouds formed at the aphelion belt, or the too strong water vapor release in the atmosphere at the North pole during the Northern Hemisphere Summer ([4]).

To solve these discrepancies, further studies, such as the refinement of the horizontal resolution (1°x1° instead of 4°x6°), and a parametrisation of sub-grid scale clouds, have been carried out by Alizée Pottier [5]. Athough some improvement have been obtained, the global improvement of the simulated water cycle is not significant considering the numerical cost of such implementations. Moreover, recent studies have revealed the importance of vertical resolution to reproduce night-time convection detected under water ice clouds [2], which has been simulated by a mesoscale model (vertical resolution of 750m) [6]. Therefore, further investigation focuses on the refinement of the vertical resolution of the model.

2. Refinement of the vertical resolution

The standard vertical resolution adopted in the GCM is refined near to the surface (from around 10 to 500m) in order to properly resolve the planetary boundary layer (PBL), however it gradually decreases from the top of the PBL up to the top of the atmosphere. It is then roughly of 2km around 10km altitude and 4km around 30km altitude. The comparison between results obtained with the standard and a high vertical resolution, of about 800m around 10km altitude and 1.5km around 30km altitude, reveals that a higher vertical resolution allows to reproduce the observed mixing layers within night-time formed water ice clouds (see Figure 1). However, this higher vertical resolution doesn't

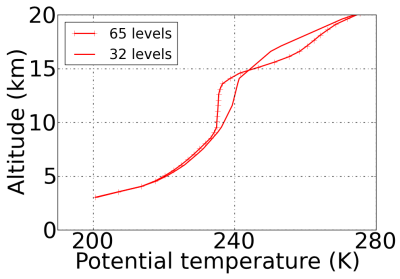

Figure 1: Potential temperature profiles at latitude 20° along the altitude above the martian aeroid at Ls=150°, LT=2AM obtained respectiveley with standard GCM vertical resolution (continuous line, standard 32 vertical levels) and the high vertical resolution (line with dashes, 65 vertical levels)

seem to significantly impact the global water cycle, in particular it doesn't make the polar hood thinner (not shown here).

3. Temporal resolution

The standard temporal resolution is of 1.5 minutes for the dynamics, of 15 minutes for the physics, and of 30 seconds for the microphysics of clouds. Another vertical resolution, of about 500m around 10km and 650m around 30km altitude, has been studied (very high vertical resolution, not shown here). In this case, the temporal resolution requires to be increased to preserve the numerical stability of the model. The physical timestep is reduced to 7.5 minutes, other dynamical and microphysical timesteps being unchanged. However, simulations run with such a temporal resolution, and with the standard vertical resolution, have revealed that the effect of an increased physical temporal resolution has much more impact on the global water cycle than the increased vertical resolution (see Figures 2 and 3). This result, actually independent of the microphysical timestep, suggests that some significant coupling between processes is not taken into account in the microphysics of clouds.

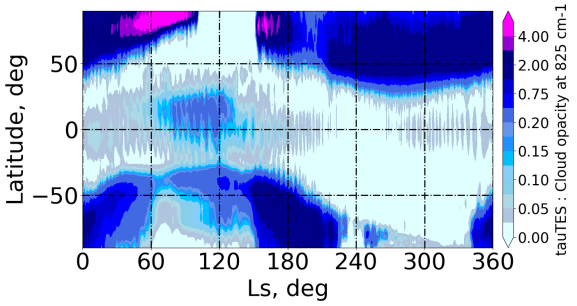

Figure 2: Zonal mean GCM cloud opacity at 2p.m. local time with the standard physical timestep (15 minutes)

4. Summary and Conclusions

An increased vertical resolution applied to the LMD GCM has positive effects on the water cycle regarding the representation of mixing layers observed within night-time clouds. Further investigation has revealed the importance of a refined coupling of microphysical processes involved in the water ice cloud formation. The study of this coupling is under investigation and results will be presented at the conference.

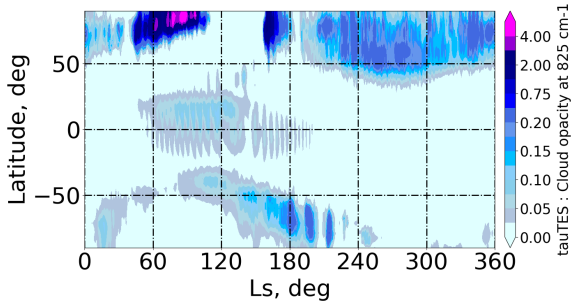

Figure 3: Zonal mean GCM cloud opacity at 2p.m. local time with a high physical timestep (7.5 minutes)

References

[1] Forget et al.: Improved general circulation models of the Martian atmosphere from the surface to above 80 km, *J. Geophys. Res.*, 104:24,155–24,176, 1999.

[2] Hinson, D. P. and Wilson, R. J.:Temperature inversions, thermal tides, and water ice clouds in the Martian tropics, Journal of Geophysical Research (Planets), Vol. 109, pp. 1002-+, 2004.

[3] Madeleine, J.-B. and Head, J. W. and Forget, F. and Navarro, T. and Millour, E. and Spiga, A. and Colaïtis, A. and Määttänen, A. and Montmessin, F. and Dickson, J. L.: Recent Ice Ages on Mars: The role of radiatively active clouds and cloud microphysics, Geophysical Research Letters, Vol. 41, pp. 4873-4879, 2014.

[4] Navarro, T. and Madeleine, J.-B. and Forget, F. and Spiga, A. and Millour, E. and Montmessin, F. and Määttänen, A.: Global Climate Modeling of the Martian water cycle with improved microphysics and radiatively active water ice clouds, Journal of Geophysical Research (Planets), 2014.

[5] Pottier, A. and Forget, F. and Montmessin, F. and Navarro, T. and Spiga, A. and Millour, E. and Szantai, A. and Madeleine, J.-B.: Unraveling the Martian water cycle with high-resolution global climate simulations, Icarus, 2017.

[6] Spiga, A. and Hinson, D.P. and Madeleine, J.B. and Navarro, T. and Millour, E. and Forget, F. and Montmessin, F.: Snow precipitation on Mars driven by cloud-induced nighttime convection, Nature Geoscience, Vol. 10, pp. 652-657, 2017.

EPSC Abstracts
Vol. 12, EPSC2018-875-2, 2018
European Planetary Science Congress 2018

Study of Venus Cloud movements by comparative analysis with Terrestrial Planets

Mr.Adhithiyan Neduncheran(1,6), Mr.James Lai(2,6),Mr.Hamed Gamal(3,6), Mr. George Cristian Potrivitu(4,6), Mrs.Jessica Greech(5,6), Dr. Sinnappoo Arunan(6)

(1)University of Petroleum and Energy Studies, India, adhithiyan.n@gmail.com
(2)McMaster University, Canada
(3) SpaceForest Ltd., Poland
(4)Nanyang Technological University, Singapore
(5)University of New South Wales, Australia
(6)Space Safety & Sustainability Project Group, Space Generation Advisory Council

This paper examines the major Global Climate Models(GCM) of Venus presented so far and analyze them. The framework is followed by the comparative climate models of Earth, Mars and Venus. The main focus shall lie on Venus and its cloud physics. The sulfuric acid clouds are very dense and even block the study of surface of Venus. The super-rotation of the clouds on the planet is one of the most intriguing things so far. A comparative study of chemical reactions and chemical densities are done so as to form a general layer of accumulation in the cloud which vary along the altitude. The paper shall put forth a possibility of density driven separation of cloud layers and its viscosity which helps in the super-rotation of the clouds in the terrestrial planets. It shall also consider the effects of gravity and the surface-clouds interface.

EPSC Abstracts
Vol. 12, EPSC2018-911, 2018
European Planetary Science Congress 2018

Retrieval and characterization of carbon monoxide (CO) vertical profiles in the Martian atmosphere from observations of PFS/MEX

Jimmy Bouche (1), Marco Giuranna (2), Pierre-Francois Coheur (1), Séverine Robert (3), Shohei Aoki (3,4,5), Ann Carine Vandaele (3), Justin T. Erwin (3), Frank Daerden (3), Paulina Wolkenberg (2,6), and Sophie Bauduin (1).

(1) Université libre de Bruxelles (ULB), Atmospheric spectroscopy, Service de Chimie Quantique et Photophysique CP 160/09, Brussels, Belgium, (2) National Institute of Astrophysics INAF-IAPS, Rome, Italy, (3) Royal Belgian Institute for Space Aeronomy, Brussels, Belgium, (4) Fonds National de la Recherche Scientifique, Belgium, (5) Tohoku University, Japan and (6) Space Research Centre of Polish Academy of Sciences, Warsaw, Poland.

(e-mail : jbouche@ulb.ac.be)

Abstract

While there has been substantial progress in our understanding of the Martian global carbon cycle during the last decade, some processes at play are still subject to many questions. This is notably due to the use of retrieval methods which have not exploited fully the satellite measurements. Among the species involved in this cycle, this work targets carbon monoxide (CO) and aims at fully investigating the possibility to retrieve CO vertical profiles from PFS/Mars Express infrared nadir observations. The retrieval method used is the optimal estimation and will be explained in details. Exploiting the framework of this method, the characterization of the retrieved profiles in terms of error budget and vertical sensitivity is deeply discussed. The influence of different parameters, such as the *a priori* constraints, is investigated and will be presented.

1. Introduction

The atmosphere of Mars, largely dominated by carbon dioxide (CO_2), is subject to a global carbon cycle that is still nowadays not completely understood. The recently reported but debated detection of atmospheric methane, combined with its large apparent seasonal variability, has challenged further the understanding of this cycle. Partly due to a lack of vertically-resolved profiles of the different species involved, questions remain on all processes (sources, sinks and transport pathways) affecting the atmospheric carbon reservoir on Mars.

This work targets especially carbon monoxide (CO). While climatology of the averaged CO mixing ratios, built from CRISM (Compact Reconnaissance Imaging Spectrometer for Mars) [1] and from PFS (Planetary Fourier Spectrometer) nadir observations [2], have been recently published and delivered important information regarding the CO latitudinal and seasonal variability, there has been no systematically retrieval of the CO vertical profile from Martian nadir observations. Development of synergies exploiting different spectral ranges or instruments to retrieve information on the CO vertical distribution has been tested [3], but these are difficult to implement. The goal of this work is to deeply investigate the possibility of retrieving CO vertical profiles from PFS nadir observations. This is performed on several single PFS spectra chosen to represent different conditions of CO on Mars. Using the optimal estimation method [4], the aim of the present study is also to characterize the retrieved CO profiles in terms of error budget and vertical sensitivity. In the longer term, this work will allow to retrieve CO profiles for a larger set of PFS measurements, and by building time series and distributions, to better understand the diurnal/seasonal cycle of CO in terms of sources, transport and photochemistry.

2. The PFS instrument

PFS [5] is a double pendulum Fourier transform interferometer orbiting around Mars on-board the Mars Express spacecraft. It covers a large spectral range in the infrared (250-8200 cm^{-1}) thanks to two different channels: the long wavelength (LW) channel, recording the Martian atmospheric spectrum between 250 and 1700 cm^{-1}, and the short wavelength (SW) channel, covering the spectral range 1700-8200 cm^{-1}. In this work, around 25 apodized spectra (spectral resolution of 1.3 cm^{-1})

recorded by the SW channel have been analysed. Simultaneous PFS LW channel observations are used to retrieve surface temperatures and vertical temperature profiles. The spectra have been selected based on the latitude, the solar longitude and the topography, to have a sample of measurements representative of the known spatial and temporal variations of CO on Mars. The selection was made also based on surface temperature and the value of the radiance at 2165 cm^{-1} to ensure sufficient signal-to-noise ratio.

3. Retrieval of carbon monoxide

The retrieval of CO vertical profiles has been performed on single spectra using the optimal estimation method [4]. The idea of this method is to find the CO profile that is consistent with both the PFS observation and the knowledge of the CO vertical distribution prior to the measurement. This method is implemented in the Atmosphit software [6], a versatile line-by-line radiative transfer code initially developed for Earth atmosphere, which is successfully exploited here for the retrieval of CO vertical profiles on Mars.

The optimal estimation offers a very adequate framework to characterize the retrieved Martian CO profiles in terms of error budget and vertical sensitivity. This is done extensively in this work using two output matrices from the retrieval: the total error covariance matrix (to discuss the retrieval errors) and the averaging kernel matrix (to discuss the vertical sensitivity and information content of the retrieval). Using this characterization framework, the influence of the choice of the *a priori* constraints on the retrieved profile is discussed. Specifically, two different *a priori* covariance matrices are built, compared and tested. One consists of an ad hoc matrix that includes 50% of variability (diagonal elements) and whose off-diagonal elements are calculated using an exponential decay, considering a scale height of 11 km. The second matrix has been built using a large ensemble of CO profiles taken from the Mars Climate Database (MCD) [7,8], considering one Martian year for the climatology solar average scenario. This matrix is shown in Figure 1 along with its associated *a priori* profile. The influence of other parameters on the retrieved CO profile, such as emissivity or thermal contrast (temperature difference between the ground and the air above it) is discussed as well.

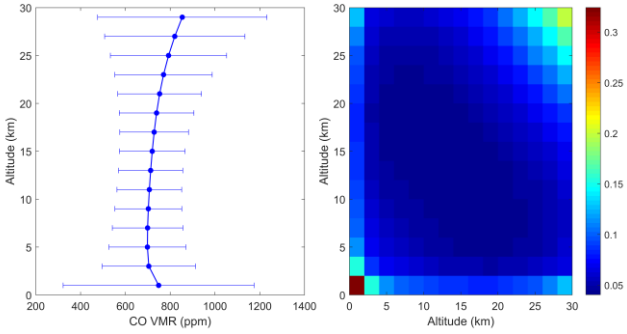

Figure 1: *A priori* profile (left) and covariance matrix (right) built using a large ensemble of CO profiles taken from the MCD database (climatology solar average scenario). The matrix is expressed in multiplicative factor. The error bars on the profile correspond to the square root of the diagonal elements of the matrix.

Acknowledgements

This work is funded by the FNRS CRAMIC project under grant number T.0171.16. PFS is funded by the Italian Space Agency under grant 2018-2-HH.0

References

[1] Smith, M. D., et al., The climatology of carbon monoxide and water vapor on Mars as observed by CRISM and modeled by the GEM-Mars general circulation model, *Icarus* **301**, 117-131, 2018.

[2] Giuranna, M., et al., New dataset of atmospheric parameters retrieved by PFS-Mex, Abstract workshop “From Mars Express to ExoMars”, 27-28 February 2018, ESAC Madrid, Spain.

[3] Robert, S., et al., Two test-cases for synergistic detections in the Martian atmosphere: Carbon monoxide and methane, *JQSRT* **189**, 86-104, 2017.

[4] Rodgers C.D., Inverse methods for atmospheric sounding: theory and practice, Singapore: World Scientific, 2000.

[5] Formisano, V, et al., The Planetary Fourier Spectrometer (PFS) onboard the European Mars Express mission, *Planetary and Space Science* **53**, 963-974, 2005.

[6] Barret, B., et al., Line narrowing effect on the retrieval of HF and HCl vertical profiles from ground-based FTIR measurements, *JQSRT* **95**, 499-519, 2005.

[7] Forget, F., et al., Improved general circulation models of the Martian atmosphere from the surface to above 80 km, *J. Geophys. Res.* **104**, 24155-24175, 1999.

[8] Millour, E., et al., The Mars Climate Database (MCD version 5.2), EPSC abstract, Vol. 10, EPSC2015-438, 2015.

EPSC Abstracts
Vol. 12, EPSC2018-917, 2018
European Planetary Science Congress 2018

High-Level Science Products of SPICAM (Mars Express) and SPICAV (Venus Express)

Nick Cox (1), Lucio Baggio (2), Jean-Loup Bertaux (2), Laurent Blanot (1), Lauriane Delaye (1), Gaetan Lacombe (2), Franck Lefèvre (2), Emmanuel Marcq (2), Franck Montmessin (2)
(1) ACRI-ST, France (nick.cox@acri-st.fr), (2) LATMOS, France

Abstract

In this contribution we present new high-level science products derived from nadir and stellar occultation observations obtained with the UV spectrometers SPICAM and SPICAV on board the Mars Express and Venus Express spacecrafts. We describe the scope of the new level 2 processing and the contents of the corresponding data products that have been ingested into the ESA planetary science archive (PSA). We present examples of scientific results obtained with these data sets and our plans for follow-up work.

1. SPICAM/SPICAV UV data

For the new level 2 processing of nadir and stellar occultation measurements we selected those obtained between orbits 0 and 7624 (SPICAM) and between 0 and 1583 (SPICAV). Observations were reprocessed starting from the most recent level 1b data.

We note that for the Venus stellar occultation observations particular care was taken to estimate and subtract the Nitric Oxide (NO) emission from the limb in order to reveal the true occultation signal.

The full details of the L2 processing are described in the Algorithm Theoretical Definition Documents (ATBDs) available through the PSA. The delivered products (Table 1) adhere to the PDS3 standard.

Table 1: New SPICAM and SPICAV products delivered to the Planetary Science Archive (PSA) of ESA.

Type of observation	Planet	Number of observations	Product level	Product type
Nadir	Mars	2218	L2a	Radiance
		2090	L2b	Atmosphere
	Venus	635	L2a	Radiance
		634	L2b	Atmosphere
Stellar occultation	Mars	1661	L2a	Transmittance
		1492	L2b	Atmosphere
	Venus	373	L2a	Transmittance
		373	L2b	Atmosphere

2. High-level science products

2.1. Nadir observations

For the Nadir observations of Mars and Venus the level 2a data products provide the absolute spectral radiances, radiance factors and geometrical parameters. When available, the associated level 2b data provide for Mars the columns of O3, the UV-averaged surface albedo, the dust aerosol optical thickness and the geometrical data. For Venus the mixing ratios of SO_2 (at 70 km) and O_3 (at 55-70 km), cloud top altitude, and the aerosol imaginary refractive index at 250 nm are provided.

2.2. Stellar occultation observations

For the stellar occultation measurements the level 2a data products comprise the wavelength dependent transmission spectra as well as the spectral flux of the reference star spectrum. For the level 2b products we include the column (line) and local densities for CO_2/SO_2/O_3 (where applicable), as well as the atmospheric temperature profiles. The altitude sampling Δz is 1–3 km for Mars and 0.2–7 km for Venus.

3. Scientific outcome (examples)

3.1. Mars: SPICAM Nadir

The new dataset comprises Martian Years (MY) 27 to 29 (2004–2009) thus covering a time span appropriate for climatological studies of ozone and dust. Figure 1 shows the assimilated information on the ozone column (top) and dust opacity (bottom) ([1], [3]).

3.2. Venus: SPICAV Nadir

For each orbit the radiance factor is given as a function of wavelength, from 200-320 nm, at different geometrical coordinates. The radiance factors are used, together with atmospheric radiative transfer models, to retrieve the levels [in ppbv] of O_3 and SO_2. An example (for orbit 0108A07) is shown in Figure 2. SPICAV routinely detects O_3 at higher latitudes ([4]). At lower

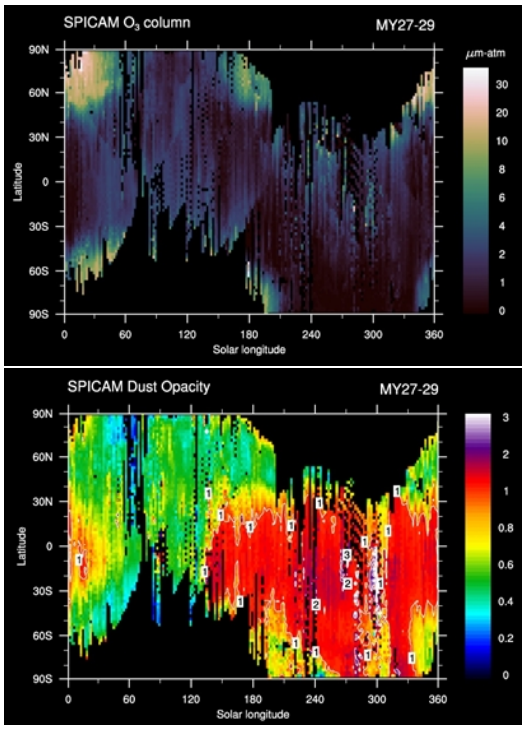

Figure 1: SPICAM retrieval of the ozone column (top) and the dust opacity (bottom) on Mars.

latitudes the cloud top is at 75±2 km. Venus is darker (UV dust opacity) at lower latitudes, consistent with known features (see [4]).

3.3. Stellar occultation on Venus/Mars

Stellar occultation provides a radiography of the vertical distribution of CO_2, O_3 and aerosols. The CO_2 profile gives the vertical temperature profile. These data can then be compared with different global climate/atmosphere models (e.g. [2]).

4. Summary and Outlook

New high-level science products for the SPICAM and SPICAV UV instruments have been delivered to the ESA PSA and will be available to the community (pending internal review, the release is foreseen before the end of 2018). This contribution presents an overview of the delivered data products (level 2a and 2b) and provides some examples of the scientific content.

Work in progress includes the level 2 processing of the second part of the SPICAV/SPICAM UV Nadir and Stellar occultation data (up to orbit 2900 for

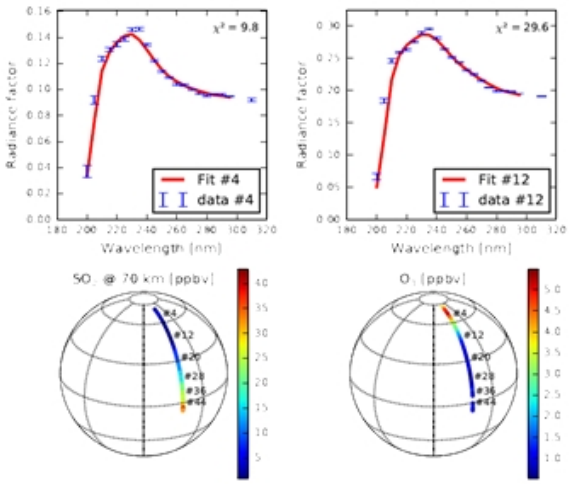

Figure 2: SPICAV-Nadir retrieval results. Example for orbit 0108A07 (produced from the FITS files delivered to the PSA).

SPICAV and orbit 10299 for SPICAM) to extend the temporal and spatial coverage for Venus and Mars.

Acknowledgements

This project is supported by an EXPRO contract with ESA. EM acknowledges support from CNES and PNP.

References

[1] Montmessin, F., O. Korablev, F. Lefèvre, et al. 2017b. "SPICAM on Mars Express: A 10 Year in-Depth Survey of the Martian Atmosphere", 2017, Icarus 297, 195-216

[2] Piccialli, A., Montmessin, F., Belyaev, D.,, et al. "Thermal Structure of Venus Nightside Upper Atmosphere Measured by Stellar Occultations with SPICAV/Venus Express", 2015, Planetary and Space Science, Volume 113, p. 321-335

[3] Willame, Y.; Vandaele, A. C.; Depiesse, C.; Lefèvre, F.; Letocart, V.; Gillotay, D.; Montmessin, F., "Retrieving cloud, dust and ozone abundances in the Martian atmosphere using SPICAM/UV nadir spectra", 2017, Planetary and Space Science, Volume 142, p. 9-25

[4] Marcq, E., Lefévre, F., Stolzenbach, A., Baggio, L., Montmessin, F., Belyaev, D., Korablev, O., Bertaux, J.-L., "Discovery of cloud top ozone on Venus", submitted to Icarus

EPSC Abstracts
Vol. 12, EPSC2018-950, 2018
European Planetary Science Congress 2018

VENUS NEAR SURFACE TEMPERATURE

N. T. Mueller[1,4], C. Tsang[2], S. Lebonnois[3], S. Smrekar[4]. [1]will be: Institute of Planetary Research, DLR, Rutherfordstr. 2, 12489 Berlin, Germany. nils.mueller@dlr.de, [2]Department of Space Studies, Southwest Research Institute, Boulder, CO 80302 USA. [3]Laboratoire de Météorologie Dynamique (LMD/IPSL), Sorbonne Université, CNRS, 75252 Paris, France. [4]Jet Propulsion Laboratory, California Institute of Technology, 4800 Oak Grove Drive, Pasadena, CA 91109 USA

Abstract

In this work we show that the thermal emission observed by VIRTIS on Venus Express indicates lateral and temporal variations of surface temperature, which is coupled to atmospheric temperature. These variations are similar to self-consistent temperatures predicted by a General Circulation Model (GCM).

1. Introduction

The current temperature at and near the surface of Venus is relevant for many open questions regarding its evolution as an Earth like planet. In situ data is scarce, especially close to the surface. They cannot provide the global picture, and the sparse data leave unsolved questions. The Venus International Reference Atmosphere (VIRA) [1] provides laterally and temporally averaged temperature for the lowest atmosphere, with a vertical temperature profile extrapolated from Pioneer Venus and Venera measurements higher up. Yet the only high-resolution descent profile from the VeGa-2 lander [2] shows an apparently dynamically unstable lapse rate, which led [3] to hypothesize that the supercritical CO_2 causes a density driven compositional gradient. Remote observations of thermal emission through the near infrared atmospheric windows are sensitive to surface temperature, which is closely coupled to atmospheric temperature.

2. VIRTIS Observations

We correct the VIRTIS data for detector non-linearities and instrumental straylight following the approach of [4]. To invert the data to emissivity we use the radiative transfer model (NEMESIS) developed for Venus by [5] to model the radiances of the near infrared atmospheric windows between 1000 and 1400 nm. The atmospheric temperature and pressure profile is based on [1] as in previous studies of deep atmosphere and surface emissions [6, 7].

The result is a map of surface emissivity in three bands at approximately 1020, 1100 and 1180 nm, all showing some residual trend with topography. Such trends of emissivity have been reported by other studies with the same assumptions on surface temperature [6, 7]. The new observation here is that the trend varies with location and local time. The trend can be interpreted as deviation of Venus surface temperature from the VIRA profile assumed for the radiative transfer modeling. The absolute deviation is not well constrained, but relative differences are.

3. General Circulation Model

We use results of a GCM developed for Venus by [8]. The model is based on an Earth GCM with several modifications. The main modification is the radiative transfer model, developed specifically for Venus, allowing the GCM to provide self-consistent temperatures. There are two GCM runs, one with constant abundance of N_2 (as in VIRA) and one with an artificially imposed gradient of N_2 between approximately 0 and 6 km altitude as proposed by [3] to explain the VeGa-2 profile. At lower altitudes, N_2 is completely absent and lapse rates between the model runs are almost identical.

4. Results

Fig. 1 shows the VIRTIS derived temperature deviation from the VIRA profile for two regions at the same latitude of 58°S to 42°S, and different longitudes -41°E to -4°E (Themis Regio), -105°E to -68°E (Lavinia Planitia), and the GCM surface temperatures of these two regions.
Temperature lapse rate in both model and observations are most consistent with the VIRA profile near 1km elevation, but indicate a lower lapse rate at lower elevations, which make up the bulk of VIRTIS data.

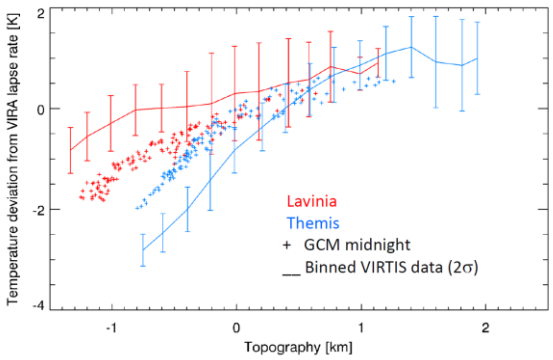

Figure 1: Observed and modeled surface temperatures relative to the VIRA profile for two regions in the same latitude band

The lowlands in Lavinia and Themis show distinct temperature lapse rates both in data and model, although the difference is more pronounced in the data.

The VIRTIS data has to be averaged over many observations to yield reasonable signal to noise. We separate the nightside data set in two wide local time intervals, before and after local midnight. The resulting VIRTIS maps are more noise but still show a similar cooling rate over the course of the Venus night as the GCM in both regions.

Fig. 2 shows all of the VIRTIS data, which is limited to southern latitudes, and the global GCM results for the two model runs.

5. Discussion and Conclusions

The potential impact of these observations is clear. The GCM predictions testable by remote observation were previously limited to the upper boundary winds and atmospheric temperature fields above roughly 40 km altitude [9]. Near infrared data provides constraints for the planetary boundary layer. On the other hand, the GCM model temperatures differing from the VIRA temperatures provide a physical meaning to the empirical corrections of emissivity trends that were necessary in previous work [6, 7].

At present we cannot show whether a gradient in N_2 provides a better fit to the VIRTIS data due to the limited altitude range covered in the data.

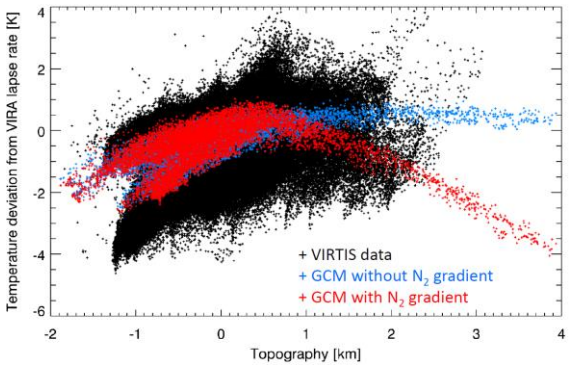

Figure 2: VIRTIS data of the southern hemisphere and global GCM results

Future observations could provide a better temporal resolution, a wider range of observed surface elevations, and a much better SNR, and more reliable altimetry of highlands, each of which will significantly improve the interpretability of the data.

References

[1] Seiff et al. (1985). Models of the structure of the atmosphere of Venus from the surface to 100 kilometers altitude. Adv. Space Res. 5 (11), 1–305.

[2] Seiff (1987). Further information on structure of the atmosphere of Venus derived from the VEGA Venus balloon and lander mission Adv. Space Res., 7, 323–328.

[3] Lebonnois and Schubert (2017). The deep atmosphere of Venus and the possible role of density-driven separation of CO_2 and N_2. Nature Geoscience, vol 10, 473-479.

[4] Kappel et al. (2012). Refinements in the data analysis of VIRTIS-M-IR Venus nightside spectra. Adv. Space Res. 50, 228–255.

[5] Tsang et al (2008). A correlated-k model of radiative transfer in the near-infrared windows of Venus JQSRT 109 (6), 1118–1135

[6] Basilevsky et al. (2012). Geologic interpretation of the near-infrared images of the surface taken by the Venus Monitoring Camera, Venus Express. Icarus 217, 434–450.

[7] Kappel et al. (2016). Multi-spectrum retrieval of Venus IR surface emissivity maps from VIRTIS/VEX nightside measurements at Themis Regio. Icarus 265, 42–62.

[8] Lebonnois et al. (2010). Superrotation of Venus' atmosphere analyzed with a full general circulation model. JGR, vol. 115, E06006.

[9] Limaye et al. (2017). The thermal structure of the Venus atmosphere: Intercomparison of Venus Express and ground based observations of vertical temperature and density profiles. Icarus 294, 124–155

EPSC Abstracts
Vol. 12, EPSC2018-1029-1, 2018
European Planetary Science Congress 2018

Spectral Scan and Line Catalogue of the Martian Atmosphere from Herschel/HIFI Observations

Miriam Rengel (1), Christopher Jarchow (1) and Paul Hartogh (1)
(1) Max-Planck-Institute für Sonnensystemforschung, Germany (rengel@mps.mpg.de)

Abstract

The Heterodyne Instrument for the Far-Infrared (HIFI) [1] was the very high-resolution spectrometer (resolving power of up to 10^7) on-board the Herschel Space Observatory [2]. It offered a spectral coverage in the ranges [480–1270] and [1430–1910] GHz. Herschel/HIFI has observed the Martian atmosphere in its different seven HIFI mixer bands and using its spectral line and spectral scan observing capabilities, covering from a Martian northern spring to mid -summer, in the framework of the Herschel Solar System Observations (HssO) Key Programme [3].

We have conducted a dedicated work in order to extract, identify and catalogue spectral lines (species and transitions) from these observations. The observations were primary processed with the standard Herschel Interactive Processing Environment (HIPE) modules [4].

The Catalogue is being made available through the Herschel Science Archive (HSA) [1] as an User-Processed Data Product (UPDP)[2], and we provide here further information about the content of this scientific data-set and examples of the observations and data-analysis. This catalogue will facilitate current and future studies of the Martian atmosphere.

Acknowledgments

HIFI has been designed and built by a consortium of institutes and university departments from across Europe, Canada and the United States under the leadership of SRON Netherlands Institute for Space Research, Groningen, The Netherlands and with major contributions from Germany, France and the US. Consortium members are: Canada: CSA, U.Waterloo; France: CESR, LAB, LERMA, IRAM; Germany: KOSMA, MPIfR, MPS; Ireland, NUI Maynooth; Italy: ASI, IFSI-INAF, Osservatorio Astrofisico di Arcetri-INAF; Netherlands: SRON, TUD; Poland: CAMK, CBK; Spain: Observatorio Astronómico Nacional (IGN), Centro de Astrobiología (CSIC-INTA). Sweden: Chalmers University of Technology - MC2, RSS & GARD; Onsala Space Observatory; Swedish National Space Board, Stockholm University - Stockholm Observatory; Switzerland: ETH Zurich, FHNW; USA: Caltech, JPL, NHSC.

References

[1] de Graauw, T., Helmich, F.P., Phillips, T.G. et al. 2010, A&A, 518, L4

[2] Pilbratt, G.L., Riedinger, J.R., Passvogel, T. et al. 2010, A&A, 518, L1

[3] Hartogh, P., Lellouch, E., Crovisier, J. et al. 2009, PSS 57, 1596

[4] Ott, S. 2010, ASP Conference Series, 434, 139

[1] https://www.cosmos.esa.int/web/herschel/home

[2] https://www.cosmos.esa.int/web/herschel/user-provided-data-products

EPSC Abstracts
Vol. 12, EPSC2018-1051, 2018
European Planetary Science Congress 2018

Comparison of a 1D column model with temperature soundings in the Martian atmosphere

Mark Paton (1), Ari-Matti Harri (1) Hannu Savijärvi (2)
(1) Finnish Meteorological Institute, Helsinki, Finland, (2) University of Helsinki, Finland (mark.paton@fmi.fi)

Abstract

A 1D column model is compared to temperature soundings from the Mars Climate Sounder (MCS) aboard the Mars Reconnaissance Orbiter currently orbiting Mars. Such comparisons could help isolate non-local and local climate phenomena and so help improve our understanding of the regional and global-scale atmospheric processes on Mars.

This investigation could also help to further verify the accuracy of a 1D column model by including more representative atmospheric properties. For example by including more representative temperature profiles imported from a climate model.

1. Background

A 1D column model, previously used to investigate the properties of the atmosphere and surface at spacecraft landing sites, is used [1,2]. The observed temperature soundings are obtained from MCS. The Mars Climate Database, which includes results from a global climate model, will provide temperature profiles for greater realism when running the 1D column model.

2. Investigation methodology

Python code has been written that searches the MCS data and imports a temperature profile for a specific date, time and location. The 1D column model can then be automatically run by the code at the specified location and then the resulting temperature profile can be compared to the MCS temperature profile. The comparison is made by first calculating the average temperatures for both the observed profile and model profile.

There is also the option available to fit the 1D column model to the MCS profile by automatically varying a parameter in the model such as, e.g. thermal inertia, albedo, dust content. The 1D column model thermal inertia and albedo is initialised from published global maps of Mars.

3. Results

The results so far suggest that the 1D column model can accurately reproduce the observed temperature profile up to or above the middle of the troposphere. Above this altitude temperature variations are present in the observations presumably due to regional-scale processes.

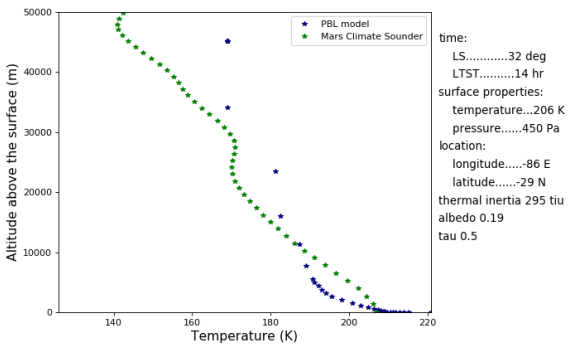

Figure 1. One of the first examples produced by the Python code for comparing a 1D column model with observation from MCS.

References

[1] Savijärvi, H. I., Paton, M. and Harri, A-M., New column simulations for the Viking landers: Winds, fog, frost, adsorption?, Icarus, Vol. 310, pp. 40-53, 2018.

[2] Paton, M. D., Harri, A. -M., Savijärvi, H., Mäkinen, T., Kemppinen O. and Hagermann, A., Thermal and microstructural properties of fine-grained material at the Viking Lander 1 site, Icarus, Vol. 271, pp. 360-374, 2016.

EPSC Abstracts
Vol. 12, EPSC2018-1101, 2018
European Planetary Science Congress 2018

Mars' upper atmosphere with varying EUV flux

Ute V. Amerstorfer (1), Tanja Amerstorfer (1), **Herbert Lichtenegger** (1), and Colin Johnstone (2)
(1) Space Research Institute, Austrian Academy of Sciences, Graz, Austria, (2) Department of Astrophysics, University of Vienna, Vienna, Austria (ute.amerstorfer@oeaw.ac.at)

Abstract

We study the upper atmosphere of Mars and its response to varying solar EUV radiation with the KompotCode ([1]). Different EUV fluxes correspond to different times in the past of the Martian evolution. We compare the results of the KompotCode, i.e. profiles of neutral and ion species, and profiles of temperatures, with existing models for today's and early Mars. Finally, we compare our results with MAVEN observations.

1. Introduction

Throughout their evolution, planetary atmospheres are strongly influenced by the radiation and particle emissions from their host star. The Sun's radiation in the extreme ultraviolet (EUV) part of the solar spectrum was higher in the past, and thus, the planetary atmospheres are exposed to varying external conditions.

2. Simulations for today's Mars

At first, we simulate the Martian atmosphere with today's solar EUV flux (1 EUV case). The results show reasonable agreement with other existing models, of e.g. [2] and [3]. Further, we compare our results with observations made by the MAVEN spacecraft.

3. Simulations for different EUV fluxes

Next, we increase the EUV flux and discuss the atmosphere's reaction to such an increase. A higher EUV input to the atmosphere results in different densities and temperatures, and thus has a direct influence on the thermal and non-thermal loss processes of different species, such as oxygen and carbon. We compare our results with the model by [3], which considers 3, 10 and 20 times the present solar EUV flux.

Acknowledgements

U.V. Amerstorfer, T. Amerstorfer, and H. Lichtenegger are supported by the Austrian Science Fund (FWF): P24247-N16.

References

[1] Johnstone, C. P., M. Güdel, H. Lammer, and K. G. Kislyakova (2018), The Upper Atmospheres of Terrestrial Planets: Carbon Dioxide Cooling and the Earth's Thermospheric Evolution, submitted to Astronomy & Astrophysics.

[2] Fox, J. L., and A. B. Hac (2009), Photochemical escape of oxygen from Mars: A comparison of the exobase approximation to a Monte Carlo method, Icarus, 204, 527–544, doi:10.1016/j.icarus.2009.07.005.

[3] Tian, F., J. F. Kasting, and S. C. Solomon (2009), Thermal escape of carbon from the early Martian atmosphere, Geophys. Res. Lett., 36, L02205, doi:10.1029/2008GL036513. ∫

EPSC Abstracts
Vol. 12, EPSC2018-1121, 2018
European Planetary Science Congress 2018

Dynamical Processes of Dust Lifting in the northern Mid-latitude region of Mars during the Storm Season

Jing Xiao, Kim-Chiu Chow, Kwing-lam Chan
Space Science Institute, Macau University of Science and Technology, Macao, China. (Jxiao@must.edu.mo)

Abstract

By numerical simulation with the general circulation model for Mars, the dynamical processes of Martian dust storms in the northern mid-latitude region during the storm season have been studied.

1. Introduction

Previous observations [1] show that the regular annual activity of Martian dust storms is more active at northern mid-latitude region during the second half of the Martian year, especially concentrated in two episodic periods (Ls = 220° - 260° and Ls = 310° - 340°). They have been suggested to be dominated by the transient mid-latitude waves with the zonal wave number of 1~3, and the period of 2~7 sols [2][3]. However, due to the limited temporal resolution of the satellite observations and the prescribed dust content applied in most GCM simulations, the processes with a period less than 2 sols and result in the dust lifting may have been missed. In this study, these two issues as well as the asymmetric terrain effect would be focused.

2. Numerical Experiments

The basic configuration of the simulations is generally similar to that used in [4]. The model includes an active dust scheme and a dust devil scheme similar to those used in [5]Newman and Richardson (2015). Then the suspended dusts may change the atmospheric radiation and so the circulations. The simulation in the second year is considered as the control simulation 'CTRL' and the results are dumped out every 2hrs.

In order to test the terrain effect, the asymmetric terrains north than 15 ºN have been smoothed as a sensitive experiment named 'RmTerrain'.

3. Figures

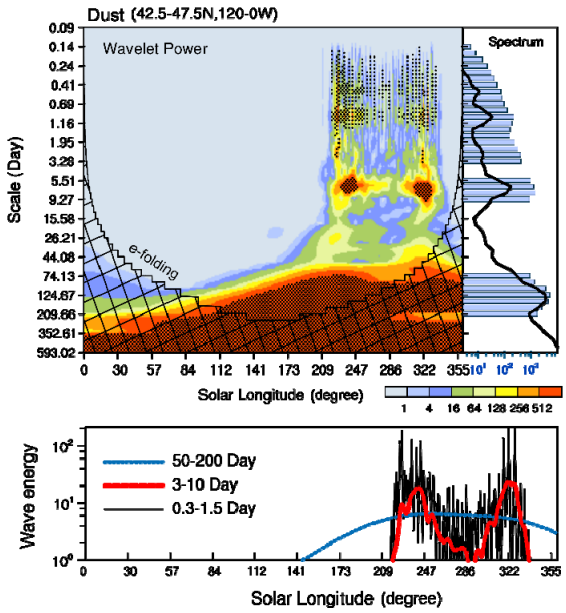

Figure 1: Wavelet analysis on the time series of simulated dust mixing ratio near surface averaged in the mid-latitude region near Alba Patera (42.5º - 47.5º N and 120º - 0º W). The shading depicts the spectrum power (significant region is dotted and the mesh marks where it is above the e-folding line), and the time-averaged spectrum is shown in the upper right (curve is the total energy profile and bars are the effective energy). The bottom subplot shows the time series of wave energy of the interested wave bands.

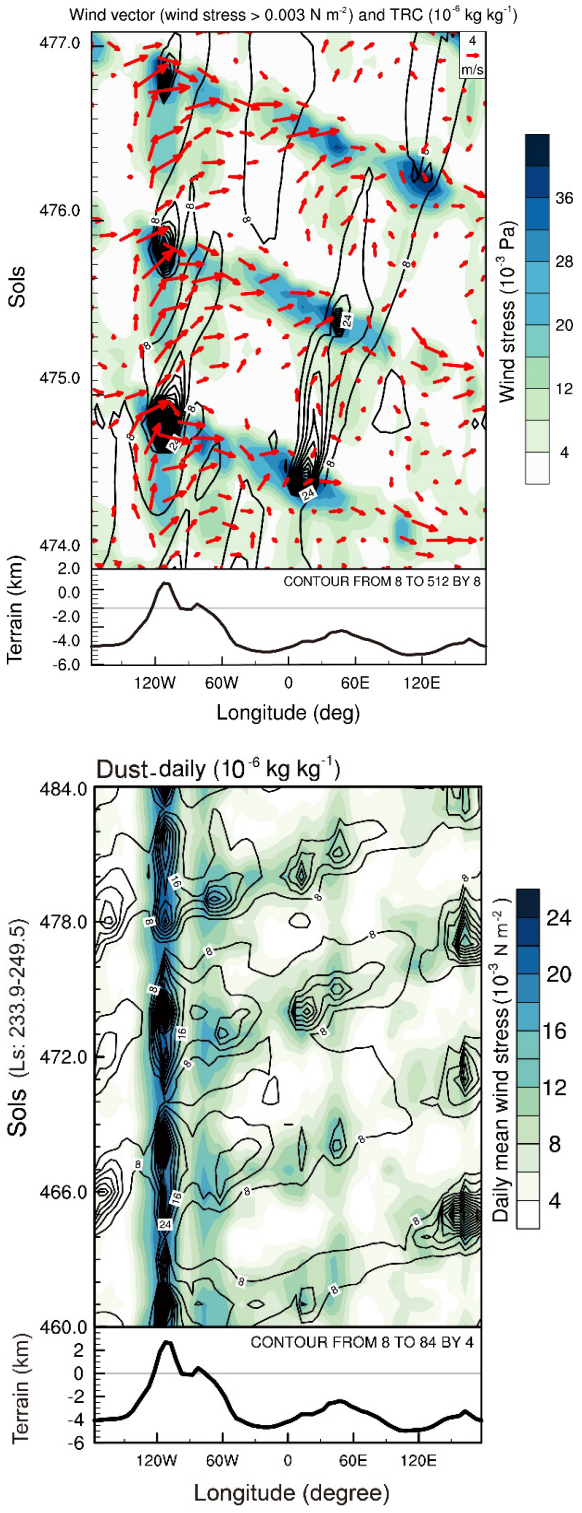

Figure 2: Hovmöller diagram of surface dust mixing ratio (contours, 10^{-6} kg kg^{-1}) and wind stress (shading, 10^{-3} N m^{-2}) averaged between 42.5º and 47.5ºN

during (a) sols 474.0 - 477.0 and (b) sols 460.2 - 484.2 (Ls = 233.9º - 249.5º). (a) also shows surface winds (red vectors) when wind stress is significant (> 0.003 N m-2), and in (b) the variables are daily mean. The corresponding profile of terrain (km) in the region is shown in the bottom. Summary and Conclusions

- The Martian dust storm activities can be well interpreted by the GCM model MarsWRF, especially the dust source region and the double-peak episodes.
- Three distinct periods of dust lifting activities can be identified: semi-diurnal to diurnal (0.5-1.5 sols), synoptic (3-7 sols) and seasonal (50-200 sols).
- Dust lifting is dominated by the diurnal thermal tide near three high terrains. Then the suspended dust are advected downstream by the baroclinic waves.
- The asymmetric high terrains have a pivotal role in triggering the dust, but have little effects on baroclinic waves.

Acknowledgements

This research is funded by the grants from the FDCT of Macau (grant no. 119/2017/A3 and 080/2015/A3)..

References

[1] Montabone, L., Forget, F., Millour, E., et al., 2015. Eight-year climatology of dust optical depth on Mars. Icarus 252, 65 – 95..

[2] Hinson, D.P., Wang, H., 2010. Further observations of regional dust storms and baroclinic eddies in the northern hemisphere of Mars. Icarus 206 (1), 290–305.

[3] Wang, H., Toigo, A.D., 2016. The variability, structure and energy conversion of the northern hemisphere traveling waves simulated in a Mars general circulation model. Icarus 271, 207–221.

[4] Chow, K. C., Chan, K. L., Xiao, J.: Dust Activity over the Hellas Basin of Mars during the Period of Southern Spring Equinox. *Icarus*, v311, 306 – 316, 2018.

[5] Newman, C.E., Richardson, M.I., 2015. The impact of surface dust source exhaustion on the martian dust cycle, dust storms and interannual variability, as simulated by the MarsWRF General Circulation Model. Icarus 257, 47 - 87.

EPSC Abstracts
Vol. 12, EPSC2018-1135, 2018
European Planetary Science Congress 2018

X ray spectroscopy of planetary atmospheres

S. Panini (1), **S. Narendranath** (2) P. Sreekumar (1) and V C Babu(2)

(1) Indian Institute of Astrophysics (2) URSC, Indian Space Research Organisation (kcshyama@isac.gov.in)

Abstract

X ray emission in the solar system though ubiquitous [1] is a less explored area for studying atmospheres. A variety of physics processes contribute to these emissions and are time variable with dependencies on the emission from the Sun as well as local magnetic field dynamics. We are developing an X ray concentrator based spectrometer to study these emissions in orbits around the planets. The design aspects and preliminary performance is discussed.

1. Introduction

X ray emission in the Solar system arises from a variety of processes (1) X ray fluorescence (XRF)(2) X ray scattering (3) electron bremsstrahlung leading to aurorae (4) Solar wind charge exchange emission (SWCX) and (5) Particle induced X ray emission (PIXE). While XRF is a commonly used technique for remotely mapping the surface composition of airless bodies [such as Apollo 15 and 16, SMART-1 DCIXS, Chandrayaan-1- C1XS, Kaguya-XRS, MESSENGER-XRS], soft X ray spectroscopy of atmospheres are limited.

2. An X ray concentrator

X ray imaging spectroscopy yields the maximum information for any of the processes mentioned earlier. X ray telescopes are challenging for planetary missions in terms of the resources they demand. An instrument is under development for soft X ray mapping of planetary atmospheres with high spatial and temporal resolutions.

The instrument consists of an X ray concentrator optics with a X ray CCD at the focus. A short focal length (80 cm) X-ray concentrator is designed to focus soft X-rays (<1 keV). X-ray concentrator consists of 8 concentric shells of gold coated mirrors placed at grazing incident angles. Parallel beam X-rays from the source undergoes single reflection from the concentrator and focuses to the detector at the focal plane. Figure 1 shows the schematic of the soft X-ray concentrator design with proposed dimensions. Table 1 gives the detailed specification of the instrument.

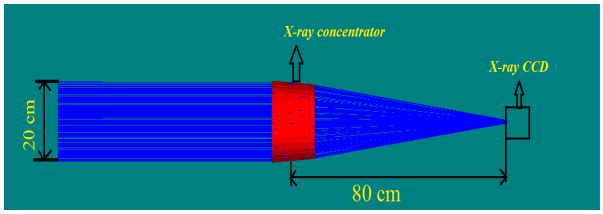

Figure 1: Schematic of the soft X ray concentrator

Table 1: Specifications

Parameter	Quantity
Focal length	80 cm
Diameter	20 cm
Number of shells	8
Coating of mirrors	Gold
Substrate of mirrors	Al
Band width of operation	0.2 keV-1 keV
Number of reflections	1
Effective area	75 cm^2 @0.5 keV

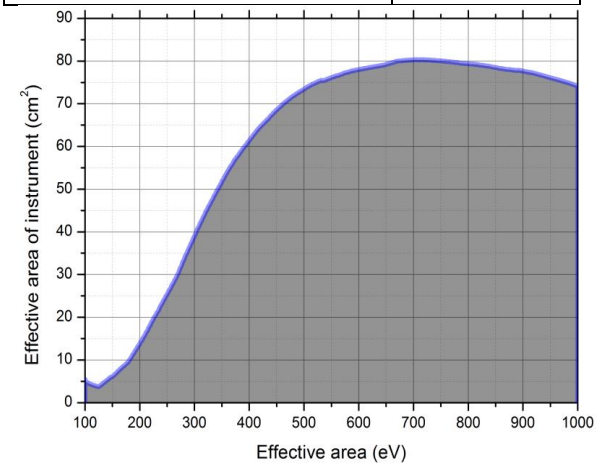

Figure 2: Effective area of the instrument including optics and a focal plane CCD

3. Results

A proto-type structure of the concentrator was fabricated with a 3D printer and gold plated mirrors were assembled. Figure 3 shows the test set up to assess the degree of concentration achieved using visible light.
Of the 20 cm diameter of the concentrator, 70% was illuminated with a parallel beam from the Sun. The spot size was 4 mm well within the proposed X ray CCD size of 1.3 x 1.3 cm.

4. Future work

We are in the process of design optimization towards measuring weak emissions such as SWCX from the exosphere of Venus, Earth and Mars. Such an instrument in orbits around these planets would yield for the first time X ray emission maps and its variability with time.

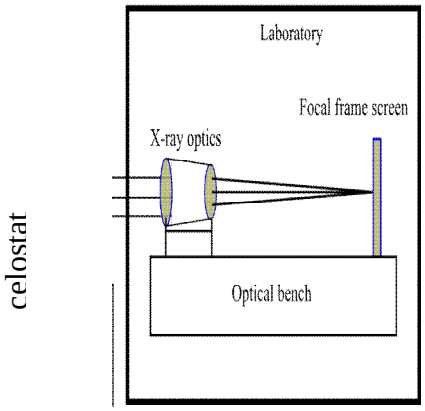

Figure 3: Schematic test set up

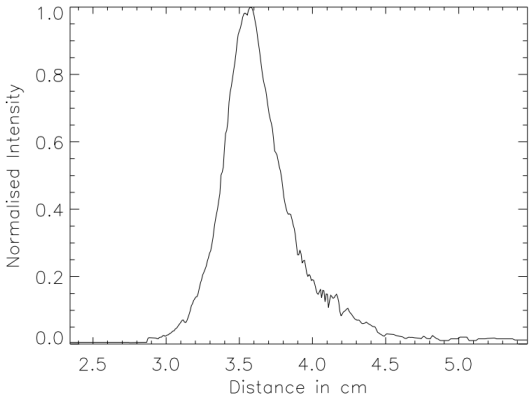

Figure 4: Spot size of 4 mm measured at the focus

Acknowledgements

We thank Prof. K P Singh and his team and Director, Tata Institute of Fundamental Research, India for generously donating the gold coated X ray mirrors used in this instrument. We thank Mr. Saurabh Gupta and team at USRC for 3D printing the structure.

References

[1] Bhardwaj, Anil., Elsner, Ronald F., Randall, Gladstone., G.,Cravens, Thomas., Lisse, Carrey M., Dennerl, Konrad., Branduardi-Raymont, Graziella., Wargelin, Bradford J., Hunter, Waite,J., Robetrson, Ina., Ostgaard, Nikolai,. Beiersdorfer, Peter., Snowden, Steven L., Kharchenko, Vasili: X rays from solar system objects, Planetary and Space Science, Vol. 55, pp. 1135-1189, 2007.

EPSC Abstracts
Vol. 12, EPSC2018-1179, 2018
European Planetary Science Congress 2018

Discussion about the Physical Origin of the Venus Low Atmosphere Chemical Gradient

D. Cordier (1) S. Lebonnois (2) D. Bonhommeau (1)
(1) GSMA - UMR CNRS 7331 Campus Moulin de la Housse - BP 1039 Université de Reims Champagne-Ardenne 51687 REIMS – France (2) LMD, Sorbonne Universités, UPMC Univ. Paris 06, ENS, PSL Research University, Ecole Polytechnique, Université Paris Saclay, CNRS, 75252 Paris, France

Abstract

Venus shares many similarities with the Earth but, concomitantly, some of its features are extremely original. This is especially true for its atmosphere, where high pressures and temperatures are found at ground level. In these conditions, carbon dioxide, the main component of Venus atmosphere, is a supercritical fluid. Recent works have suggested the existence of a vertical gradient of nitrogen abundances, around 5 ppm per meter, in the deep atmosphere of Venus. An analogous chemical gradient is observed in terrestrial hydrocarbon reservoirs, but in that case, the fluids are trapped in a porous medium which efficiently impede fast large scale transport, leaving diffusion at work over long timescales. The venusian separation mechanism had to be faster than the mixing produced by atmospheric large scale circulation. Our goal was then to discuss which physical processes could lead to the establishment of a nitrogen gradient, around the expected value, in the deep atmosphere of Venus. Using an appropriate equation of state, we have explored the thermodynamic properties of the binary mixture CO_2-N_2, under supercritical conditions. We have particularly focused our attention on a possible pressure diffusion transport, caused by gravity.

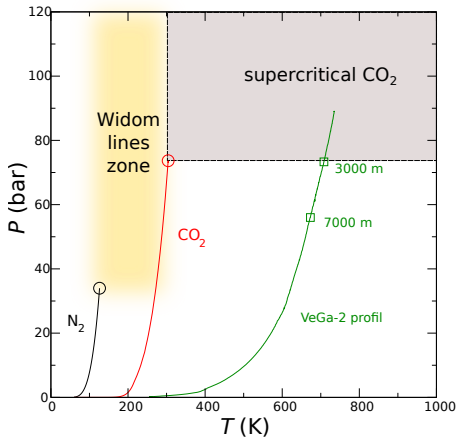

Figure 1: Simplified phase diagram of CO_2. The position of the critical point of pure CO_2 has been plotted, together with its position when a small fraction of nitrogen is added to the system. The introduction of N_2 shifts the position of the critical point by a few bars and a few kelvins (Goos et al. 2011). The green and the blue lines refer respectively to pressure-temperature of Venus atmosphere derived respectively from GCM simulations (Lebonnois & Schubert, 2017) and measurements performed by the VeGa-2 probe (Lorenz et al. 2018).

1. Introduction

At ground level, the Venus air is under hellish conditions, where the temperature is close to 740 K and the pressure not too different than 90 bars. Since carbon dioxide dominates the atmospheric composition, with a mole fraction around 97%, at low altitude the venusian air is a supercritical fluid. The second most abundant atmospheric compound is molecular nitrogen, N_2, with a mole fraction of about 3%. Therefore, nitrogen is also in a supercritical state. In the phase diagram, plotted in Fig. 1, we have recalled the position of carbon dioxide and nitrogen respective critical points, this, complemented by the pressure-temperature atmospheric profile measured during the descent of the VeGa-2 probe (Lorenz et al. 2018). Recently, the existence of a composition gradient in the Venus deep atmosphere, *i.e.* for layers below the altitude of $\sim$ 7000 m, has been suggested (Lebonnois & Schubert, 2017). The abundance of nitrogen seems to decreases from $\sim$ 3.5% at 7000 m, to zero at ground level; yielding to a gradient of about 5 ppm m^{-1}. As it can be seen in Fig. 1, this deep atmosphere is partially in CO_2 supercritical domain

and entirely in that of N_2. Then, we first checked that the apparent composition gradient could not be only an effect of compressibility properties of the CO_2-N_2 mixture. For this purpose, we have employed an equation of state (Duan et al. 1996), specifically developed for mixture like CO_2-N_2, under supercritical conditions. We found that the compressibility factor Z stays around 1 in the deep atmosphere of Venus. Actually, Z measures the deviation of real gases from ideal gases behavior, a value around the unity shows a compressibility behavior similar to what we have with an ideal gas. Then, this result, also supported by laboratory measurements (Mohagheghian et al. 2015), tends to confirm the existence of compositional variations.

2. The Effect of Molecular Diffusion

For almost a century, chemical composition variations are known among terrestrial reservoirs of hydrocarbons, *i.e.* containing gases or petroleum (Sage & Lacey, 1939), or both. These variations are horizontal, but also vertical: in that case, for a given well, the abundances of species evolves with depth. The emergence of such a gradient of composition is due to the effect of gravity and, also to thermodiffusion. In this context, the convection is not very efficient since the fluid is trapped in a porous medium. Here, we focus our attention on the physics of the vertical compositional grading. If the air mixing, due to atmospheric circulation, is slow or inefficient enough, deep atmosphere of Venus could be the subject of analogous physical processes, leading to the suspected gradient of nitrogen concentration.
Assuming a steady state, an ideal gas, and using the pressure and temperature gradient, provided by the VeGa-2 probe (Lorenz et al. 2018), the nitrogen mole fraction (x_1) gradient is given by

$$\frac{\partial x_1}{\partial z} = -\frac{x_1}{P}\left(1-\frac{M_1}{\bar{M}}\right)\left.\frac{\partial P}{\partial z}\right|_{\mathrm{VeGa2}} - \frac{\alpha_{T\,1,2}}{T}\,x_1(1-x_1)\left.\frac{\partial T}{\partial z}\right|_{\mathrm{VeGa2}} \quad (1)$$

Thanks to the kinetic theory of gases (Chapman & Cowling, 1970), the thermal diffusion coefficient $\alpha_{T\,1,2}$ may be estimated for the system N_2-CO_2. By integrating Eq. (1) from the top of the Venus deep atmosphere, *i.e.* from an altitude of 7000 m, down to the surface, we obtained a nitrogen mole fraction gradient of ~ 0.6 ppm m^{-1}. This value is roughtly one order of magnitude lower than the expected gradient (Lebonnois & Schubert, 2017) of ~ 5 ppm m^{-1}.
Now we can turn to a more realistic model, taking into account non-ideal effects, the relevant equation is then (Ghorayeb & Firoozabadi, 2000)

$$\left.\frac{\partial \ln f_1}{\partial \ln x_1}\right|_{P,T}\frac{\partial x_1}{\partial z} + \frac{x_1}{RT}\left(\bar{V}_1-\frac{M_1}{\rho}\right)\left.\frac{\partial P}{\partial z}\right|_{\mathrm{VeGa2}} - \frac{\alpha_{T\,1,2}}{T}\,x_1(1-x_1)\left.\frac{\partial T}{\partial z}\right|_{\mathrm{VeGa2}} = 0 \quad (2)$$

where f_1 denotes the fugacity of compound (1) (here nitrogen), $\bar{V}_1$ is the nitrogen partial molar volume and the density of the mixture is called ρ. All these quantities are evaluated with the EoS published by Duan et al. (1996) and relevant for supercritical carbon dioxide. With this new equation, we may expect enhanced composition gradient $\partial x_1/\partial z$. Indeed, close to the critical point the derivative $\partial \mathrm{ln} f_1/\partial \mathrm{ln} x_1$ tends to zero. Unfortunately, even with this more realistic modeling, the computed gradient is not in agreement with the value suspected for Venus deep atmosphere. In addition, the estimated molecular diffusion coefficient of N_2 in supercritical CO_2 leads to relaxation time around 16 mega-years, largely incompatible with dynamic mixing timescale computed by Lebonnois & Schubert (2017).

3. Summary and Future Work

Even for a supercritical material, like the mixture of CO_2 and N_2 present at Venus, the diffusional properties cannot explain the compositional gradient of ~ 5 ppm m^{-1} proposed by Lebonnois & Schubert, (2017). We are now turning our attention to "exotic" properties of supercritical system, like those liked to the existence of the so-called "Frenkel line" (Bolmatov et al. 2013; Brazhkin et al. 2013; Bolmatov et al. 2014). We plan to perform molecular dynamics simulations in order to identify some, still unknown, physical processes which could lead to a kind of "phase transition" in the supercritical domain.

References

Lebonnois & Schubert, 2017; Mohagheghian et al. 2015, Sage & Lacey, 1939; Duan et al. 1996; Lorenz et al. 2018; Chapman & Cowling, 1970; Ghorayeb & Firoozabadi, 2000.